Southern Hemisphere atmospheric history of carbon monoxide over the late Holocene reconstructed from multiple Antarctic ice archives

Xavier Faïn[1], David M. Etheridge[2,3], Kévin Fourteau[4], Patricia Martinerie[1], Cathy M. Trudinger[2,3], Rachael H. Rhodes[5], Nathan J. Chellman[6], Ray L. Langenfelds[2], Joseph R. McConnell[6], Mark A. J. Curran[13,3], Edward J. Brook[7], Thomas Blunier[8], Grégory Teste[1], Roberto Grilli[1], Anthony Lemoine[1], William T. Sturges[9], Boris Vannière[10,11], Johannes Freitag[12], Jérôme Chappellaz[1,14]

[1]Univ. Grenoble Alpes, CNRS, INRAE, IRD, Grenoble INP, IGE, 38000 Grenoble, France
[2]CSIRO Environment, 3195, Aspendale, Victoria, Australia
[3]Australian Antarctic Program Partnership, Institute for Marine and Antarctic Studies, University of Tasmania, Hobart, Tasmania, Australia
[4]Univ. Grenoble Alpes, Université de Toulouse, Météo-France, CNRS, CNRM, Centre d'Études de la Neige, Grenoble, France
[5]Department of Earth Sciences, University of Cambridge, Cambridge, CB2 3EQ, UK
[6]Division of Hydrologic Sciences, Desert Research Institute, Reno, NV 89512, USA
[7]College of Earth, Ocean, and Atmospheric Sciences, Oregon State University, Corvallis, OR 97331, USA
[8]Physics of Ice, Climate and Earth, Niels Bohr Institute, University of Copenhagen, Copenhagen, Denmark
[9]Centre for Ocean and Atmospheric Sciences, School of Environmental Sciences, University of East Anglia, Norwich, UK
[10]Institute of Plant Sciences, Oeschger Centre for Climate Change Research, University of Bern, Switzerland
[11]MSHE, Chrono-environnement, CNRS, Université de Franche-Comté, Besançon, France
[12]Alfred Wegener Institut Helmholtz Zentrum für Polar und Meeresforschung, Bremerhaven, Germany
[13]Australian Antarctic Division, Kingston, Tasmania, Australia
[14]Ecole Polytechnique Fédérale de Lausanne EPFL, CH-1951, Sion, Switzerland

Correspondence to: Xavier Faïn (xavier.fain@univ-grenoble-alpes.fr)

Abstract.

Carbon monoxide (CO) is a naturally occurring atmospheric trace gas, a regulated pollutant and one of the main components determining the oxidative capacity of the atmosphere. Evaluating climate-chemistry models under different conditions than today and constraining past CO sources requires a reliable record of atmospheric CO mixing ratios ([CO]) since pre-industrial times. Here, we report the first continuous record of atmospheric [CO] for Southern Hemisphere (SH) high latitudes over the past three millennia. Our continuous record is a composite of three high-resolution Antarctic ice core gas records and firn air measurements from seven Antarctic locations. The ice core gas [CO] records were measured by continuous flow analysis (CFA) using an optical-feedback cavity-enhanced absorption spectrometer (OF-CEAS), achieving excellent external precision (2.8-8.8 ppbv, 2σ), and consistently low blanks (ranging from 4.1±1.2 to 7.4±1.4 ppbv), enabling paleo-atmospheric

1

interpretations. Six new firn air [CO] Antarctic datasets collected between 1993 and 2016 CE at the DE08-2, DSSW19K, DSSW20K, South Pole, ABN, and Lock-In sites (and one previously published firn CO dataset at Berkner) were used to reconstruct the atmospheric history of CO from ~1897 CE using inverse modeling that incorporates the influence of gas transport in firn. Excellent consistency was observed between the youngest ice core gas [CO] and the [CO] from the base of the firn, and between the recent firn [CO] and atmospheric [CO] measurements at Mawson station (East Antarctica), yielding a consistent and contiguous record of CO across these different archives. Our Antarctic [CO] record is relatively stable from -835 to 1500 CE with mixing ratios within a 30-45 ppbv range (2σ). There is a ~5 ppbv decrease in [CO] to a minimum at around 1700 CE, during the Little Ice Age. CO mixing ratios then increase over time to reach a maximum of ~54 ppbv by ~1985 CE. Most of the industrial period [CO] growth occurred between about 1940 to 1985 CE, after which there was an overall [CO] decrease, as observed in Greenland firn air and later at atmospheric monitoring sites and attributed partly to reduced CO emissions from combustion sources. Our Antarctic ice core gas CO observations differ from previously published records in two key aspects. First, our mixing ratios are significantly lower than reported previously, suggesting previous studies underestimated blank contributions. Second, our new CO record does not show a maximum in the late 1800s. The absence of a [CO] peak around the turn of the century argues against there being a peak in Southern Hemisphere biomass burning at this time, which is in agreement with (i) other paleofire proxies such as ethane or acetylene and (ii) conclusions reached by paleofire modeling. The combined ice core and firn air [CO] history, spanning -835 – 1992 CE, extended to the present by the Mawson atmospheric record, provides a useful benchmark for future atmospheric chemistry modeling studies.

1 Introduction

CO is a reactive trace gas that plays a crucial role in the interactions between climate and atmospheric chemistry. CO acts on the budgets of both hydroxyl radical (OH) and ozone (O_3), and thus has a strong impact on the global oxidative capacity of the atmosphere. With up to 40% of the OH radicals reacting with CO in the modern troposphere (Lelieveld et al., 2016), CO is the principal sink for tropospheric OH. Consequently, CO indirectly affects the lifetime of many atmospheric constituents such as methane (CH_4), volatile organic compounds (VOCs), and hydrofluorocarbons (HCFCs). Oxidation of CO by OH in the presence of high levels of nitrogen oxides (NOx) can result in significant production of tropospheric ozone, and ultimately leads to CO_2 production (Crutzen, 1973).

CO is produced by atmospheric oxidation of different gaseous precursors and emitted by various surface processes. Atmospheric oxidation of CH_4 and VOCs represents about half of the modern sources (Duncan et al., 2007). Modern terrestrial sources mainly include biomass burning (van der Werf et al., 2017) and incomplete combustion of anthropogenic fossil fuels and biofuels (Hoesly et al., 2018). Minor contributions come from the ocean (Conte et al., 2019) and plant leaves (Tarr et al., 1995; Bruhn et al., 2013). Oxidation by OH is the dominant sink of CO, which results in a modern mean global CO tropospheric lifetime of about 2 months (Khalil et al., 1999). However, CO lifetime strongly varies with latitude and season, ranging from

2

Supprimé: around the world and in Greenland firn air

Supprimé: day

Supprimé: , with m

80   20–40 days in the tropics to up to 3 months in polar areas (Duncan et al., 2007). In the pre-industrial (PI), CO emissions from fossil fuel combustion and oxidation of anthropogenic VOCs were negligible, and limited variations in the methane-oxidation CO source were likely as a consequence of relatively stable atmospheric CH_4 mixing ratios. Thus, the PI CO budget is expected to be driven principally by biomass burning and oxidation of biogenic VOCs (BVOCs), thereby providing an opportunity to use PI atmospheric CO to reconstruct past biomass burning.

85   Vegetation fires are an important component of the climate system. Fire emissions affect atmospheric chemistry and composition, biogeochemical cycling, radiative balance, or surface albedo (Archibald et al., 2018; Bowman et al., 2009). Biomass burning is also a major driver of vegetation changes and of ecosystem dynamics (Bond et al., 2005). In return, changes in climate (e.g., variations in temperature or precipitation) drive changes in fire as well as changes in vegetation that provide the fuels for fire. Understanding past fire dynamics is required to improve understanding of the climate-fire relationship on

90   centennial and millennial time scales, which will be essential to project future biomass burning and climate change. There is still a debate about how biomass burning emissions varied in the past and the extent to which humans have impacted the natural fire system (Vannière et al., 2016).

      Numerous proxies, exhibiting varying atmospheric lifetimes and consequently different footprints, have been investigated to reconstruct past biomass burning. These proxies, which include southern Hemisphere (SH) reconstructions of Antarctic [CO]

95   (Wang et al., 2010; Haan et al., 1996; 1998), generally suggest that SH biomass burning was high during the Medieval Period (MP) spanning 1000–1500 CE, with a decrease in burning during the 1400-1500 CE period reaching a minimum sometime during the 1600–1800 CE cool period (Little Ice Age or LIA). However, there are inconsistencies between different records regarding the timing and magnitude of changes during the last three centuries, i.e. the transition from the LIA to the industrial times. The Wang et al. (2010) dataset suggests that, following the LIA minimum, biomass burning emissions increased rapidly

100   during the 1700s and 1800s and peaked during the late 19th century at a level roughly 3 to 4 times the modern ones. By contrast, other fire proxies such as ethane (Nicewonger et al., 2018), acetylene (Nicewonger et al., 2020a), or black carbon (Liu et al., 2021; McConnell et al., 2021) indicate that SH biomass burning remained low throughout the 1800s. Improving our understanding of past burning variability requires more fire paleorecords. Specifically new [CO] records from Antarctic ice archives are needed to document biomass burning history in the SH.

105   Ground-based and satellite-derived CO data are only available for the last three to four decades. Ancient air preserved in glacial ice and firn is thus a unique archive for reconstructing the past atmospheric [CO] record prior to the 1990s. Firn is the upper layer of an ice sheet where snow is slowly transformed into ice. A large amount of air can be sampled from the interconnected open pores of the firn. Mean ages of atmospheric gases increase with firn depth. Analysis of air trapped in bubbles in solid ice below the firn layer is required to extend reconstructions further back in time. Over the last decade, Continuous Flow Analyses

110   (CFA) of ice core CO mixing ratios utilising laser spectroscopy has become a new tool in palaeoclimatology (Faïn et al., 2014; 2022). The CFA-based [CO] measurements exhibit excellent external precision and achieve consistently low blank levels, with absolute calibration enabling paleo-atmospheric interpretations. Faïn et al. (2022) applied CFA to multiple Greenland ice cores, allowing for reconstruction of an atmospheric trend for Northern Hemisphere CO over the past 300 yrs.

3

Supprimé: ,
Supprimé: ,
Supprimé: ,
Supprimé: m
Supprimé: p
Supprimé: s
Supprimé: concentrations
Supprimé: CO
Supprimé: history

In this study, we report [CO] firn air depth profiles from seven Antarctic sites, and continuous CO data measured on a set of five Antarctic ice cores. By combining the analysis conducted on these archives, we build a new composite record of

125 atmospheric [CO] in the SH for the last three millennia. This new dataset is compared with [CO] data previously published (Wang et al., 2010, Haan et al., 1996;1998) which suggest an increase of about 100% in biomass burning by the late 1800s, as well as with other biomass burning proxies. We focus on interpreting the pre-industrial trends in atmospheric [CO] largely related to biomass burning and BVOC oxidation sources. Climate-chemistry models and/or Earth System Models can produce simulated atmospheric [CO] at ground level in Antarctica, from the PI era to present-day. Such models are evaluated presently

130 within the Aerosol Chemistry Model Intercomparison Project (AerChemMIP) (Collins et al., 2017). Comparing the past evolution of Antarctic atmospheric [CO] extracted from ice archives for the specific period covering 1850 to present day with AerChemMIP model simulations is out of the scope of this paper. Such comparison, which should also provide improved constraints on inventories of CO emissions, will be addressed in a future study.

135 **2 Sampling and methods**

2.1 Firn air samples

Firn air samples used in this study were recovered between 1993 and 2016 from seven different Antarctic sites: Lock-In (LI), Berkner Island (BKN), DE08-2, DSSW20K, DSSW19K, Aurora Basin North (ABN), and South Pole (SP) (Fig. S1). Site descriptions are reported in Table 1. The LI site is located 136 km away from Dome C along the traverse road joining the

140 Concordia and Dumont d'Urville stations (Fourteau et al., 2019). BKN is an island surrounded by the Filchner-Ronne Ice Shelf (Assonov et al., 2007). ABN is located in inland East Antarctica approximately mid-distance between the coast and Dome C, in the Indian Ocean sector. DE08-2, DSSW20K and DSSW19K are located within 20 km of the Law Dome summit, about 120 km southeast of Casey Station (Etheridge et al., 1996; Trudinger et al., 2002).

Firn air sampling site (Fig. S1)	Sampling date	Analysis date	Deepest sampling (m)	Accum. Rate (cm w eq yr^{-1})	Mean annual Temp. (°C)
Lock-In 74°08' S, 126°09' E 3209m elevation	7-14 Jan. 2016	April 2016	108	3.6 [a]	-53 [a]
Berkner 79°33' S, 45°41' W 900m elevation	10-26 Jan. 2003	unknown	63 [b]	13 [b]	-26 [b]
DE08 66°43' S, 113°12' E 1250m elevation	17 Jan. - 28 Feb. 1993	May - June 1993	80 [c]	110 [c]	-19 [c]
DSSW20K 66°46' S, 112°21' E 1200m elevation	16-20 Dec. 1997	Feb. - April 1998	52	15 [d]	-22 [d]
DSSW19K 66°46' S, 112°22' E 1200m elevation	26-30 Oct. 2004	Dec. 2004	51	15 [d,h]	-22 [d,h]
ABN 71°10' S, 111°22' E 2690m elevation	25-30 Dec. 2013	Feb. - May 2014	102	11.9 [e]	-44 [e]
South Pole 90°S, 0°E 2835m elevation	22-23 Jan. 2001	March 2001	120 [f]	8 [g]	-49 [g]

Table 1. Locations, site characteristics and other relevant information for firn air sampling sites featured in this study. Deepest levels may have experienced contamination during sampling and may not be suitable for paleoatmospheric interpretations. [a] Fourteau et al. (2019), [b] Mulvaney et al. (2002), [c] Etheridge et al. (1996), [d] Trudinger et al. (2002), [e] Servettaz et al. (2020), [f] Butler et al. (2001), [g] Battle et al. (1996), [h] Trudinger et al., (2016).

2.2 Firn air sampling

The firn air extraction technique was originally described by Schwander et al. (1993). Briefly, at each site a shallow ice core drill progressively penetrates the firn column, stopping every few meters to allow recovery of the firn air using a firn air sampling device (FASD). Firn air is sampled at intervals of about 10 m from the surface down to the beginning of the lock-in zone where the age of the gases increases more rapidly. Within the lock-in zone, firn air sampling is typically conducted at intervals of 1-3 m. At each sampled depth, the borehole is sealed by the FASD's inflatable rubber bladder. Two continuous tubes (commonly made of Dekabon, with internal diameter 0.25 in.) pass through the bladder and its end caps. At BKN, LI, ABN, and SP, a "Bender baffle" (e.g., Assonov et al., 2007) was attached below the lower end caps of the bladder for venting firn-air in direct contact with the bladder, while the sample line below the baffle is directed towards gas analysers and canisters (Schwander et al.,1993).

CO sampling from the BKN firn is described by Assonov et al. (2007). The samples collected at the deepest levels of the BKN site were likely contaminated by a leak in the pumping system (Worton et al., 2007) and thus are not included in this study.

5

165 Firn air sampling techniques at DE08-2, DSSW19K, DSSW20K and SP are reported by Etheridge et al. (1996), Sturrock et al. (2002) and Rubino et al. (2019). Only two depths (surface and 119 m) at SP were available for our analysis due to a sample pump failure (previous studies have reported full depth profiles for other gases, e.g. Battle et al., 1996).

At LI and ABN, the CO_2, CO, and CH_4 mixing ratios of the extracted firn air were continuously monitored. Specifically, [CO_2] was monitored using an infrared analyzer (LI-COR, LI-7000) and [CO] and [CH_4] with an optical analyzer (SARA, OF-CEAS

170 technology, Morville et al., 2005). These real time measurements were used to indicate when uncontaminated air was extracted from the borehole, and thus samples were only collected when CO_2, CO, and CH_4 were stable and below modern ambient levels.

Measurements of ambient air at the DE08-2, DSSW19K, DSSW20K, SP, ABN and LI sites sampled through the FASD were in agreement with concomitant measurements of atmospheric air samples collected at Mawson Station and collected at the site

175 (typically 1 ppbv or less discrepancy), suggesting minimal air contamination or loss of CO during firn air sampling. Measurement uncertainty is further discussed in SI Sect. 2.2.

2.3. Firn air CO analysis

The DE08-2, DSSW20K, DSSW19K, SP and ABN firn air samples were analyzed at CSIRO by gas chromatography using a Trace Analytical Reduction Gas Analyser (Langenfelds et al., 2023). Only containers that demonstrated reliable storage for

180 CO were used (glass flasks and electropolished stainless steel tanks) and small time-dependent corrections (e.g. -0.0058 ppbv/day in CSIRO 0.5 L glass flasks fitted with PFA o-rings, -0.0030 ppbv/day or less for electropolished stainless steel tanks) were applied to allow for the remaining drift in [CO] between sample collection and analysis. Uncertainty of CSIRO flask data, including experimental precision and correction for storage, was generally within ±1 ppbv. LI firn air was collected in 3 L stainless steel canisters (Silcocan) pressurized to 3 bar. However, such pressure could not always be reached at the

185 deepest levels sampled, where most of the firn porosity was fully closed. LI samples were measured at IGE (France) in April 2016 (i.e., four months after field collection) using a SARA analyzer (Morville et al., 2005). A subset of LI canisters was reanalyzed 6 months later, demonstrating no [CO] drift related to storage. The BKN firn air was analyzed for [CO] at MPI (Max Planck Institute, Mainz, Germany) using accurate volumetric determination (Brenninkmeijer et al., 2001), along with CO isotopic ratios (Assonov et al., 2007).

190 Firn air [CO] analyses conducted at CSIRO are reported on the CSIRO2020 CO calibration scale (see SI for more details). LI firn air [CO] measurements conducted at IGE are reported on the WMO-X2014 scale. A comparison of CSIRO2020 and WMO-X2014 scales, based on NOAA analysis in 2015/16 of CSIRO's primary standards samples, indicates their consistency within about ±1 ppbv over the 28 - 487 ppbv range (Langenfelds et al., 2023). The BKN CO dataset is reported on the MPI scale, which was 8% higher than the WMO CO_X2004A scale when BKN firn air was analyzed (Assonov et al., 2007). The

195 WMO-X2004 scale gives ~1 ppbv lower values for [CO] below 200 ppbv compared to WMO-X2014 scale, with [CO] reported by Assonov et al. (2007) all below 200 ppbv. Uncertainties reported in this study for BKN firn air [CO] account for calibration scale differences.

6

2.4. Modeling trace gas transport in firn

Due to diffusive mixing, the composition of firn air at any depth does not correspond exactly to the atmospheric composition at a specific time in the past, rather it is a mix of air over a range of past times so corresponds to a distribution of ages (Schwander et al., 1993). Molecular diffusion through the open porosity of firn, followed by porosity closure, results in increasing gas ages and gas age distribution widths with depth in the firn. Trace-gas records in ice cores are further smoothed by progressive gas enclosure into individual bubbles. Models of gas transport in firn (e.g. Buizert et al., 2012, Witrant et al., 2012, Trudinger et al., 2013) take these effects, and more generally the firn physics, into account and thereby allow reconstruction of past atmospheric variations.

In this study we use the IGE-GIPSA and the CSIRO firn air transport models and inverse models to reconstruct the temporal evolution of CO mixing ratio from our firn depth profiles (Sect. 2.1). The physical basis of the IGE-GIPSA and the CSIRO firn models are described in Witrant et al. (2012) and Trudinger et al. (1997, 2013), respectively. Briefly, these models include molecular diffusion, gravitational settling and advection of air due to firn sinking. Firn models use a site-specific diffusivity-depth profile which is tuned using reference gases that have a well constrained past atmospheric trends (major greenhouse gases and anthropogenic halocarbons). Diffusivity tuning for our seven firn sites has been described in previous studies (Witrant et al., 2012; Trudinger et al., 2013; Yeung et al., 2019). The diffusivity-depth profile for DSSW19K was assumed to be the same as for DSSW20K due to their close proximity.

Two different inverse approaches are used to reconstruct atmospheric trends of CO from the firn observations. The IGE-GIPSA inverse model is based on the transfer function approach by Rommelaere et al. (1997) and uses a new definition of the optimal solution (Witrant and Martinerie, 2013) intended to favor robustness (Lukas, 2008). It has already been used to reconstruct several atmospheric trends of trace gas mixing ratios and isotopic ratios (e.g. Helmig et al., 2014; Laube et al. 2016; Trudinger et al., 2016; Yeung et al., 2019 and references therein). The seasonal CO cycle is damped in the firn due to diffusive mixing. The summer minimum is reflected by low near-surface values, and the seasonality variation quickly damps with depth so that below about 30m depth, the CO firn signal mostly reflects annual mean variations (Wang et al., 2012, Petrenko et al., 2013). The IGE-GIPSA inverse firn model cannot reconstruct the CO seasonality (Wang et al., 2012), therefore CO measurements above a depth of 30 to 40 m depending on the site investigated were excluded from the model input. Modeling several firn sites simultaneously to reconstruct a single atmospheric trend provides a much stronger constraint than a single firn site and allows evaluation of the consistency of the firn datasets. Best constraints are obtained when simultaneously modeling firn sites with very different physical characteristics (temperature, snow accumulation rate, etc.) and drilling dates, which is the case for our sites. The model can use data from firn air pumping and ice core analysis simultaneously, and here we link our reconstruction based on the firn measurements to the shallowest measurements of the ice core record. Trace gas records in ice are affected by an additional smoothing process compared to firn air: bubbles in an ice sample close at a range of times. This process is less well constrained than trace gas transport in firn (e.g. Fourteau et al., 2020) but is driven primarily by the snow accumulation rate which controls the firn sinking speed. Similarly to the approach in Yeung et al. (2019), we use synthetic

data points in BKN ice, which has almost the same accumulation rate as ABN to simulate the constraint from ice core data. The best estimates of CO mixing ratios corresponding to five gas age values ranging between 1882 and 1889 CE were attributed to depth levels with the same gas age in the BKN ice.

The CSIRO inverse model used here is based on the Bayesian synthesis inversion described in Trudinger et al. (2002; 2016) but formulated to infer annual mixing ratios rather than annual sources. As with the IGE-GIPSA inverse model, the CSIRO inverse model infers a single atmospheric trend from multiple firn datasets modeled simultaneously. Both inverse models use Green's functions, which represent gas age distributions, to relate the mixing ratio of a trace gas at the measurement depths to atmospheric mixing ratio of that gas over a range of times (Rommelaere et al., 1997; Trudinger et al., 2002). The modeled CO at a depth in firn can be calculated by convolving the atmospheric CO history with the relevant Green's function (assuming diffusivity versus depth is constant in time). The CSIRO inverse model takes a different approach than the IGE-GIPSA model due to the strong influence of seasonality in atmospheric CO on the upper firn mixing ratio profile. Instead of excluding observations in the upper firn, the effect of seasonality in atmospheric CO on the firn mixing ratio profile is calculated with a forward run of the CSIRO firn model forced with a Thoning et al. (1989) fit at daily resolution to the Mawson atmospheric CO record from mid-1992 and mean seasonality calculated from the Mawson record before that. The resulting modeled mixing ratios at the observation depths are subtracted from the firn observations before they are used in the inversion, so that the inversion infers annual values of the atmospheric CO trend up to 1992.0 (with CO from 1993.0 taken from the Mawson atmospheric record). This allows the complete profiles for firn measurements to be used. A melt layer at the DE08-2 site was observed to have been a partial barrier to firn air mixing (Trudinger et al., 1997). The melt layer is advected with the ice downwards away from the snow surface, but this cannot be incorporated into the inversion using the Green's function representation that assumes diffusivity versus depth is constant with time. The influence of the melt layer at DE08-2 is therefore calculated with a forward simulation of the firn model, and the result subtracted from the firn data before the inversion. The CSIRO inversion calculation is regularized by including a term in the cost function to be minimized that is the sum over all years of the change in mixing ratio from one year to the next, as described in Trudinger et al. (2016). At the end of the firn reconstruction, the regularization term compares the final firn reconstruction value with the 1993 to 1997 mean for Mawson. The deep SP firn sample has a small contribution from the atmospheric [CO] history before 1900 (i.e. part of the Green's function from the firn model for this SP sample extends before 1900). The CSIRO inversion can either reconstruct atmospheric [CO] from 1900 assuming constant CO before 1900 (the [CO] value inferred at 1900 is extended back in time and convolved with the part of the Green's function before 1900), or it can reconstruct atmospheric [CO] from 1898 assuming the atmospheric CO history from the ice reconstruction up to 1897 (the ice reconstruction is convolved with the part of the Green's function extending before 1898), with the regularization described above applied to the change in [CO] between the last annual ice reconstruction CO value in 1897 and the first annual firn reconstruction value in 1898 (to ensure a smooth and continuous reconstruction from ice and firn). Uncertainties in the CSIRO firn reconstruction are calculated by a bootstrap method (Trudinger et al., 2016), whereby the inversion is repeated many times with firn measurements, the Mawson atmospheric record and the ice reconstruction all randomly perturbed according to their uncertainties, and used with firn Green's functions

drawn randomly from an ensemble of Green's functions for each site (chosen during firn model calibration to represent uncertainty in the firn model parameters). The uncertainty calculation is discussed in more detail in Supplementary Information (SI) Sect. 2.4. The best-fit atmospheric history is calculated without any perturbations.

In this study, we apply a multi-site reconstruction inverse method to using both the IGE-GIPSA and the CSIRO models to determine the atmospheric reconstruction that fits the investigated sites for each model. Five sites (DE08-2, DSSW20K, SP, LI, BKN) were investigated with the IGE-GIPSA model, and 5 sites (DE08-2, DSSW20K, SP, DSSW19K, ABN) with the CSIRO model. As different models, methodologies and site combinations were used, the comparison of IGE-GIPSA and CSIRO model results provides insights about the robustness of our results.

2.5. Ice core samples

Five ice cores extracted from Antarctica were investigated in this study (Fig. S1). The DC12, ABN, and Taldice (TD) ice cores (Table 2) were used to investigate the past atmospheric history of carbon monoxide over the late Holocene. Two additional Antarctic ice cores, EDML-B40 and Solarice (Fig. S1), which provided complementary, short datasets supporting paleo-atmospheric interpretations, are described in SI (Table S3 and SI Sect. 2.6 and 2.7). High resolution CO mixing ratios (See Sect. 2.6) were measured continuously along with those of methane.

Ice core & location	Depth interval (m)	Gas age interval (yrs CE)	Accum. Rate (cm weq yr^{-1})	Mean annual Temp. (°C)
DC12 Dôme Concordia 75°0.6' S, 123°2' E 3233m elevation	108-151; 156-177	1619 ; -835	2.5 [a]	-53 [b]
ABN Aurora Basin 71°10' S, 111°22' E 2690m elevation	108 - 303	1897 ; 22	11.9 (period 1979-2013) [c]	-44 [c]
TD Talos Dome 159°11'E, 72°49' S 2315m elevation	27 sections distributed from 88 to 136 m depth	1876 ; 652	8.6 [d]	-41 [d]

Table 2. Locations, site characteristics and other relevant information for ice cores featured in this study. [a] Gautier et al. (2016), [b] Fabre et al. (2000),[c] Servettaz et al. (2020), [d] Stenni et al. (2002).

DC12 ice core. This shallow ice core was drilled in 2012 at Concordia Station (Dome C) and fully analyzed for CO mixing ratio. The continuous methane record for this shallow Dome C ice core has been reported previously (Fourteau et al., 2020).

Supprimé: Uncertainties in the CSIRO firn reconstruction are calculated by a bootstrap method (Trudinger et al., 2016) that incorporates uncertainty in the firn measurements, the firn model parameters (using an ensemble of firn Green's functions), the Mawson atmospheric record and the ice reconstruction (when used).

Supprimé: constrain

Supprimé: and

Supprimé: and

Supprimé: Supplementary information (

Supprimé:)

ABN ice core. A single summer drilling campaign was conducted in the 2013–2014 season at the ABN site. This drilling site (Servettaz et al., 2023) is located on the lower elevation edge of the East Antarctic Plateau, ~500 km inland of the coastal station Casey, approximately halfway to Concordia station on Dome C (Fig. S1). The entire ABN ice core below close off was analyzed for CO mixing ratio.

320 *TaldIce ice core.* The TaldIce drilling was conducted from 2004 to 2008 at Talos Dome, an ice dome on the edge of the East Antarctic plateau and adjacent to the Victoria Land mountain (Stenni et al., 2002; Frezzotti et al., 2007). Talos Dome is located about 290 km from the Southern Ocean and 250 km from the Ross Sea. In the framework of this study, discontinuous sections spanning 19 m were analyzed.

These three sites experience accumulation rates ranging from 2.5 to 11.9 cm weq yr^{-1} and mean annual surface temperature
325 between -41 and -53°C (Table 2). Ice and gas chronologies for the three ice cores are described in Table S1.

2.6. CO continuous flow analyses

Over the past decade, continuous and high resolution CFA-based CO analyses have greatly improved, including lowering the CO blank and characterizing how CO is preferentially dissolved during CFA process so as to establish absolute calibration (Faïn et al., 2022). The excellent precision of CO analyses has been confirmed, and the designs of CFA setups themselves
330 have been optimized to limit the instrumental smoothing and improve signal resolution. These improvements have been reported in detail by Faïn et al. (2022), which describe CO continuous analyses of five ice cores from Greenland. Here we report here the first application of this method to Antarctic ice cores.

2.6.1. System operation

The ice cores listed in Table 1 were analyzed using a continuous ice core melter system coupled with online gas measurements
335 (Stowasser et al., 2012; Fourteau et al., 2017; Faïn et al., 2022). Ice core sticks are cut at a 34 mm x 34 mm cross section and processed on a melter-head located in a cold room. The melter-head is composed of inner and outer collection areas with the inner area dedicated to sample collection. To prevent contamination, a water overflow from the inner to the outer melter-head areas of >10% is created by lowering the sample pumping speed. The water and gas bubble mixture is continuously pumped via a debubbler into a temperature-controlled gas extraction unit maintained at 30°C. The gas/water volume ratio of the sample
340 is about 10% before the debubbler, and 50% after the debubbler. Water sample without gas bubbles is thus also available at the debubbler for complementary chemical analyses in the liquid phase. The gas is extracted along the sample line after the debubbler by applying a pressure gradient across a gas-permeable membrane (Transfer-Line degasser, Idex). Then, the gas is dried by a custom-made Nafion (Perma Pure) dryer. Finally, CO (and/or CH$_4$) mixing ratios are continuously measured by a laser spectrometer.

The Idex degassing membrane operated in this study does not recover dissolved gases from the water phase efficiently. Carbon

350 monoxide (or methane) has higher solubility than N_2 or O_2. Consequently, mixing ratios of CO in the gas phase of the sample flow exhibit lower values than exist initially in the ice bubbles. As melting ice contains ~10% air, a 10:90 mixture of synthetic air with known mixing ratios of CO (and/or CH_4) and degassed deionized (DI) water can be introduced into the system via a 4-port valve located directly after the melter head. The water is sourced from a 2 L reservoir degassed by constantly bubbling ultra-pure helium through it. The air–water mixture follows the same path through the system as the ice core sample before

355 being analyzed by the laser spectrometer. However, it is not fully identical as it includes more components such as an additional peristaltic pump and tubing. This pathway for synthetic standard analysis will be designed as the "calibration loop".

The DC12 and TD ice cores were analyzed at the Institut des Geosciences de l'Environnement (IGE, Grenoble, France) in 2014 during two different analytical campaigns (in June and November, respectively). The ABN core was analyzed at the Desert Research Institute (DRI, Reno NV, USA) in October 2015, immediately after the PLACE (Greenland) core (Faïn et al.,

360 2022) without modification of the CFA setup. Descriptions of the IGE and DRI setups are reported by Faïn et al. (2022).

A unique spectrometer (SARA, developed at Laboratoire Interdisciplinaire de Physique, University Grenoble Alpes, France) operating optical feedback cavity enhanced absorption spectrometry (OF-CEAS, Morville et al., 2005) was used to analyze carbon monoxide (and simultaneously, methane) at both IGE and DRI. Detailed description of this instrument, which was used for CO measurements along Greenland ice cores is reported by Faïn et al. (2022). The OF-CEAS instrument was always

365 carefully calibrated before melting ice cores (SI Sect.1.3).

2.6.2. Precision of continuous CO analyses

We apply the Allan-Werle statistical method (Allan, 1966, Werle 1993) to the calibration loop datasets to evaluate internal precision and stability of gas-CFA measurements. Observed optimal integration time (i.e., time of lowest Allan-Werle deviation) was determined for each analytical campaign, and is larger than 500 s for DRI, and 1000 s for IGE CFA setups (Fig.

370 S2). Gas data were all averaged over a 10 sec integration time, allowing full resolution of the variability of the Antarctic CO records. Internal precision, defined as twice the Allan-Werle deviation at chosen integration time, was 0.7 and 1.0 ppbv for the IGE (i.e., DC12 and TD) and DRI (i.e., ABN) analytical campaigns (Table S2).

External precision of the continuous CO measurements (i.e., including all sources of errors or bias) was investigated by melting replicate Greenland ice sticks on different days on a gas-CFA setup, yielding 2.8 ppbv and 8.8 ppbv (2σ) for the IGE and DRI

375 CFA setups, respectively (SI Sect. 1.5).

2.6.3. Absolute calibration and accuracy

11

CFA–based gas records must be corrected for (i) analytical blank and (ii) under-recovery of gases dissolved in the water stream to obtain absolute values on the WMO-X2014 calibration scale. Evaluation of analytical blanks indicated 4.1 and 7.4 ppbv for the IGE and DRI CFA setups, respectively (SI Sect. 1.6, Table S3).

The calibration loop is an appropriate approach to evaluate the magnitude of CO preferential dissolution (Faïn et al., 2022). We hypothesize that CO and methane dissolution follow the same physical laws: consequently, if a calibration loop is able to reproduce methane preferential dissolution, it should also reproduce CO losses related to dissolution. In the case of methane, discrete datasets allow for an external validation of this CFA internal calibration. In this study, we extracted calibration factors for CO from calibration loop experiments for each CFA setup (SI).

Overall, CO losses driven by preferential dissolution ranged from 6.0 to 7.4%. Replicate measurements show that the fraction of CO not recovered at the outlet of the CFA system was very stable during analytical campaigns, both at IGE and DRI. Based on repeated calibration loop measurements throughout the campaigns we conservatively estimate the uncertainty of the SC factor to be ±1% (2σ).

2.6.4. Signal Smoothing

Mixing of gases and meltwater during sample transfer from the melt-head to the laser spectrometer induces a CFA experimental smoothing of the signal. The extent of the CFA-based damping was determined for each CFA setup by performing switches between synthetic mixtures of synthetic air standards of different CO mixing ratios and degassed deionized water. Cut-off wavelengths, defined as the wavelength of a sine signal experiencing a 50% attenuation in amplitude, of 1.6 cm and 9.3 cm were observed for the IGE and DRI CFA setups, respectively (Table S2; see SI Sect. 1.3 in Faïn et al., 2022, for a description of differences and similarities between DRI and IGE CFA setups).

2.6.5. Data processing

The occasional entry of ambient air into the analytical system when core breaks are encountered could cause contamination. The SARA spectrometer simultaneously measures carbon monoxide and methane mixing ratios, and such contamination events were characterized by a sharp increase in methane (ca 1900 ppbv) followed by an exponential decrease. Data were manually screened for ambient air contamination.

3. Results and discussion

In this study, we report new CO records from firn air and ice cores, spatially distributed across the Antarctic ice sheet. In Sect. 3.1, we investigate the spatial variability of CO mixing ratios in the modern Antarctic atmosphere. In Sect. 3.2, we describe

12

our CO firn air and ice core records. In Sect. 3.3, we combine all records to reconstruct the evolution of the past [CO] in the Antarctic atmosphere for the last 3000 years. In Sect. 3.4, we compare this new reconstruction with other paleofire proxies, and Sect. 3.5 discusses new insights on SH past fire history.

3.1. Spatial variability of [CO] in the modern Antarctic atmosphere

420 Before combining multiple [CO] records from firn air and ice archives collected at sites spatially distributed across East Antarctica (Fig. S1), it is important to assess if atmospheric [CO] exhibits similar levels and trends at these sites. Monitoring of [CO] in the Antarctic atmosphere has been conducted routinely by CSIRO and NOAA. Over recent decades, CSIRO has collected atmospheric [CO] at Casey (Loh et al., 2021a), South Pole (Loh et al., 2021b), and Mawson (Loh et al., 2021c). These three stations are distributed across East Antarctica, with South Pole located on the plateau, and Casey and Mawson

425 both located on the coast (Fig. S1). Over the period spanning 1997-2020 CE, CO mixing ratio at the three CSIRO monitoring sites exhibit almost identical and highly correlated patterns (Fig. S5 and S6) as might be expected given the absence of CO sources across Antarctica. We conclude that [CO] records extracted from firn air and ice core archives at the sites investigated in this study (Fig. S1) can be combined to produce a robust history of atmospheric [CO] in the Antarctic atmosphere. Note that the high [CO] annual mean in 2020 is observed at the three Antarctic stations and Kennaook/Cape Grim (40.7° S in Tasmania; Langenfelds et al., 2023) and is likely from the emissions from the 2019-2020 Australian bushfires. [CO] has since returned

430 to the longer term trend at these stations.

To further investigate the spatial representativity of an Antarctic record based on firn air and ice cores, we compared the [CO] outputs simulated for the year 2000 in the framework of the ACCMIP exercise (Lamarque et al., 2013) and averaged over three latitudinal bands: 30-90°S, 45-90°S, and 70-90°S. The 70-90°S latitudinal band encompasses the Antarctic ice sheet.

435 Average [CO] over the 45-90°S, and 70-90°S areas are similar, with levels of 51.9 and 51.0 ppbv, respectively. An atmospheric [CO] of 54.1 ppbv is simulated for the 30-90°S latitudinal band, i.e. about 5% higher than [CO] simulated over Antarctica. These modeling results are in agreement with observations: the annual mean [CO] difference in CSIRO measurements between Kennaook/Cape and Mawson and Casey Stations since 2000 CE is only 2.2 ppbv, the coastal Antarctic Stations being lower. These results suggest that the absolute CO mixing ratios derived from our datasets not only are representative of Antarctica,

440 but more widely of the mid-high latitude Southern Hemisphere (45-90°S) atmosphere. Also, the temporal changes depicted by our composite record probably have a larger spatial significance, including at least the 30-90°S latitudinal band.
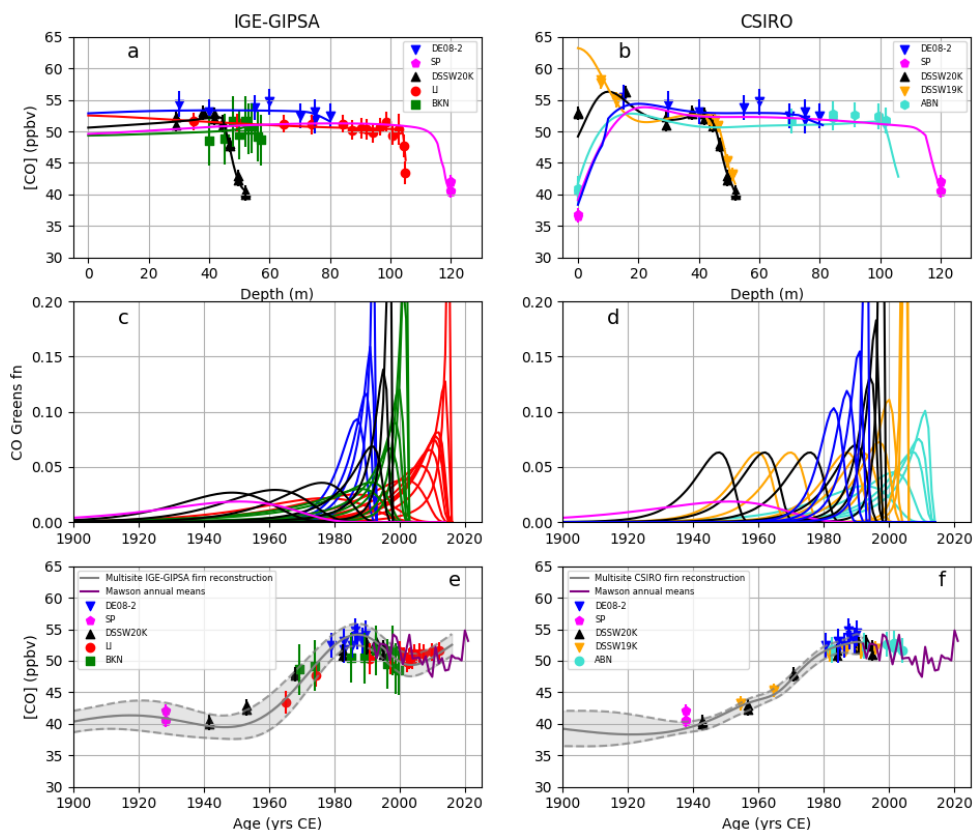
3.2. [CO] datasets

3.2.1 Firn air datasets

CO mixing ratios measured in the firn air at LI, BKN, DE08-2, DSSW19K, DSSW20K, ABN and SP are presented as a

445 function of depth below snow surface in Fig. 1a and 1b. The number of depths sampled varies among sites, with firn air collected at 15 depths at LI, and only one deep level measured for [CO] at SP by CSIRO.

13

Figure 1. (a) and (b) Depth profiles of carbon monoxide mixing ratio in the firn air at seven Antarctic sites (Lock-In, DE08-2, DSSW20K, DSSW19K, Berkner, South Pole, ABN). Lines show forward model results using optimum atmospheric [CO] history (Sect. 3.3) as input; symbols are measurements with 2σ uncertainties. (a) reports IGE-GIPSA modeling results: the IGE-GIPSA model does not reconstruct the CO seasonality, and CO measurements above a depth ranging 30-40 m were excluded from the model inputs. (b) shows CSIRO modeling results. (c) and (d) show Green's functions from the IGE-GIPSA (c) and CSIRO (d) firn models (there is one line for each firn sampling depth, with the colors corresponding to those for different sites in panels (a) and (b)). (e) and (f) Best-fit atmospheric history of Antarctic [CO] obtained with the inverse modeling IGE-GIPSA (e) and CSIRO (f) technique (gray line, with the envelope representing 2σ uncertainty). Firn air measurements (symbols) are plotted as a function of mean ages extracted from the modeled age distributions (excluding the upper firn measurements strongly affected by seasonality). We note that firn air data plotted versus mean age are not strictly comparable with the modeled time trends which account for the age distribution widths in the samples. Annual mean [CO] at Mawson Station is shown in purple - the annual means are calculated from a smooth fit at daily resolution to measurements conducted by CSIRO since 1992 on flask samples of background air collected fortnightly (SI Sect. 2.1).

14

[CO] exhibits a strong seasonal cycle in the Antarctic troposphere, with mixing ratios lower (higher) in summer (in winter) when OH levels are elevated (resp. low) (Fig. S5). The seasonal signal diffuses down in the upper firn layers, and affects the top 30-40 m of the firn depending on the site, with attenuation of seasonality mostly complete below this. Variations in CO mixing ratios observed in the shallowest firn air (Fig.1a and 1b) thus are driven mainly by the atmospheric [CO] seasonal cycle. All firn air sampling described in this study, except DSSW19K, was conducted during summer, and thus surface sampling (denoted as 0 m in Fig. 1a and 1b) exhibited low [CO]. On the contrary, maxima in [CO] are observed at ~10m depth at these sites, reflecting diffusion of elevated wintertime atmospheric [CO] into the firn. Sampling at DSSW19K was conducted in spring (Table 1) and thus exhibits higher [CO] surface levels.

[CO] profiles with depth (Fig. 1a and 1b) differ depending on the sampling site. The oldest and most interesting parts of the firn [CO] records for inferring long-term changes are in deep firn i.e., located below the lock-in depths (Table 1). All sites show a decrease with depth indicating lower atmospheric [CO] levels in the past in the Antarctic atmosphere. Low open porosity of the firn at the bottom of the lock-in zone makes firn air contamination possible during sampling, which results in the partial rejection of measurements at the deepest levels. In this study, we were careful to report only uncontaminated [CO] values. Contamination was identified by deploying specific analyzers in the field ($[CO_2]$, $[CH_4]$ or [CO], Sect. 2.2) and/or by detection of anomalous values for species which are expected at very low levels in old air (e.g. halocarbons such as [SF6] or [CFC-11] because they have been emitted to the atmosphere only recently by human activities (Witrant et al., 2012). The [CO] decreases observed in the lock-in zones reveal different shapes. The thickness of the lock-in zone, and the possibility for older gas to be preserved in the firn, depends on climatic conditions such as temperature and snow accumulation (Witrant et al., 2012), which differ between sites. Differences in [CO] depth profiles (Fig. 1a and b) are also related to the age distributions in the firn air samples, which depend on firn physics and on the date of the firn air sampling campaigns (between 1993 and 2016, see Table 1). Interestingly, DE08-2 firn depth profile which was sampled in 1993 (Table 1) exhibits higher [CO] (Fig. 1a). Although some residual contamination or effects of the firn air sampling device can't be ruled out completely in 1993 when firn air sampling was a new methodology, the mean Antarctic atmospheric [CO] also was higher three decades ago.

Concerns about the potential of CO production on snow surfaces (e.g. Assonov et al., 2007) led us to investigate whether [CO] in firn air and therefore in deeper ice core air could be elevated above background atmospheric levels. Measurements were made of [CO] in air sampled via pump inlets at the snow surface or inserted 5-10 cm into the snow at three regions of Law Dome (a cold, high accumulation region near the summit, a lower accumulation region at DSSW19K and a warmer, snow ablation site near the ice sheet margin). A similar experiment was conducted at Concordia Station (a very low accumulation site where the DC12 ice core was drilled, Table 2), with pump inlets at the snow surface or inserted 10-70 cm into the snow. At all sites, the CO mixing ratios in air sampled during daylight hours at or just below the snow surface were not systematically different, within measurement uncertainty, from those sampled at night or during the day but from about 3 meters above the snow surface. Firn [CO] measurements in the upper 30 m also agree well with the CSIRO model simulations (Fig. 1b) which

15

Supprimé:

Supprimé: s

Supprimé: [CO]

Supprimé: S

at this depth range are driven by atmospheric observations at Mawson. From this we conclude that the firn and ice samples are
505 not significantly affected by photochemical [CO] production, presumably due to low CO production in Antarctic snow and/or
ventilation of produced CO away from the surface snow layer.

Finally, annual mean values of the CSIRO atmospheric [CO] record from Mawson Station since 1992 CE are also displayed
in Fig. 1e and 1f. These direct measurements of atmospheric [CO] in the Antarctic atmosphere, which use the CSIRO2020
calibration scale, exhibit good agreement with firn air datasets.

510 **3.2.2. Continuous [CO] records along Antarctic ice cores**

The [CO] new records available from the DC12, ABN, and TD ice cores are reported in Fig. 2 and plotted for a period spanning
-835 to 1897 CE (gas age, see Table S1). The high resolution datasets represent the CFA output calibrated (WMO-X2014
scale, Sect. 2.6.3. and SI), filtered to remove lab air infiltrations (Sect. 2.6.5), with an integration time of 10 s. Splines based
on the high resolution signals can be used to produce an average CO history for each site. The envelopes report 2σ uncertainties,
515 and combine uncertainties evaluated specifically (Tarantola, 2005) for each analytical setup on CO blanks, solubility
calibration factors, and external precision of CO CFA measurements (see SI and previous sections). The high resolution DC12
CO record exhibits a 6 m gap, for gas ages spanning -114 to -209 CE, because samples were damaged during transport. To
infer the [CO] trend in this missing data interval, we analyzed a section of the Solarice core, which was drilled at Concordia
Station in January 2016, 2 km away from the DC12 borehole. Solarice measurements reveal a smooth evolution of CO mixing
520 ratio for the missing period in the DC12 records and we consequently extract a continuous spline from the DC12 dataset (SI
Sect. 2.7, Fig. S15). None of the Antarctic records revealed high and variable mixing ratios that were previously observed in
Greenland ice cores and interpreted as in situ CO production (Faïn et al., 2014; 2022). The DC12, ABN, and TD records exhibit
stable and low MAD (median absolute deviation) values, with mean MAD values over the entire datasets ranging from 1.1 to
2.4 ppbv, depending on the records. These values are much lower than the MAD values reported for Greenland [CO] records
525 impacted by in situ production, which ranged from 10 to 80 ppbv (Faïn et al., 2022).
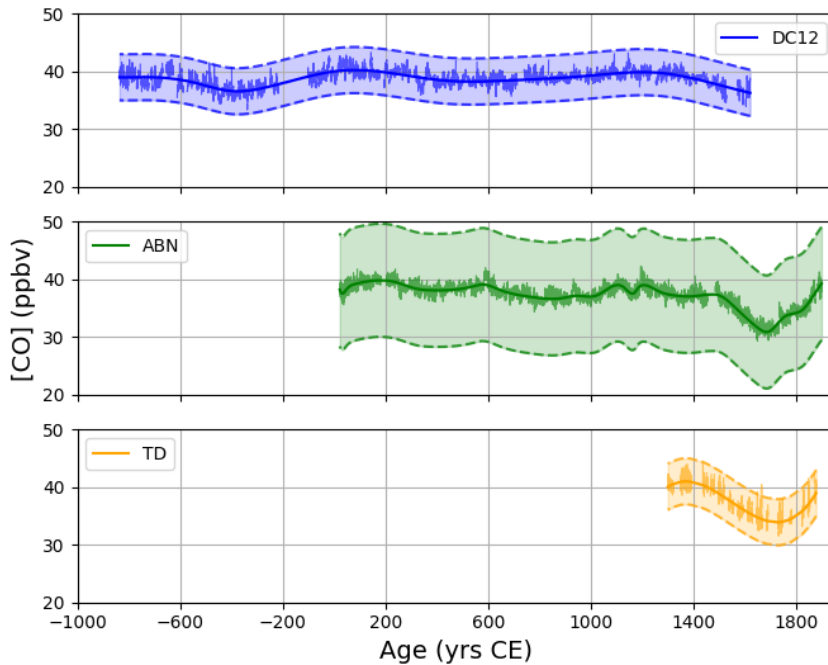
Supprimé: vetted for lab air infiltrations

Supprimé: concentrations

16

Figure 2. Continuous [CO] records collected along the DC12 (blue), ABN (green), and TD (orange) Antarctic ice cores. The integration time of high resolution datasets is 10 s. A spline is applied to each high resolution dataset. The noise displayed by high resolution solid lines only represents the internal precision, while the envelopes report 2σ uncertainties combining uncertainties on CO blanks, solubility calibration factors, and external precision of CO CFA measurements derived from the reproducibility measurements.

The ABN and TD CO records both show a minimum in CO mixing ratio in ~1700 CE. The DC12 record does not extend to 1700 CE, but still shows a decreasing trend in [CO] from 1400 to 1620 CE. All records exhibit rather stable CO levels for periods prior to ~1400 CE. Although some fluctuations in [CO] can be seen prior to 1400 CE, they are not significant compared to the width of the uncertainty envelopes.

The occurrence of a minimum in atmospheric Antarctic [CO] centered in 1700 CE is supported by CFA analyses of the EDML-B40 ice core (SI Sect. 2.6). Although absolute calibration of the EDML-B40 CFA CO dataset was not possible, this record also reveals a minimum in [CO] in the 1700s.

3.3. Atmospheric [CO] history over the last 3000 yrs

3.3.1. A reconstruction spanning 1897 to 1992 CE from firn air data

545   We applied the inverse IGE-GIPSA and CSIRO firn and inverse models (Sect. 2.4) to the [CO] firn depth profiles (Fig. 1a and 1b) to reconstruct the temporal evolutions of [CO] in the Antarctic atmosphere. The IGE-GIPSA reconstruction extends to 2016 CE, and is constrained in 1862-1889 CE by five synthetic data points in BKN ice with mean ages and CO mixing ratios consistent with the ice core composite presented in Sect. 3.3.2. Simulations performed with and without this ice constraint provide consistent results (within uncertainty limits of one another, for more details, see Sect. 2.4 and SI Sect. 2.3.2).

550   The CSIRO firn reconstruction extends to 1992 CE, after which the atmospheric history follows the atmospheric measurements from Mawson station, as described in Sect. 2.4. By using the Mawson record with daily resolution to calculate the influence of seasonality in the upper firn, it is possible to use all of the firn measurements. Fig. S9 shows how the atmospheric history before and after 1992 affects the modeled depth profiles. The CSIRO firn air reconstruction begins in 1898 and uses the ice reconstruction (see Sect. 3.3.2) to give the atmospheric history up to 1897 (with regularization in the inversion preventing the
555 difference between the last ice record value in 1897 and the first firn record value in 1898 being too large). A firn reconstruction run without the ice core record before 1897, instead assuming constant CO before 1900, differs in 1897 from the ice core reconstruction by only 1 ppbv, therefore within the uncertainty envelopes (SI, Fig. S10).

    The Green's functions used in the inversions are shown in Fig. 1c and 1d. Optimal atmospheric [CO] histories obtained by both models are reported in Fig. 1e and 1f with the envelope reporting 2σ uncertainty. [CO] firn air data are plotted as a
560 function of mean ages in Fig. 1e and 1f (however note that the Green's functions are a more accurate representation than mean age for the age of firn air, and it is more appropriate to assess the agreement between models and measurements by comparing the [CO] depth profiles in 1a and 1b than the reconstructed [CO] time histories and measurements versus mean ages in 1e and 1f). Both IGE-GIPSA and CSIRO firn models were then operated in forward mode to simulate a [CO] depth profile at each firn site from the inferred optimal history (lines in Fig. 1a and 1b). Due to mixing by diffusion, CO mixing ratio profiles in
565 firn are smoothed and the model interprets the CO variability between adjacent depth levels as noise, reflected in the uncertainty envelope. The detailed site by site comparisons of model results with firn data (Fig. S7 and S11), do not show site-specific systematic shifts that would be indicative of inconsistencies between the datasets.
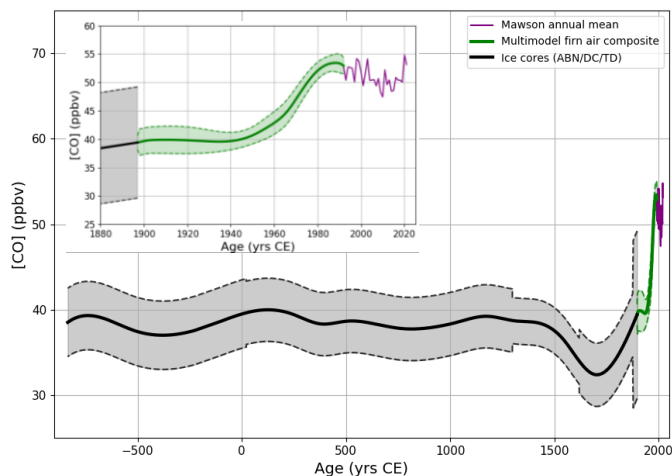
    The IGE-GIPSA atmospheric [CO] history based on firn air samples (Fig. 1e) reveals the following patterns: (i) from 1897 to 1945 CE, the record is stable overall with [CO] values remaining in the 37-44 ppbv range; (ii) from 1945 to 1985 CE, the
570 record indicates an increase in [CO] from 37-41 ppbv to 52-56 ppbv, with a mean rate of 0.4 ppbv yr^{-1}; (iii) Antarctic [CO] declines from 1985 to 2000 CE; (iii) over the 2000-2016 CE time period, [CO] slightly increases (+3 ppbv) to reach present-day levels, in agreement with direct [CO] monitoring at Mawson station. The CSIRO atmospheric [CO] record (Fig. 1f)

18

exhibits a similar pattern, but with the fast increase in [CO] starting ~5 yrs earlier. Overall, IGE-GIPSA and CSIRO reconstructions are in good agreement, always with overlapping uncertainty envelopes.

Both inversions need some degree of regularization to prevent unrealistic solutions with wildly oscillating atmospheric CO levels, as demonstrated by Rommelaere et al 1997. The two inversions use different approaches to regularisation, and this leads to different degrees of smoothing of the reconstructed atmospheric history. However it is an advantage in this study to be able to present two independent inversion methods, and their differences reflect part of the overall uncertainty. Over the period spanning 1920 to 1992, we average the IGE-GIPSA and CSIRO records' annual values to produce a multimodel firn air [CO] reconstruction. For the 1897-1920 CE period, a polynomial weight was introduced in the annual averaging of the two firn records. Such approach (Fig. S12) allowed (i) to weight the multimodel record toward the CSIRO reconstruction in 1897 CE, and (ii) to match the [CO] growth rates (ie. in ppbv yr^{-1}) of the firn and ice core reconstructions in 1897 and 1920 CE. The multimodel firn air reconstruction is shown in Fig. 3, with the envelope representing the 2σ uncertainty interval.

3.3.2. A reconstruction spanning -835 to 1897 CE from ice core data

Figure 3 reports a history of atmospheric [CO] spanning the last 3000 yr in 45-90°S latitudinal band (Sect. 3.1). Prior to 1897 CE, it is an average multisite record based on ice core continuous datasets. The DC12, ABN, and TD high resolution [CO] records reported along the age scale are merged, and a spline fit of the data from the three sites is used to define the multi-site record. Site specific uncertainties are combined, and the grey envelope reported in Fig. 3 depicts a 2σ uncertainty. The recent atmospheric [CO] history retrieved from firn air (Sect. 3.3.1) covers the period from 1897 to 1992 (Fig. 3).

19

600

Atmospheric [CO] was rather stable from -835 to 1500 CE, with mixing ratios remaining in a 30-45 ppbv range (2σ). Then, [CO] showed a decreasing trend from 38.5±2.7 ppbv in ~1500 CE to a minimum of 32.5±3.7 ppbv in ~1700 CE. After 1700

605 CE, [CO] increased until reaching a maximum of 53.6±1.6 ppbv in ~1985 CE. Over the 1700-1900 CE time period, [CO] increased at a moderate rate of 0.035 ppbv yr^{-1}. The subsequent growth rate in SH atmospheric [CO] during the latter half of the 20th century is 10-fold higher (Sect. 3.3.1) than prior to the industrial times (i.e., prior to 1850 CE).

Supprimé: concentrations

3.4. Comparison with previous ice core CO records

Figure 4 reports a comparison of our new record with [CO] datasets collected earlier from Antarctic ice cores from Vostok

610 (VST, Haan el al., 1998), D47 (Haan et al., 1996; Wang et al., 2010), and South Pole (SP, Wang et al., 2010). Error bars on the VST, D47, and SP represent 2σ uncertainties. The VST [CO] (Haan et al., 1998) which shows stable ~50 ppbv [CO] from -230 to 1370 CE, is only partially shown on Fig. 4. The D47, VST, and SP records suggest stable CO levels prior to 1400 CE, a minimum in [CO] in ~1600 CE, and an increase in [CO] to the onset of the 20th century reaching higher values than today.

20
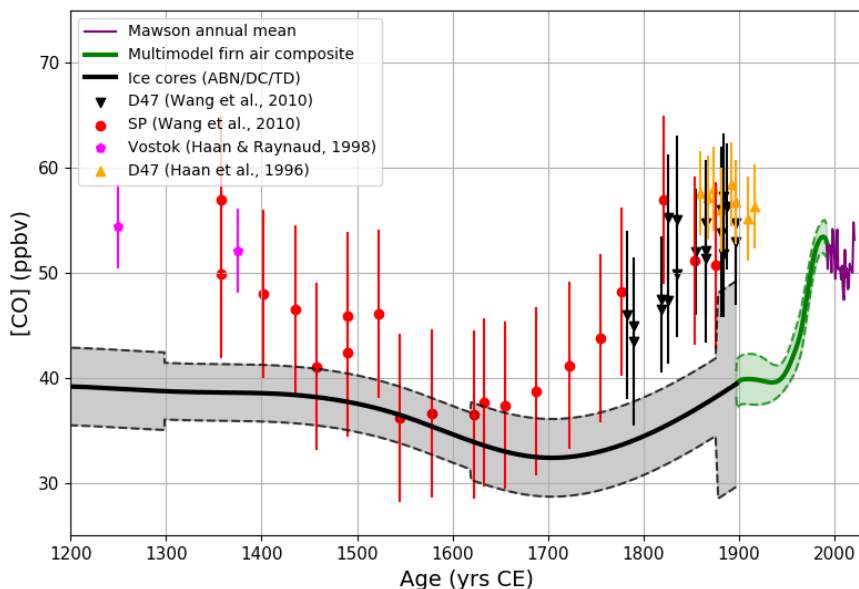
Figure 4. Comparison of the [CO] atmospheric reconstruction based on ABN, DC12, and TD ice core with previously published CO ice core datasets reported with 2σ uncertainties: South Pole (Wang et al., 2010), Vostok (Haan et al., 1998) and D47 (Haan et al., 1996; Wang et al., 2010) archives. Seven more Vostok data points are available in the time period spanning -236 to 1093 yrs CE, with [CO] ranging from 48 to 53 ppbv (Haan et al., 1998).

There are substantial differences between our new record and the published D47/VST/SP dataset. First, the D47/VST/SP dataset exhibits about 10 ppbv higher [CO] than our record prior to 1500 CE, and in the early 1900s (Fig. 4). This difference is larger than our 2σ uncertainty envelope and therefore significant. Such disagreement is puzzling: the published datasets of D47, Vostok, and South Pole agree with each other although they were measured 15 years apart in different laboratories with different analytical methods. On the other hand, our new ice record is internally consistent between the four Antarctic sites (including Solarice core, SI Sect. 2.7). Our new record also includes firn air datasets measured in three different laboratories (IGE, CSIRO, and MPI) with different methods, and unlike the earlier records, are contiguous with modern [CO] atmospheric monitoring (Fig. 4). We showed in Section 3.1 that atmospheric CO is relatively uniform over Antarctica, so these differences cannot be explained by spatial gradients between the different ice core sites.

Haan's studies report [CO] on the CSIRO94 calibration scale which is 3% lower than the CSIRO2020 scale. Wang et al. (2010) calibrated their dataset using a single 141 ppbv gas cylinder certified on the WMO-X2004 scale. The WMO-X2014 scale gives higher values by around 1 ppbv for mixing ratios lower than 200 ppbv compared to WMO-X2004 scale, including for the [CO]

21

635 range reported by Wang et al. (2010). In this study, consistent calibrations (WMO-X2014 and CSIRO2020) have been applied to all new firn air and ice core datasets. Consequently, a direct comparison of our new record with previously published CO datasets reported in Fig. 4 is possible.

Second, our [CO] record and the South Pole dataset (Wang et al., 2010) both exhibit a minimum during the LIA, but the exact timing of this minimum is different, with our record showing a minimum 100 yr later than at South Pole (i.e., ~1700 CE,

640 instead of ~1600 CE). The three ice core records in this study all exhibit a minimum in ~1700 CE, i.e. ABN, TD, and EDML-B40 (Fig. 2 and Fig S13). However, Wang et al. (2010) used SP and D47 chronologies based on the pioneering studies of Schwander and Stauffer (1984) and Barnola et al. (1995), and report uncertainties of ±100 yr (resp. ±20 yr) for the SP (resp. D47) gas dating. Such large uncertainties may explain the mismatch observed for the timing of the minimum in [CO] during the LIA, between the Wang et al. (2010) dataset and our record.

645 Third, the amplitude of the decrease in [CO] during the LIA is only 5 ppbv for the new record reported in this study, compared to a 20 ppbv amplitude observed on the South Pole ice core by Wang et al. (2010). We investigated if the ABN and TD records, which constrain in this study a 5 ppbv amplitude for the minimum in [CO] during the LIA, could smooth atmospheric signals by either analytical or gas trapping processes. The response times of the IGE and DRI CFA setup have been documented earlier (Faïn et al., 2022, and SI) and are fully able to resolve the whole amplitude of variation in [CO] observed during the LIA which

650 spans meters (e.g., 40 m along the ABN core). During the LIA, the ABN accumulation rate is lower than modern values (such as reported in Table 1), but it is similar to the South Pole accumulation rate (Servettaz et al., 2023). Thus the ABN record is not expected to be more affected by smoothing than the South Pole record during the LIA. Furthermore, we estimate that the smoothing effect from gas transport in firn and from progressive trapping in ice on the ABN or TD CO ice records is likely insignificant (SI Sect. 2.8, Fig. S16 and S17).

655 Overall, the lack of consistency between our new record and the published D47/VST/SP dataset is reminiscent of a previous study where we were not able to reconcile the Greenland [CO] Eurocore dataset of Haan and Raynaud (1998) and Haan et al. (1996) with multiple new Greenland ice core CO measurements made using both discrete and continuous analytical methods, including the PLACE ice core drilled 1km away from the Eurocore site (Faïn et al., 2022). Similarly, our Antarctic CO results call into question the accuracy of the CO values reported for the D47/VST/SP ice core. The SP/D47 CO isotopic ratios

660 published by Wang et al. (2010) could also be impacted by additional, extraneous CO and thus should be interpreted with caution.

An early Law Dome record of [CO] spanning 200-1600 CE was reported by Ferretti et al. (2005). The general pattern of the Law Dome CO record differs from both our study and the D47/VST/SP (Haan et al., 1996, Wang et al., 2010) dataset. Notably, Law Dome [CO] exhibits higher mixing ratios in the 50-90 ppbv range, with no significant decrease in [CO] during the 1400s.

665 The Law Dome [CO] data were a by-product of the methane isotopic measurements by Ferretti et al. (2005) and had significantly higher measurement uncertainty and blank corrections than the dedicated [CO] measurements reported here.

22

Supprimé: s

Supprimé: 2022

Supprimé: We could speculate as a possible explanation for the difference that the quantification of CO contamination through the different discrete methods used for the D47/VST/SP ice cores significantly underestimated the true analytical bias introduced by these methods.

3.5. Implications for pre-industrial SH fire history

In this study, we report an atmospheric history for [CO] in the SH for the last three millennia (Fig. 3). Temporal variations in atmospheric [CO] could, in theory, result from changing emissions of CO and/or changing oxidation of CO during its transport from source areas to Antarctica. Oxidation by OH is the dominant sink of CO but past levels and variations of OH are notoriously difficult to quantify. Earth system models including atmospheric chemistry schemes suggest a stable global average OH-budget from pre-industrial times to 1980 CE (Stevenson et al., 2020). Given the absence of data-based constraints on the OH budget over the last three millennia, we adopt these findings and assume that the PI [CO] variability is primarily driven by changes in emissions rather than changes in the OH sink.

This section therefore discusses the evolution of CO sources and implications for fire history for pre-industrial times. It includes discussion of other proxies of PI biomass burning in the Southern Hemisphere (Rubino et al., 2016a). Such proxies include ethane (Nicewonger et al., 2018), acetylene (Nicewonger et al., 2020a), and black carbon (Liu et al., 2021; McConnell et al., 2021) retrieved from ice cores, and charcoal in sediments (Marlon et al., 2016; Power et al., 2008). Acetylene is released from incomplete combustion processes, and it is lost in the atmosphere via reaction with the OH radical, resulting in a global mean lifetime of roughly 2–3 weeks (Burkholder et al., 2015; Xiao et al., 2007). Biomass burning has been reported as the only major source of acetylene to the pre-industrial atmosphere (Nicewonger et al., 2020a). Ethane is emitted in the modern atmosphere by the production and use of oil and natural gas, burning of biofuels and biomass, and natural geologic seeps (Etiope and Ciccioli, 2009; Helmig et al., 2016; Tzompa-Sosa et al., 2017). The major sink of atmospheric ethane is via oxidation with the OH radical resulting in a global mean lifetime of roughly 2 months (Burkholder et al., 2015; Xiao et al., 2008). Charcoal accumulation in lake or peatbog sediments has been shown to reflect biomass burning within tens of kilometers of the sampling site. Composite stratigraphies based on multiple charcoal records from lake sediments and peats have been built to infer biomass burning history (Vannière et al. 2016; Marlon et al., 2016; Power et al., 2008). Far smaller than charcoal fragments, light-absorbing black carbon (BC) aerosols are primarily emitted from fires during the pre-industrial and can be transported from the SH middle to high latitudes to Antarctica where they are deposited on snow surfaces (Bisiaux et al., 2012; Liu et al.; 2021, McConnell et al., 2021). Overall, these proxies exhibit varying atmospheric lifetimes and consequently different footprints. Stable isotopic composition of methane ($\delta^{13}CH_4$) also has been used to reconstruct the pre-industrial methane budget, including variation of its biomass burning source (Beck et al., 2018; Bock et al., 2017; Ferretti et al., 2005; Mischler et al., 2009; Sapart et al., 2012). However, the atmospheric lifetime of methane is almost 10 years making $\delta^{13}CH_4$ a proxy of global PI biomass burning.

3.5.1. Evolution of non-fire CO sources during pre-industrial times

The main sources of CO in the pre-industrial atmosphere are biomass burning and atmospheric production through the oxidation of methane and VOCs. The PI methane-oxidation source is almost constant, as a consequence of the relatively small changes in CH_4 atmospheric mixing ratio prior to 1850 (Rubino et al., 2019). Using a chemical-transport model, Wang et al.

(2010) evaluated a nearly constant contribution of the methane oxidation source to [CO] at South Pole in the 10-12 ppbv range for the period spanning 1350-1900 CE. Consequently, SH atmospheric oxidation of VOCs, along with biomass burning, likely drive the pre-industrial evolution in CO mixing ratio observed in the Antarctic record.

VOCs relevant during the PI are mainly biogenic VOCs. Little is known about past evolution of BVOC emissions in the atmosphere. Isoprene and monoterpenes constitute ~65% of the BVOCs emitted by the terrestrial biosphere (e.g., Guenther et al., 2012), and the processes driving isoprene and monoterpene emissions are complex and still not fully understood (Hantson et al., 2017, and reference therein). BVOC emissions are sensitive to climate, CO_2 mixing ratios, vegetation type and foliage density. BVOCs emissions from forests account for more than 70% of the total VOC emissions in the 1990s (Guenther et al., 1995). Pongratz et al. (2008) suggest that SH forest area had been fairly constant from 1000 to 1800 CE. Similarly, Goldewijk et al. (2017) suggests that the fraction of land impacted by anthropogenic activities increased from 2.6 to 7.3% between 0 and 1700 CE, reflecting a limited pressure of humans on natural ecosystems and forests prior to industrial times. Using two independent modeling approaches, Acosta et al. (2014) simulate the evolution and driving factors of isoprene and monoterpene emissions during the past millennium. These authors simulate limited decreases in isoprene and monoterpene emissions for the period spanning 1000 CE to 1850, with (i) global isoprene emissions decreasing from 779 TgC yr^{-1} during years 1000–1200 CE to 725 TgC yr^{-1} in 1800 CE, and (ii) a slight decrease in monoterpene emissions between the beginning of the millennium and the pre-industrial time (from 83 to 80 TgC yr^{-1} and from 25 to 24 TgC yr^{-1}, according to MEGAN and LPJ-GUESS models, respectively). They find that climate change can have short-term global effects on isoprene emissions, with e.g., a decrease in BVOC emissions during the LIA. A decrease in gross primary production and a larger decrease in ecosystem respiration was also reconstructed during the LIA using a global numerical simulation of atmospheric carbonyl sulfide (COS) mixing ratios (Rubino et al., 2016b). Considering the limited variation in atmospheric CO_2, forest coverage and natural landscape prior to 1000 CE, it is unlikely that BVOC emissions have experienced significant changes over the last 3000 yrs. Evaluating the contribution of BVOC-oxidation to the Antarctic [CO] in PI times requires CO isotope datasets (e.g., Wang et al., 2010) or a 3D chemistry transport model constrained with BVOC emission inventories (e.g., Rowlinson et al., 2021; Sect. 3.5.3). Decrease in BVOC emissions over the last millennia (Acosta et al., 2014) should in principle be reflected by a decrease in the fraction of atmospheric [CO] produced by the BVOC oxidation source, a decrease possibly enhanced during the LIA (Acosta et al., 2014). However, because such a decrease in BVOC emissions is likely limited, we conclude that atmospheric CO in the SH has not experienced large fluctuation driven by the BVOC oxidation source in PI times.

3.5.2. Evolution of the CO fire source during pre-industrial times

Our atmospheric history for [CO] in the SH for the last three millennia (Fig. 3) exhibits stable mixing ratios prior to 1500 CE, i.e. the onset of the LIA. Although some variations in [CO] exist prior to 1500 CE, they are not significant within the 2σ uncertainty envelope. Combined continuous CO measurements conducted along the ABN and TD ice cores (supported by the EDML-B40 CO dataset, Sect. SI 2.4) also reveal a decrease in [CO] in the Antarctic atmosphere from the MP to the LIA in the 1500s, with a minimum around ~1700 CE during the LIA. Such a decrease is unique over the last three millennia. These

24

patterns are very similar to the ethane and acetylene records retrieved from Antarctica ice (Nicewonger et al., 2018; Nicewonger et al., 2020a). The ethane record (Nicewonger et al., 2018; Fig. 5b) is of particular interest as both CO and ethane have similar atmospheric lifetime (~2 months in the Antarctic atmosphere).

Using a 3D chemical transport model (UCI-CTM), Nicewonger et al. (2020b) demonstrated that Antarctic ice core records of ethane and acetylene are ~~more~~ sensitive to biomass burning emissions from non-boreal regions, and primarily reflect tropical burning. Ethane and acetylene records thus suggest stable biomass burning emissions in the period spanning 1000 to 1500 CE, and a gradual decline in fire emissions from the MP to the LIA in the 1500s with the LIA as a minimum in burning. This decline is estimated to be 30-45% (resp. 50%) by the ethane (resp. acetylene) datasets (Nicewonger et al., 2018, 2020a). Our atmospheric history of Antarctic [CO] supports this finding - considering the small changes in the methane and BVOC oxidation CO sources (Sect. 3.5.1), stable fire CO emissions are required to explain the stable atmospheric [CO] retrieved from the DC12 and ABN ice cores (Fig. 3). A slight decrease in BVOC emissions during the LIA (Acosta et al., 2014) may partially explain a decrease in [CO] during that period, but a reduction in biomass burning during the LIA is also likely to be dominant contributor. Similarly to ethane, CO in the Antarctic atmosphere is likely primarily ~~sensitive~~ to fire emissions occurring at tropical latitudes.

To further investigate the tropical fire emission footprint of our SH atmospheric [CO] record, we extracted from the Global Paleofire Database (https://database.paleofire.org) two unpublished regional charcoal indexes for the intertropical latitudinal band (25°N – 25°S) and the extratropical SH (25°S – 60°S) (Fig. S18). Charcoal indexes reflect a more regional component of biomass burning relative to Antarctic CO, because of the fast deposition of charcoal particles. Our atmospheric [CO] record exhibit similarities with the tropical charcoal index (Fig. 5c), with stable burning during the MP, and a minimum in burning during the LIA followed by a sharp increase. While both the tropical charcoal index and [CO] increase simultaneously in ~1750 CE, the tropical charcoal index start declining in 1150 CE, i.e. 250 years earlier than CO, ethane and acetylene. We conclude that CO variability over Antarctica is driven by integrated fire variability occurring over a wider area, with a significant contribution from the extratropical southern hemisphere (Fig. 5d). Charcoal index integrated at the extratropical SH scale does not exhibit à decline during the LIA, in agreement with an Antarctic black carbon record from the East Antarctic Plateau which integrates fire emissions south of 40°S (McConnell et al., 2021). This stable trend, however, also masks regional variability in fire emissions driven by both climatic factors (e.g., shift in the location of the Intertropical Convergence Zone impacting precipitation patterns) and anthropogenic humans factors (e.g., new human settlements in Oceania, or the catastrophic collapse that occurred in the Americas following the European arrival after 1492; McConnell et al., 2021; Koch et al., 2019).
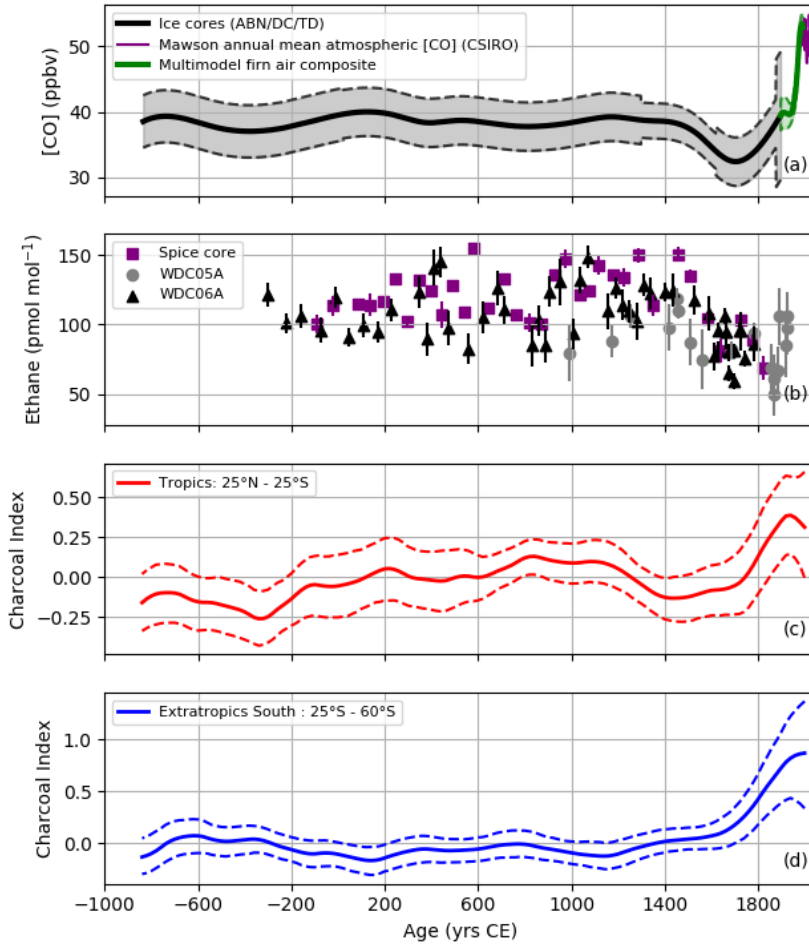
Figure 5. <u>Antarctic Ice core and firn air CO (panel a; this study), and ethane (panel b; Nicewonger et al. ,2018) records.</u> **Charcoal indexes for the** <u>intertropical 25° N, 25° S latitudinal band (panel c) and the extratropical SH 25° S – 60 °S (panel d)</u> **for the last 3000 years, extracted from the Global Paleofire Database (https://database.paleofire.org). Charcoal indexes are average Z-scores of transformed charcoal influx per region (100 yr smoothing window/1000 yr bootstrap). Dotted-line envelopes** <u>on the charcoal indexes</u> **represent the upper and lower 95% confidence intervals from the bootstrap analysis.**
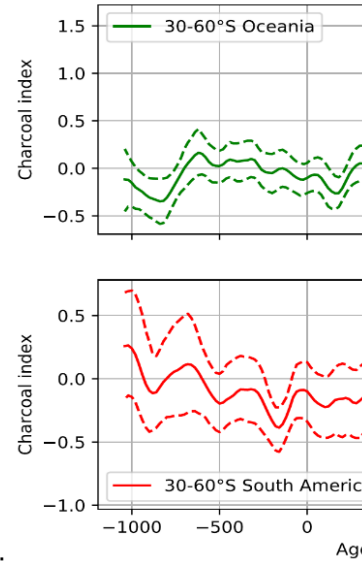
830

Finally, PI fire modeling conducted by Van der Werf et al. (2013) suggests that the contribution of fire to the Antarctic [CO] in 1400 CE was ~35% below present-day level, with the largest drop due to lower deforestation in South America in 1400 CE. This finding is in disagreement with Wang et al. (2010), who estimated that fire emissions contributed to ~30 ppbv to [CO] in the Antarctic atmosphere in 1350 CE, i.e. a contribution larger than modern fire emissions estimated at 7 ppbv (van der Werf et al., 2013). The lower [CO] levels revealed by our new CO record are thus in better agreement with the paleofire modeling of van der Werf et al. (2013), for the period prior to 1400 CE.

3.5.3. Did biomass burning peak at the onset of the industrial period?

The CO records (mixing ratios and isotopic ratios) from Wang et al. (2010) suggest that biomass burning emissions increased rapidly during the 1700s and 1800s and peaked during the late 19th century at rates roughly 3 times modern levels (defined as the 1997–2016 CE period of global satellite records of biomass burning). On the other hand there is no evidence in the three ice core hydrocarbon records (Mishler et al., 2009; Sapart et al., 2012; Nicewonger et al., 2018; 2020a), as well as in the BC Antarctic dataset (Liu et al., 2021), for such a large peak in fire emissions/activity in the late 1800s. Marlon et al. (2008) suggest that the sharp increase in the charcoal index from ~1750 CE onwards, on a global scale, may be related to the increase in human activities worldwide as a result of population growth. The decline after ~1850 CE would be associated with changes in land use on a global scale, due to more intensive practices and coupled with fire suppression.

SH biomass burning proxies are used to evaluate biogeochemical and atmospheric chemical transport models that investigate PI biomass burning rates. The output of such models is closely related to PI biomass burning emission inventories. Such inventories are still subject to debate, with contradictory hypotheses discussed. On one side, biomass burning emission inventories (such as the CMIP6 inventories) commonly scale up fire emission with population (e.g., van der Werf, 2013; van Marle et al., 2017), suggesting lower biomass burning emission in PI compared to present day. On the other side, hypothesizing a decline in burned areas with increasing population density due to land use changes (Knorr et al., 2014; Andela et al., 2017) leads to biomass burning reaching higher levels in the PI compared to present day (e.g., Hamilton et al., 2018; Liu et al., 2021, Rowlinson et al., 2021).

Hypothesizing a positive relationship between fire and population density, van der Werf et al. (2013) inferred how PI fire emissions could have contributed to [CO] in the Antarctic atmosphere. These authors find that all the SH non-forest land would have to burn annually or bi-annually to explain the Wang et al. CO levels (i.e., a 30 ppbv contribution from fires to Antarctic [CO] in 1900 CE). They conclude that such a scenario is unlikely, notably because in arid regions, not all savannas build up enough fuel each year to be able to burn annually. Murray et al. (2014) used a chemical transport model (GEOS-Chem) coupled with land cover and fire emissions from dynamic global vegetation models (BIOME4 and LPJ-LMfire) to simulate the PI atmospheric composition. They established a "low PI fire" scenario by scaling the LPJ-LMfire total dry matter consumed to

27

Supprimé: Overall, prior to the LIA, charcoal and ice core proxies (black carbon, ethane, acetylene) indicate stable biomass burning levels in the SH. Our atmospheric history of Antarctic [CO] supports this finding - considering the small changes in the methane and BVOC oxidation CO sources (Sect. 3.5.1), stable fire CO emissions are required to explain the stable atmospheric [CO] retrieved from the DC12 and ABN ice cores (Fig. 3). ¶

Supprimé: 3.5.3. Evolution of the CO fire source during the LIA¶

Supprimé: Combined continuous CO measurements conducted along the ABN and TD ice cores (supported by the EDML-B40 CO dataset, Sect. SI 2.4) reveal a decrease in [CO] in the Antarctic atmosphere over the last three millennia. A slight decrease in BVOC emissions during the LIA (Acosta et al., 2014) may partially explain this decrease in [CO], but a reduction in biomass burning during the LIA is also likely to contribute. Indeed, ethane and acetylene show the LIA as a minimum in burning, with a gradual decline in fire emissions from the MP to the LIA, in the 1500s. This decline is estimated to be 30-45% (resp. 50%) by the ethane (resp. acetylene) datasets (Nicewonger et al., 2018, 2020a). The minimum in the SP [CO] dataset (Wang et al., 2010) was attributed to a decrease in fire emission, using isotopic CO measurements. Charcoal indexes from South America and Oceania areas do not exhibit decreasing trends during the LIA (Fig. 5). However, charcoal signals can be influenced by local and small fires (e.g. caused by human activities) that can mask a regional decrease in biomass burning (e.g., driven by climatic factors). The limited number of charcoal records available also limits the interpretation of charcoal indexes as regional proxies.¶

Supprimé: 4

Supprimé: The Southern America and Oceania charcoal datasets exhibit opposite patterns at the onset of the industrial period, with increasing fires in Australia, and decreasing biomass burning in Southern America (Fig. 5). Because of such spatial heterogeneities in charcoal indexes, comparing Antarctic [CO] with a hemispheric or global charcoal index (e.g., Marlon et al., 2016) may not be relevant due to lack of documentation, high variability between sites and, finally, poor knowledge of human fire practices, which must include a complex land economy and various land use techniques.

match emissions implied by the charcoal accumulation rates from the Global Charcoal Database (Power et al., 2008, 2010; van der Werf et al., 2010). Such a "low-fire" scenario yields 35 ppbv surface total [CO] at the South Pole in 1770 CE. This value is significantly lower than the SP [CO] of 47±4 ppbv (Wang et al., 2010), but compares well with the 33.5±5.0 ppbv reconstructed in this study (Fig. 3). More recently, Rowlinson et al. (2021) simulated PI [CO] levels using the TOMCAT chemical transport model (which include BVOC chemistry) with CMIP6 fire emission inventory (van der Marle et al., 2017). Simulated Antarctic CO mixing ratios using PI CMIP6 emissions in 1750 CE are 37 ppbv, also substantially lower than the Wang et al. (2010) value of 45±5 ppbv, but similar to our CO reconstruction which exhibits 33.0±5.0 ppbv for CO mixing ratio in the Antarctic atmosphere.

The PI LMfire and PI SIMFIRE-BLAZE fire emissions inventories consider that land use changes imply a decline in burned areas with increasing population density (Hamilton et al., 2018). Similarly, Murray et al. (2014) reported a "high fire" PI fire inventory using the LMFire model and assuming decreases in passive fire suppression (due to less fragmentation in the landscape and reduced live-stock grazing) and the absence of active fire suppression. These three inventories lead to biomass burning reaching higher levels in the PI compared to present days (Hamilton et al., 2018; Liu et al., 2021; Murray et al., 2014), and substantially larger than the PI CMIP6 emissions. Notably, Liu et al. (2021) concluded that fire emissions remained relatively stable in the SH between 1750 CE and ~1920 CE followed by a 30% decrease until about 1990 CE. This conclusion is supported by a comparison of simulated black carbon (BC) deposition fluxes with BC measurement conducted on an array of ice cores (14 Antarctica records, and one record from the Andes). When using SIMFIRE-BLAZE and LMfire emissions, Antarctic [CO] in 1750 CE are estimated at 48 and 61 ppbv, respectively (Rowlinson et al., 2021). The "high fire" inventory reported by Murray et al. (2014) also yields elevated [CO] in the Antarctic atmosphere, with PI mixing ratios reaching 63 ppbv in 1770 CE. Such values are significantly larger than our continuous [CO] ice-core record (Fig. 3).

Large uncertainty remains about PI SH biomass burning, with implications for our understanding of the magnitude of the historical radiative forcing due to anthropogenic aerosol emissions (e.g., Hamilton et al., 2018). All fire inventories discussed previously fall within the current uncertainty range for fire emissions (Pan et al., 2020). Although simulating larger PI fire emissions, Hamilton et al. (2018) could not reproduce the enhancement in PI CO emissions from fires reported by Wang et al. (2010), and Liu et al. (2021) do not report a maximum in fire emission in the SH at the onset of the 20th century. The trend and levels of SP/D47 CO SH record (Fig. 3, Wang et al., 2010) are often difficult to reconcile with fire modeling. Our new SH [CO] atmospheric reconstruction, which does not exhibit a maximum in the late 19th century, is in agreement with paleofire proxies such as acetylene, ethane, methane isotope or BC retrieved from Antarctic ice cores (Nicewonger 2018; 2020a; Sapart 2012, Mischler et al. ,2009; Liu et al., 2021), and can bring new constraints on paleofire simulations.

3.6. Increase in SH atmospheric [CO] during the industrial era

Our multimodel atmospheric record based on firn air samples reveals rather stable [CO] from 1900 to 1945 CE, followed by an increase in [CO] from 40.0±1.5 to 53.5±1.5 during the period spanning 1945 to 1987 CE (Fig. 3). This period exhibits the

28

Supprimé: concentration

Supprimé: is

Supprimé: ,

Supprimé: concentrations

Supprimé: There again, a possible analytical bias in the estimate of CO contamination by the discrete measurements conducted by Wang et al., 2010, could explain the discrepancy.

highest atmospheric [CO] growth rate in SH atmospheric [CO] record over the last three millennia, with a mean rate of 0.32 ppbv yr^{-1}. Antarctic [CO] declined slightly over the period 1988 – 1992 CE (firn air reconstruction). From 1993 to 2021 CE, the Mawson [CO] record shows inter-annual variability reaching 5 ppbv, but remains below 53.5 ppbv when such inter-annual variability is smoothed out with a 5 yrs running windows. Our record thus suggests that the late 80s are a maximum in atmospheric [CO] over the last three millennia.

During the industrial era, the atmospheric Antarctic [CO] can be interestingly compared with the [CO] record extracted from Greenland archives. By analyzing [CO] depth profiles collected from firn air at three different Greenland sites (NGRIP, Summit, and NEEM), Petrenko et al. (2013) obtained a reconstruction of atmospheric [CO] spanning 1950-2010 CE. This reconstruction has been recently extended back to 1700 CE with the CFA analysis of 4 different Greenland ice cores (NGRIP, PLACE, NEEM, and D4) (Faïn et al., 2022). Faïn et al. (2022) could not fully exclude the possibility that the Greenland ice archive CO reconstruction could be slightly positively biased by chemical processes (in situ production) occurring within the Greenland ice. Therefore, the atmospheric [CO] history extracted from Greenland should be considered as an upper bound of the past [CO] abundance in the Arctic (Faïn et al., 2022). The Greenland firn air reconstructed history suggests that Arctic [CO] in 1950 CE was 140–150 ppbv, rose by 10–15 ppbv from 1950 CE to the 1970s, and peaked in the early 1980s before a ~30 ppbv decline to today's levels. Consequently, atmospheric [CO] exhibits a maximum in the 1980s at the global scale, with [CO] levels about 3 fold higher in the NH. However, the increasing trend in atmospheric [CO] prior to the 1980s maximum differs among hemisphere, with [CO] starting to increase in the late 1800s in the NH and in 1945 CE in the SH.

Changes in CO over the past century would be the net result of several possible factors: direct emissions from natural and anthropogenic sources, biomass burning, chemical loss of CO by OH-oxidation partly offset by CO production from the oxidation of CH_4 and other hydrocarbons by OH.

The peak in CO in our SH record and subsequent decrease from the 1980s has similar timing to that found in the NH firn and ice core measurements (Petrenko et al., 2013; Faïn et al., 2022). The NH decrease was attributed to reduced anthropogenic emissions, resulting from improved fossil fuel combustion efficiency and pollution controls in the transport sector through the use of catalytic converters (Wang et al., 2012). Reduced CO emissions from transport are also found for this time in inventory emissions estimates (Hoesly et al., 2018) and, together with biomass burning reductions, attributed to the continued decrease in global [CO] since 2000 inferred from inverse modelling (Zheng et al., 2019). The [CO] peak and the subsequent decrease in the SH is less pronounced than in the NH, despite the age resolution of our Antarctic firn air record that would record rapid atmospheric changes with minimal smoothing. This implies that emissions from sources that are more concentrated in the NH, likely anthropogenic and fossil fuel emissions, also contributed to the peak and subsequent decrease of CO in the SH.

Atmospheric surface [CO] simulated by state of the art global chemistry-climate models (e.g., Collins et al., 2017) is required to better understand the roles of CO source variations and coupled CO-OH-CH_4 chemistry for the period spanning 1850 to present. Because emissions from anthropogenic, biomass burning and chemical sources and CO loss by oxidation have different relative contributions in the high latitude SH and NH, we would expect the Antarctic and Arctic CO reconstructions

29

to provide valuable modeling constraints. A modeling study for the industrial period is beyond the scope of the present work but is underway for a future paper.

4. Summary and Conclusions

990 We have produced a firn air record of past atmospheric CO mixing ratio for the high SH latitudes based on 7 different Antarctic firn air sites (Berkner, DE08-2, DSSW20K, DSSW19K, Lock-In, South Pole, and ABN) for the period covering 1897-2016 CE. The quality of this firn air record is supported by the good agreement with direct atmospheric measurements of [CO] at Mawson Station from 1992 CE, which extends the record to 2021. New continuous profiles of [CO] have been measured covering the past 3 millennia by coupling ice core melter systems with online measurements (SARA spectrometer) along three

995 Antarctic ice cores (DC12, ABN, and TaldIce archives), with supplementary data from the EDML-B40 and Solarice cores. None of the Antarctic records revealed high and variable concentrations that were previously observed in Greenland ice cores and interpreted as in situ CO production (Faïn et al., 2014; 2022). We calculated a multisite average ice core record, extending the firn air history of [CO] in the Antarctic atmosphere to -835 CE.

Our reconstruction of past atmospheric [CO] at the southern latitudes reveals (i) stable levels prior to 1500 CE at levels of

1000 about 40 ppbv, (ii) a ~5 ppbv decrease between the medieval period and the LIA, and (iii) a progressive increase from a minimum of 32.5±3.7 ppbv in ~1700 CE to near present-day levels of 53.6±1.6 ppbv by 1985 CE. This trend relies on an excellent agreement between 10 firn air and ice core [CO] records and is contiguous with modern [CO] atmospheric monitoring. Our new CO record exhibits substantial differences with the CO data from the D47, South Pole, and Vostok ice cores (Haan et al., 1996; 1998; Wang et al., 2010): the CO record reported in this study exhibits overall lower levels (e.g., ~10

1005 ppbv lower prior to 1400 CE), a minimum during the LIA occurring about 100 yrs later, and no maximum in [CO] in the late 1800s. Our new [CO] record is in agreement with other ice core SH biomass burning proxies such as ethane or acetylene (e.g., Nicewonger et al., 2018; 2020a) and fire modeling (e.g., van der Werf 2013, Hamilton et al., 2018) that do not reproduce a large biomass burning in the SH at the onset of the 20th century.

Overall, large uncertainties remain on pre-industrial fire history (Nicewonger et al., 2020b), with implication on the PI to

1010 modern evolution in aerosol radiative forcing (Hamilton et al., 2018). Nicewonger et al. (2020b) used chemical-transport models to investigate if a single global burning history could be extracted from the three hydrocarbon ice core records. They could not find a consistent fire history even assuming unrealistic changes in spatial distribution of fire and biomes.

These ice-core, firn and atmospheric [CO] measurements, spanning -835-2021 CE, provide a benchmark record of past variations in the high southern latitude [CO] for future atmospheric chemistry model studies. Since the early 20th century,

1015 industrial activities have impacted biogeochemistry resulting in large CO changes (Szopa et al., 2021). Rapid growth in [CO] from the mid 1900s was likely due to combustion sources and the indirect CO production from atmospheric CH_4 oxidation.

30

Supprimé: four

Supprimé: , and EDML-B40

Supprimé: ten

Disentangling the roles of these sources and possible changes in the OH sink in this [CO] growth and the subsequent [CO] decrease over the past 3 decades involves understanding of the coupled CO-OH-CH$_4$ system. A natural extension of this work will be the comparison of our ice and firn-based atmospheric [CO] reconstruction for the period covering 1850 to present with model outputs from the AerChemMIP exercise (Collins et al., 2017).

Supprimé: The following datasets will be accessible on PANGAEA:

Supplement. A supplement related to this article is available

References

Acosta Navarro, J. C., Smolander, S., Struthers, H., Zorita, E., Ekman, A. M. L., Kaplan, J. O., Guenther, A., Arneth, A. and
Riipinen, I.: Global emissions of terpenoid VOCs from terrestrial vegetation in the last millennium, J. Geophys. Res. Atmos.,
119(11), 6867–6885, doi:10.1002/2013JD021238, 2014.

Allan, D. W.: Statistics of atomic frequency standards, Proc. IEEE, 54(2), 221–230, doi:10.1109/PROC.1966.4634, 1966.

Andela, N., Morton, D. C., Giglio, L., Chen, Y., van der Werf, G. R., Kasibhatla, P. S., DeFries, R. S., Collatz, G. J., Hantson,
S., Kloster, S., Bachelet, D., Forrest, M., Lasslop, G., Li, F., Mangeon, S., Melton, J. R., Yue, C. and Randerson, J. T.: A
human-driven decline in global burned area, Science, 356(6345), 1356–1362, doi:10.1126/science.aal4108, 2017.

Archibald, S., Lehmann, C. E. R., Belcher, C. M., Bond, W. J., Bradstock, R. A., Daniau, A. L., Dexter, K. G., Forrestel, E.
J., Greve, M., He, T., Higgins, S. I., Hoffmann, W. A., Lamont, B. B., McGlinn, D. J., Moncrieff, G. R., Osborne, C. P., Pausas,
J. G., Price, O., Ripley, B. S., Rogers, B. M., Schwilk, D. W., Simon, M. F., Turetsky, M. R., Van Der Werf, G. R., and Zanne,
A.: Biological and geophysical feedbacks with fire in the Earth system. Environ. Res. Lett., 13, 033003,
https://doi.org/10.1088/1748-9326/aa9ead, 2018.

Assonov, S. S., Brenninkmeijer, C. A. M., Jockel, P. J., Mulvaney, R., Bernard, S. and Chappellaz, J.: Evidence for a CO
increase in the SH during the 20th century based on firn air samples from Berkner Island, Antarctica, Atmos. Chem. Phys., 7,
295–308, 2007.

Barnola, J. M., Anklin, M., Porcheron, J., Raynaud, D., Schwander, J. and Stauffer, B.: CO2 evolution during the last
millennium as recorded by Antarctic and Greenland ice, Tellus, 47B, 264–272, 1995.

Bisiaux, M. M., Edwards, R., McConnell, J. R., Curran, M. A. J., Ommen, T. D. Van, Smith, A. M., Neumann, T. A., Pasteris, D. R., Penner, J. E. and Taylor, K.: Changes in black carbon deposition to Antarctica from two high-resolution ice core records , 1850 – 2000 AD, Atmos. Chem. Phys., 12, 4107–4115, doi:10.5194/acp-12-4107-2012, 2012.

Battle, M. O., Bender, M., Sowers, T., Tans, P. P., Butler, J. H., Elkins, J. W., Ellis, J. T., Conway, T., Zhang, N., Lang, P. and Clarke, A. D.: Atmospheric gas concentrations over the past century measured in air from firn at the South Pole, Nature, 383, 231–235, 1996.

Beck, J., Bock, M., Schmitt, J., Seth, B., Blunier, T. and Fischer, H.: Bipolar carbon and hydrogen isotope constraints on the Holocene methane budget, Biogeosciences, 15(23), 7155–7175, doi:10.5194/bg-15-7155-2018, 2018.

Bock, M., Schmitt, J., Beck, J., Seth, B., Chappellaz, J. and Fischer, H.: Glacial/interglacial wetland, biomass burning, and geologic methane emissions constrained by dual stable isotopic CH_4 ice core records., Proc. Natl. Acad. Sci. U. S. A., 114(29), 2017.

Bond, W. J. and Keeley, J. E.: Fire as a global "herbivore": the ecology and evolution of flammable ecosystems, Trends Ecol. Evol., 20(7), 387–94, doi:10.1016/j.tree.2005.04.025, 2005.

Bowman, D. M. J. S., Balch, J. K., Artaxo, P., Bond, W. J., Carlson, J. M., Cochrane, M. A., D'Antonio, C. M., DeFries, R. S., Doyle, J. C., Harrison, S. P., Johnston, F. H., Keeley, J. E., Krawchuk, M. A., Kull, C. A., Marston, J. B., Moritz, M. A., Prentice, I. C., Roos, C. I., Scott, A. C., Swetnam, T. W., van der Werf, G. R., and Pyne, S. J.: Fire in the Earth System, Science, 324, 481–484, https://doi.org/10.1126/science.1163886, 2009.

Brenninkmeijer, C. A. M., Koeppel, C., Rockmann, T., Scharffe, D. S., Braunlich, M. and Gros, V.: Absolute measurement of the abundance of atmospheric carbon monoxide, J. Geophys. Res., 106, 3–10, 2001.

Buizert, C., Martinerie, P., Petrenko, V. V., Severinghaus, J. P., Trudinger, C. M., Witrant, E., Rosen, J. L., Orsi, A., Rubino, M., Etheridge, D. M., Steele, L. P., Hogan, C., Laube, J. C., Sturges, W. T., Levchenko, V. A., Smith, A. M., Levin, I., Conway, T. J., Dlugokencky, E. J., Lang, P. M., Kawamura, K., Jenk, T. M., White, J. W. C., Sowers, T., Schwander, J. and Blunier, T.: Gas transport in firn: multiple-tracer characterisation and model intercomparison for NEEM, Northern Greenland, Atmos. Chem. Phys., 12(9), 4259–4277, doi:10.5194/acp-12-4259-2012, 2012.

Burkholder, J. B., Sander, S. P., Abbatt, J., Barker, J. R., Huie, R. E., Kolb, C. E., et al. (2015). Chemical kinetics and photochemical data for use in atmospheric studies evaluation no. 18. Pasadena: JPL publication 15-10, jet Propulsion Laboratory. https://jpldataeval.jpl.nasa.gov.

Butler, J. H., Montzka S. A., Battle M., Clarke A. D., Mondeel D. J., Lind J. A., Hall B. D., and Elkins J. W.: Collection and analysis of firn air from the South Pole, Abstract A51F-0145 presented at 2001 Fall Meeting, San Francisco (CA, USA), AGU, 2001.

Collins, W. J., Lamarque, J.-F., Schulz, M., Boucher, O., Eyring, V., Hegglin, M. I., Maycock, A., Myhre, G., Prather, M., Shindell, D. and Smith, S. J.: AerChemMIP: quantifying the effects of chemistry and aerosols in CMIP6, Geosci. Model Dev., 10(2), 585–607, doi:10.5194/gmd-10-585-2017, 2017.

Supprimé: 8

33

Conte, L., Szopa, S., Séférian, R. and Bopp, L.: The oceanic cycle of carbon monoxide and its emissions to the atmosphere, Biogeosciences, 16(4), 881–902, doi:10.5194/bg-16-881-2019, 2019.

1120 Crutzen, P. J.: A discussion of the chemistry of some minor constituents in the stratosphere and troposphere, Pure Appl. Geophys., 106–108(1), 1385–1399, doi:10.1007/BF00881092, 1973.

Dlugokencky, E. J., Nisbet, E. G., Fisher, R. and Lowry, D.: Global atmospheric methane: budget, changes and dangers, Philos. Trans. A. Math. Phys. Eng. Sci., 369(1943), 2058–72, doi:10.1098/rsta.2010.0341, 2011.

Duncan, B., Logan, J. A., Bey, I., Megretskaia, I. A., Yantosca, R. M., Novelli, P. C., Jones, N. B. and Rinsland, C. P.: Global

1125 budget of CO, 1988-1997: Source estimates and validation with a global model, J. Geophys. Res., 112(D22), doi:10.1029/2007jd008459, 2007.

Etiope, G. and Ciccioli, P.: Earth's Degassing: A Missing Ethane and Propane Source, Science (80-.)., 323(5913), 478–478, doi:10.1126/science.1165904, 2009.

Etheridge, D. M., Steele, L. P., Langenfelds, R. L., Francey, R. J., Barnola, J. M. and Morgan, V. I.: Natural and anthropogenic

1130 changes in atmospheric CO_2 over the last 1000 years from air in Antarctic ice and firn, J. Geophys. Res., 101(D2), 4115–4128, 1996.

Fabre, A., Barnola, J. M., Arnaud, L. and Chappellaz, J.: Determination of gas diffusivity in polar firn: comparison between experimental measurements and inverse modeling, Geophys. Res. Lett., 27(4), 557–560, 2000.

Faïn, X., Chappellaz, J., Rhodes, R. H., Stowasser, C., Blunier, T., McConnell, J. R., Brook, E. J., Preunkert, S., Legrand, M.,

1135 Debois, T. and Romanini, D.: High resolution measurements of carbon monoxide along a late Holocene Greenland ice core: evidence for in situ production, Clim. Past, 10(3), 987–1000, doi:10.5194/cp-10-987-2014, 2014.

Faïn, X., Rhodes, R. H., Place, P., Petrenko, V. V., Fourteau, K., Chellman, N., Crosier, E., McConnell, J. R., Brook, E. J., Blunier, T., Legrand, M. and Chappellaz, J.: Northern Hemisphere atmospheric history of carbon monoxide since preindustrial times reconstructed from multiple Greenland ice cores, Clim. Past, 18(3), 631–647, doi:10.5194/cp-18-631-2022, 2022.

1140 Ferretti, D. F., Miller, J. B., White, J. W. C., Etheridge, D. M., Lassey, K. R., Lowe, D. C., Meure, C. M. M., Dreier, M. F., Trudinger, C. M., van Ommen, T. D. and Langenfelds, R. L.: Unexpected changes to the global methane budget over the past 2000 years, Science (80-.)., 309(5741), 1714–1717, doi:10.1126/science.1115193, 2005.

Fourteau, K., Martinerie, P., Faïn, X., Schaller, C. F., Tuckwell, R. J., Löwe, H., Arnaud, L., Magand, O., Thomas, E. R., Freitag, J., Mulvaney, R., Schneebeli, M. and Lipenkov, V. Y.: Multi-tracer study of gas trapping in an East Antarctic ice core,

1145 Cryosph., 13(12), 3383–3403, doi:10.5194/tc-13-3383-2019, 2019.

Fourteau, K., Martinerie, P., Faïn, X., Ekaykin, A. A., Chappellaz, J. and Lipenkov, V.: Estimation of gas record alteration in very low-accumulation ice cores, Clim. Past, 16(2), 503–522, doi:10.5194/cp-16-503-2020, 2020.

Frezzotti, M., Urbini, S., Proposito, M., Scarchilli, C. and Gandolfi, S.: Spatial and temporal variability of surface mass balance near Talos Dome, East Antarctica, J. Geophys. Res. Earth Surf., doi:10.1029/2006JF000638, 2007.

1150 Gautier, E., Savarino, J., Erbland, J., Lanciki, A. and Possenti, P.: Variability of sulfate signal in ice core records based on five replicate cores, Clim. Past, 12(1), 103–113, doi:10.5194/cp-12-103-2016, 2016.

34

Guenther, A., Hewitt, C. N., Erickson, D., Fall, R., Geron, C., Graedel, T., Harley, P., Klinger, L., Lerdau, M., Mckay, W. A., Pierce, T., Scholes, B., Steinbrecher, R., Tallamraju, R., Taylor, J. and Zimmerman, P.: A global model of natural volatile organic compound emissions, J. Geophys. Res., 100(D5), 8873, doi:10.1029/94JD02950, 1995.

1155 Guenther, A. B., Jiang, X., Heald, C. L., Sakulyanontvittaya, T., Duhl, T., Emmons, L. K. and Wang, X.: The Model of Emissions of Gases and Aerosols from Nature version 2.1 (MEGAN2.1): an extended and updated framework for modeling biogenic emissions, Geosci. Model Dev., 5(6), 1471–1492, doi:10.5194/gmd-5-1471-2012, 2012.

Goldewijk, K. K., Beusen, A., Doelman, J. and Stehfest, E.: Anthropogenic land use estimates for the Holocene – HYDE 3.2, Earth Syst. Sci. Data, 9(2), 927–953, doi:10.5194/essd-9-927-2017, 2017.

1160 Haan, D., Martinerie, P. and Raynaud, D.: Ice core data of atmospheric carbon monoxide over Antarctica and Greenland during the last 200 years, Geophys. Res. Lett., 23(17), 2235–2238, 1996.

Haan, D. and Raynaud, D.: Ice core record of CO variations during the last two millennia: atmospheric implications and chemical interactions within the Greenland ice, Tellus Ser. B-Chemical Phys. Meteorol., 50(3), 253–262, 1998.

Hamilton, D. S., Hantson, S., Scott, C. E., Kaplan, J. O., Pringle, K. J., Nieradzik, L. P., Rap, A., Folberth, G. A., Spracklen,
1165 D. V. and Carslaw, K. S.: Reassessment of pre-industrial fire emissions strongly affects anthropogenic aerosol forcing, Nat. Commun., 9(1), 3182, doi:10.1038/s41467-018-05592-9, 2018.

Hantson, S., Knorr, W., Schurgers, G., Pugh, T. A. M. and Arneth, A.: Global isoprene and monoterpene emissions under changing climate, vegetation, CO_2 and land use, Atmos. Environ., 155, 35–45, doi:10.1016/j.atmosenv.2017.02.010, 2017.

Helmig, D., Petrenko, V. V., Martinerie, P., Witrant, E., Röckmann, T., Zuiderweg, A., Holzinger, R., Hueber, J., Thompson,
1170 C., White, J. W. C., Sturges, W. T., Baker, A., Blunier, T., Etheridge, D. M., Rubino, M. and Tans, P.: Reconstruction of Northern Hemisphere 1950–2010 atmospheric non-methane hydrocarbons, Atmos. Chem. Phys., 14(3), 1463–1483, doi:10.5194/acp-14-1463-2014, 2014.

Hoesly, R. M., Smith, S. J., Feng, L., Klimont, Z., Janssens-Maenhout, G., Pitkanen, T., Seibert, J. J., Vu, L., Andres, R. J., Bolt, R. M., Bond, T. C., Dawidowski, L., Kholod, N., Kurokawa, J., Li, M., Liu, L., Lu, Z., Moura, M. C. P.,
1175 O&apos;Rourke, P. R. and Zhang, Q.: Historical (1750–2014) anthropogenic emissions of reactive gases and aerosols from the Community Emissions Data System (CEDS), Geosci. Model Dev., 11(1), 369–408, doi:10.5194/gmd-11-369-2018, 2018.

Khalil, M. A. ., Pinto, J. . and Shearer, M. .: Atmospheric carbon monoxide, Chemosph. - Glob. Chang. Sci., 1(1–3), ix–xi, doi:10.1016/S1465-9972(99)00053-7, 1999.

1180 Knorr, W., Kaminski, T., Arneth, A. and Weber, U.: Impact of human population density on fire frequency at the global scale, Biogeosciences, 11(4), 1085–1102, doi:10.5194/bg-11-1085-2014, 2014.

Koch, A., Brierley, C., Maslin, M. M. and Lewis, S. L.: Earth system impacts of the European arrival and Great Dying in the Americas after 1492, Quat. Sci. Rev., 207, 13–36, doi:10.1016/J.QUASCIREV.2018.12.004, 2019.

Lamarque, J.-F., Shindell, D. T., Josse, B., Young, P. J., Cionni, I., Eyring, V., Bergmann, D., Cameron-Smith, P., Collins, W.
1185 J., Doherty, R., Dalsoren, S., Faluvegi, G., Folberth, G., Ghan, S. J., Horowitz, L. W., Lee, Y. H., MacKenzie, I. a., Nagashima,

35

Déplacé vers le bas [1]: Laube, J. C., Mohd Hanif, N., Martinerie, P., Gallacher, E., Fraser, P. J., Langenfelds, R., Brenninkmeijer, C. A. M., Schwander, J., Witrant, E., Wang, J.-L., Ou-Yang, C.-F., Gooch, L. J., Reeves, C. E., Sturges, W. T. and Oram, D. E.: Tropospheric observations of CFC-114 and CFC-114a with a focus on long-term trends and emissions, Atmos. Chem. Phys., 16(23), 15347–15358, doi:10.5194/acp-16-15347-2016, 2016.

T., Naik, V., Plummer, D., Righi, M., Rumbold, S. T., Schulz, M., Skeie, R. B., Stevenson, D. S., Strode, S., Sudo, K., Szopa, S., Voulgarakis, a. and Zeng, G.: The Atmospheric Chemistry and Climate Model Intercomparison Project (ACCMIP): overview and description of models, simulations and climate diagnostics, Geosci. Model Dev., 6(1), 179–206, doi:10.5194/gmd-6-179-2013, 2013.

Langenfelds, R. L., Guerette E-A., Steele L. P., Krummel P. B., Spencer D. A., Loh Z. M., Gregory R. L., Thornton D. P., Howden R. T. and Fraser P. J.: Atmospheric methane, carbon dioxide, carbon monoxide, hydrogen and nitrous oxide from Cape Grim flask samples analysed by gas chromatography, in Baseline Atmospheric Program (Australia), 2014-16, R. Langenfelds, N. Derek and S. L. Cleland (eds.), Bureau of Meteorology and CSIRO Environment, Melbourne, Australia, 2023.

Laube, J. C., Mohd Hanif, N., Martinerie, P., Gallacher, E., Fraser, P. J., Langenfelds, R., Brenninkmeijer, C. A. M., Schwander, J., Witrant, E., Wang, J.-L., Ou-Yang, C.-F., Gooch, L. J., Reeves, C. E., Sturges, W. T. and Oram, D. E.: Tropospheric observations of CFC-114 and CFC-114a with a focus on long-term trends and emissions, Atmos. Chem. Phys., 16(23), 15347–15358, doi:10.5194/acp-16-15347-2016, 2016.

Loh, Z., Langenfelds, R. and Krummel, P.: Atmospheric CO at Casey by Commonwealth Scientific and Industrial Research Organisation, dataset published as CO_CYA_surface-flask_CSIRO_data1 at WDCGG, ver.2021-04-08-1004, https://doi.org/10.50849/WDCGG_0016-7004-3001-01-02-9999, 2021a.

Loh, Z., Langenfelds, R. and Krummel, P.: Atmospheric CO at South Pole by Commonwealth Scientific and Industrial Research Organisation, dataset published as CO_SPO_surface-flask_CSIRO_data1 at WDCGG, ver.2021-04-08-1004, https://doi.org/10.50849/WDCGG_0016-7011-3001-01-02-9999, 2021b.

Loh, Z., Langenfelds, R. and Krummel, P.: Atmospheric CO at Mawson by Commonwealth Scientific and Industrial Research Organisation, dataset published as CO_MAA_surface-flask_CSIRO_data1 at WDCGG, ver.2021-04-08-1004, https://doi.org/10.50849/WDCGG_0016-7005-3001-01-02-9999, 2021c.

Legrand, M., McConnell, J. R., Fischer, H., Wolff, E. W., Preunkert, S., Arienzo, M. M., Chellman, N., Leuenberger, D., Maselli, O. J., Place, P., Sigl, M., Schupbach, S. and Flannigan, M.: Boreal fire records in Northern Hemisphere ice cores: A review, Clim. Past, 12(10), 2033–2059, doi:10.5194/cp-12-2033-2016, 2016.

Lelieveld, J., Gromov, S., Pozzer, A. and Taraborrelli, D.: Global tropospheric hydroxyl distribution, budget and reactivity, Atmos. Chem. Phys., 16(19), 12477–12493, doi:10.5194/acp-16-12477-2016, 2016.

Liu, P., Kaplan, J. O., Mickley, L. J., Li, Y., Chellman, N. J., Arienzo, M. M., Kodros, J. K., Pierce, J. R., Sigl, M., Freitag, J., Mulvaney, R., Curran, M. A. J. and Mcconnell, J. R.: Improved estimates of preindustrial biomass burning reduce the magnitude of aerosol climate forcing in the Southern Hemisphere, Science Advance, 2021.

Lukas, M. A.: Strong robust generalized cross-validation for choosing the regularization parameter, Inverse Probl., 24(3), 034006, doi:10.1088/0266-5611/24/3/034006, 2008.

Marlon, J. R., Bartlein, P. J., Carcaillet, C., Gavin, D. G., Harrison, S. P., Higuera, P. E., Joos, F., Power, M. J. and Prentice, I. C.: Climate and human influences on global biomass burning over the past two millennia, Nat. Geosci., 1(10), 697–702, doi:10.1038/ngeo313, 2008.

Déplacé (insertion) [1]

36

Marlon, J. R., Bartlein, P. J., Daniau, A.-L., Harrison, S. P., Maezumi, S. Y., Power, M. J., Tinner, W. and Vannière, B.: Global biomass burning : a synthesis and review of Holocene paleo fire records and their controls, Quat. Sci. Rev., 65, 5–25, 2013

Marlon, J. R., Kelly, R., Daniau, A.-L., Vannière, B., Power, M. J., Bartlein, P., Higuera, P., Blarquez, O., Brewer, S., Brücher, T., Feurdean, A., Romera, G. G., Iglesias, V., Maezumi, S. Y., Magi, B., Courtney Mustaphi, C. J. and Zhihai, T.: Reconstructions of biomass burning from sediment-charcoal records to improve data–model comparisons, Biogeosciences, 2016.

McConnell, J. R., Chellman, N. J., Mulvaney, R., Eckhardt, S., Stohl, A., Plunkett, G., Kipfstuhl, S., Freitag, J., Isaksson, E., Gleason, K. E., Brugger, S. O., McWethy, D. B., Abram, N. J., Liu, P. and Aristarain, A. J.: Hemispheric black carbon increase after the 13th-century Māori arrival in New Zealand, Nature, 598(7879), 82–85, doi:10.1038/s41586-021-03858-9, 2021.

Mischler, J. A., Sowers, T. A., Alley, R. B., Battle, M., McConnell, J. R., Mitchell, L. E., Popp, T., Sofen, E. and Spencer, M. K.: Carbon and hydrogen isotopic composition of methane over the last 1000 years, Global Biogeochem. Cycles, 23(4), 2009.

Morville, J., Kassi, S., Chenevier, M. and Romanini, D.: Fast, low-noise, mode-by-mode, cavity-enhanced absorption spectroscopy by diode-laser self-locking, Appl. Phys. B-Lasers Opt., 80(8), 1027–1038, doi:10.1007/s00340-005-1828-z, 2005.

Mulvaney, R., Oerter, H., Peel, D. A., Graf, W., Arrowsmith, C., Pasteur, E. C., Knight, B., Littot, G. C. and Miners, W. D.: 1000 year ice-core records from Berkner Island, Antarctica, Ann. Glaciol., 35, 45–51, doi:10.3189/172756402781817176, 2002.

Murray, L. T., Mickley, L. J., Kaplan, J. O., Sofen, E. D., Pfeiffer, M. and Alexander, B.: Factors controlling variability in the oxidative capacity of the troposphere since the Last Glacial Maximum, Atmos. Chem. Phys., 14(7), 3589–3622, doi:10.5194/acp-14-3589-2014, 2014.

Nicewonger, M. R., Aydin, M., Prather, M. J. and Saltzman, E. S.: Large changes in biomass burning over the last millennium inferred from paleoatmospheric ethane in polar ice cores, Proc. Natl. Acad. Sci., 201807172, doi:10.1073/pnas.1807172115, 2018.

Nicewonger, M. R., Aydin, M., Prather, M. J. and Saltzman, E. S.: Reconstruction of paleofire emissions over the past millennium from measurements of ice core acetylene, Geophys. Res. Lett., 47(3), doi:10.1029/2019GL085101, 2020a.

Nicewonger, M. R., Aydin, M., Prather, M. J. and Saltzman, E. S.: Extracting a history of global fire emissions for the past millennium from ice core records of acetylene, Ethane, and Methane, J. Geophys. Res. Atmos., 125(20), doi:10.1029/2020JD032932, 2020b.

Pan, X., Ichoku, C., Chin, M., Bian, H., Darmenov, A., Colarco, P., Ellison, L., Kucsera, T., da Silva, A., Wang, J., Oda, T. and Cui, G.: Six global biomass burning emission datasets: intercomparison and application in one global aerosol model, Atmos. Chem. Phys., 20(2), 969–994, doi:10.5194/acp-20-969-2020, 2020.

Petrenko, V. V., Martinerie, P., Novelli, P. C., Etheridge, D. M., Levin, I., Wang, Z., Blunier, T., Chappellaz, J., Kaiser, J., Lang, P., Steele, L. P., Hammer, S., Mak, J., Langenfelds, R. L., Schwander, J., Severinghaus, J. P., Witrant, E., Petron, G., Battle, M. O., Forster, G., Sturges, W. T., Lamarque, J.-F., Steffen, K. and White, J. W. C.: A 60 yr record of atmospheric

37

carbon monoxide reconstructed from Greenland firn air, Atmos. Chem. Phys., 13(15), 7567–7585, doi:10.5194/acp-13-7567-2013, 2013.

Pongratz, J., Reick, C., Raddatz, T. and Claussen, M.: A reconstruction of global agricultural areas and land cover for the last millennium, Global Biogeochem. Cycles, 22(3), GB3018, doi:10.1029/2007GB003153, 2008.

Power, M. J., Marlon, J. R., Ortiz, N., Bartlein, P. J., Harrison, S. P., Mayle, F. E., Ballouche, a., Bradshaw, R. H. W., Carcaillet, C., Cordova, C., Mooney, S., Moreno, P. I., Prentice, I. C., Thonicke, K., Tinner, W., Whitlock, C., Zhang, Y., Zhao, Y., Ali, a. a., Anderson, R. S., Beer, R., Behling, H., Briles, C., Brown, K. J., Brunelle, a., Bush, M., Camill, P., Chu, G. Q., Clark, J., Colombaroli, D., Connor, S., Daniau, A.-L., Daniels, M., Dodson, J., Doughty, E., Edwards, M. E., Finsinger, W., Foster, D., Frechette, J., Gaillard, M.-J. J., Gavin, D. G., Gobet, E., Haberle, S., Hallett, D. J., Higuera, P., Hope, G., Horn, S., Inoue, J., Kaltenrieder, P., Kennedy, L., Kong, Z. C., Larsen, C., Long, C. J., Lynch, J., Lynch, E. a., McGlone, M., Meeks, S., Mensing, S., Meyer, G., Minckley, T., Mohr, J., Nelson, D. M., New, J., Newnham, R., Noti, R., Oswald, W., Pierce, J., Richard, P. J. H., Rowe, C., Sanchez Goñi, M. F., Shuman, B. N., Takahara, H., Toney, J., Turney, C., Urrego-Sanchez, D. H., Umbanhowar, C., Vandergoes, M., Vannière, B., Vescovi, E., Walsh, M., Wang, X., Williams, N., Wilmshurst, J., Zhang, J. H. and Goni, M. F. S.: Changes in fire regimes since the Last Glacial Maximum: an assessment based on a global synthesis and analysis of charcoal data, Clim. Dyn., 30(7–8), 887–907, doi:10.1007/s00382-007-0334-x, 2008.

Power, M. J., Mayle, F., Bartlein, P., Marlon, J. R., Anderson, R., Behling, H., Brown, K., Carcaillet, C., Colombaroli, D., Gavin, D., Hallett, D., Horn, S., Kennedy, L., Lane, C., Long, C., Moreno, P., Paitre, C., Robinson, G. S., Taylor, Z. and Walsh, M.: Climatic control of the biomass-burning decline in the Americas after AD 1500, The Holocene, 23(1), 3–13, doi:10.1177/0959683612450196, 2012.

Rommelaere, V., Arnaud, L. and Barnola, J. M.: Reconstructing recent atmospheric trace gas concentrations from polar firn and bubbly ice data by inverse methods, J. Geophys. Res., 102, 30 069-30 083, 1997.

Rowlinson, M. J., Rap, A., Hamilton, D. S., Pope, R. J., Hantson, S., Arnold, S. R., Kaplan, J. O., Arneth, A., Chipperfield, M. P., Forster, P. M. and Nieradzik, L.: Tropospheric ozone radiative forcing uncertainty due to pre-industrial fire and biogenic emissions, Atmos. Chem. Phys., 20(18), 10937–10951, doi:10.5194/acp-20-10937-2020, 2020.

Rubino, M., D'Onofrio, A., Seki, O. and Bendle, J. A.: Ice-core records of biomass burning, Anthr. Rev., 3(2), 140–162, doi:10.1177/2053019615605117, 2016a.

Rubino, M., Etheridge, D. M., Trudinger, C. M., Allison, C. E., Rayner, P. J., Enting, I., Mulvaney, R., Steele, L. P., Langenfelds, R. L., Sturges, W. T., Curran, M. A. J. and Smith, A. M.: Low atmospheric CO_2 levels during the Little Ice Age due to cooling induced terrestrial uptake, Nat. Geosci., 9(9), 691–694, doi:10.1038/ngeo2769, 2016b.

Rubino, M., Etheridge, D. M., Thornton, D. P., Howden, R., Allison, C. E., Francey, R. J., Langenfelds, R. L., Steele, L. P., Trudinger, C. M., Spencer, D. A., Curran, M. A. J., van Ommen, T. D. and Smith, A. M.: Revised records of atmospheric trace gases CO_2, CH_4, N_2O, and $d^{13}CO_2$ over the last 2000 years from Law Dome, Antarctica, Earth Syst. Sci. Data, 11(2), 473–492, doi:10.5194/essd-11-473-2019, 2019.

38

Sapart, C. J., Monteil, G., Prokopiou, M., van de Wal, R. S. W., Kaplan, J. O., Sperlich, P., Krumhardt, K. M., van der Veen,
C., Houweling, S., Krol, M. C., Blunier, T., Sowers, T. A., Martinerie, P., Witrant, E., Dahl-Jensen, D. and Rockmann, T.:
Natural and anthropogenic variations in methane sources during the past two millennia, Nature, 490(7418), 85–88, doi:Doi
10.1038/Nature11461, 2012.

Servettaz, A., Orsi, A. J., Curran, M. A. J., Moy, A. D., Landais, A., Agosta, C., Winton, V. H. L., Touzeau, A., McConnell,
J. R., Werner, M. and Baroni, M.: Snowfall and Water Stable Isotope Variability in East Antarctica Controlled by Warm
Synoptic Events, J. Geophys. Res. Atmos., 125(17), e2020JD032863, doi:10.1029/2020JD032863, 2020.

Servettaz, A. P. M., Orsi, A. J., Curran, M. A. J., Moy, A. D., Landais, A., McConnell, J. R., Popp, T. J., Le Meur, E., Faïn,
X. and Chappellaz, J.: A 2000-year temperature reconstruction on the East Antarctic plateau from argon–nitrogen and water
stable isotopes in the Aurora Basin North ice core, Clim. Past, 19(6), 1125–1152, doi:10.5194/cp-19-1125-2023, 2023.

Stenni, B., Proposito, M., Gragnani, R., Flora, O., Jouzel, J., Falourd, S. and Frezzotti, M.: Eight centuries of volcanic signal
and climate change at Talos Dome (East Antarctica), J. Geophys. Res. Atmos., 107(D9), ACL 3-1-ACL 3-13,
doi:10.1029/2000JD000317, 2002.

Stowasser, C., Buizert, C., Gkinis, V., Chappellaz, J., Schüpbach, S., Bigler, M., Faïn, X., Sperlich, P., Baumgartner, M.,
Schilt, a., Blunier, T. and Schupbach, S.: Continuous measurements of methane mixing ratios from ice cores, Atmos. Meas.
Tech., 5(5), 999–1013, doi:10.5194/amt-5-999-2012, 2012.

Sturrock, G. A.; Etheridge, D. M.; Trudinger, C. M.; Fraser, P. J.; Smith, A. M.: Atmospheric histories of halocarbons from
analysis of Antarctic firn air: Major Montreal Protocol species. Journal of geophysical research - Atmospheres. 107(D24):4765,
doi:10.1029/2002JD002548, 2002.

Schwander, J. and Stauffer, B.: Age difference between polar ice and the air trapped in its bubbles, Nature, 311(5981), 45–47,
doi:10.1038/311045a0, 1984.

Schwander, J., Barnola, J. M., Andrie, C., Leuenberger, M., Ludin, A., Raynaud, D. and Stauffer, B.: The age of the air in the
firn and the ice at Summit, Greenland, J. Geophys. Res., 98, 2831–2838, 1993.

Stevenson, D. S., Zhao, A., Naik, V., O'Connor, F. M., Tilmes, S., Zeng, G., Murray, L. T., Collins, W. J., Griffiths, P. T.,
Shim, S., Horowitz, L. W., Sentman, L. T. and Emmons, L.: Trends in global tropospheric hydroxyl radical and methane
lifetime since 1850 from AerChemMIP, Atmos. Chem. Phys., 20(21), 12905–12920, doi:10.5194/acp-20-12905-2020, 2020.

Szopa, S., V. Naik, B. Adhikary, P. Artaxo, T. Berntsen, W.D. Collins, S. Fuzzi, L. Gallardo, A. Kiendler-Scharr, Z. Klimont,
H. Liao, N. Unger, and P. Zanis, 2021: Short-Lived Climate Forcers. In Climate Change 2021: The Physical Science Basis.
Contribution of Working Group I to the Sixth Assessment Report of the Intergovernmental Panel on Climate Change [Masson-
Delmotte, V., P. Zhai, A. Pirani, S.L. Connors, C. Péan, S. Berger, N. Caud, Y. Chen, L. Goldfarb, M.I. Gomis, M. Huang, K.
Leitzell, E. Lonnoy, J.B.R. Matthews, T.K. Maycock, T. Waterfield, O. Yelekçi, R. Yu, and B. Zhou (eds.)]. Cambridge
University Press, Cambridge, United Kingdom and New York, NY, USA, pp. 817–922, doi:10.1017/9781009157896.008.

Tarantola, A.: Inverse problem theory and methods for model parameter estimation, Society for Industrial Mathematics, 2005.

1300

1305

1310

1315

1320

1325

1330

Supprimé: Servettaz, A. P. M., Orsi, A. J., Curran, M. A. J., Moy, A. D., Landais, A., McConnell, J. R., Popp, T. J., Le Meur, E., Faïn, X. and Chappelaz, J.: A 2000-year temperature reconstruction on the East Antarctic plateau, from argon-nitrogen and water stable isotopes in the Aurora Basin North ice core, Clim. Past Discuss., 2022, 1–58, doi:10.5194/cp-2022-91, 2022.

Tarr, M. A., Miller, W. L. and Zepp, R. G.: Direct carbon monoxide photoproduction from plant matter, J. Geophys. Res., 100(D6), 11403, doi:10.1029/94JD03324, 1995.

Thoning, K. W., Tans, P. P., and Komhyr, W. D., Atmospheric carbon dioxide at Mauna Loa Observatory: 2. Analysis of the NOAA GMCC data, 1974–1985, J. Geophys. Res., 94(D6), 8549– 8565, doi:10.1029/JD094iD06p08549, 1989.

Tzompa-Sosa, Z. A., Mahieu, E., Franco, B., Keller, C. A., Turner, A. J., Helmig, D., Fried, A., Richter, D., Weibring, P., Walega, J., Yacovitch, T. I., Herndon, S. C., Blake, D. R., Hase, F., Hannigan, J. W., Conway, S., Strong, K., Schneider, M. and Fischer, E. V.: Revisiting global fossil fuel and biofuel emissions of ethane, J. Geophys. Res. Atmos., 122(4), 2493–2512, doi:10.1002/2016JD025767, 2017.

Trudinger, C. M., Enting, I. G., Etheridge, D. M., Francey, R. J., Levchenko, V. A., Steele, L. P., Raynaud, D., and Arnaud, L.: Modeling air movement and bubble trapping in firn, J. Geophys. Res., 102, 6747–6763, 1997.

Trudinger, C. M., Etheridge, D. M., Rayner, P. J., Enting, I. G., Sturrock, G. A., and Langenfelds, R. L.: Reconstructing atmospheric histories from measurements of air composition in firn, J. Geophys. Res., 107, 4780, doi:10.1029/2002JD002545, 2002.

Trudinger, C. M., Enting, I. G., Rayner, P. J., Etheridge, D. M., Buizert, C., Rubino, M., Krummel, P. B., and Blunier, T.: How well do different tracers constrain the firn diffusivity profile?, Atmos. Chem. Phys., 13, 1485–1510, doi:10.5194/acp-13-1485-2013, 2013.

Trudinger, C. M., Fraser, P. J., Etheridge, D. M., Sturges, W. T., Vollmer, M. K., Rigby, M., Martinerie, P., Mühle, J., Worton, D. R., Krummel, P. B., Steele, L. P., Miller, B. R., Laube, J., Mani, F. S., Rayner, P. J., Harth, C. M., Witrant, E., Blunier, T., Schwander, J., O'Doherty, S. and Battle, M.: Atmospheric abundance and global emissions of perfluorocarbons CF_4, C_2F_6 and C_3F_8 since 1800 inferred from ice core, firn, air archive and in situ measurements, Atmos. Chem. Phys., 16(18), 11733–11754, doi:10.5194/acp-16-11733-2016, 2016.

van der Werf, G. R., Randerson, J. T., Giglio, L., Collatz, G. J., Mu, M., Kasibhatla, P. S., Morton, D. C., DeFries, R. S., Jin, Y. and van Leeuwen, T. T.: Global fire emissions and the contribution of deforestation, savanna, forest, agricultural, and peat fires (1997–2009), Atmos. Chem. Phys., 10(23), 11707–11735, doi:10.5194/acp-10-11707-2010, 2010.

van der Werf, G. R., Peters, W., van Leeuwen, T. T. and Giglio, L.: What could have caused pre-industrial biomass burning emissions to exceed current rates?, Clim. Past, 9(1), 289–306, doi:10.5194/cp-9-289-2013, 2013.

van der Werf, G. R., Randerson, J. T., Giglio, L., van Leeuwen, T. T., Chen, Y., Rogers, B. M., Mu, M., van Marle, M., Morton, D. C., Collatz, G. J., Yokelson, R. J. and Kasibhatla, P. S.: Global fire emissions estimates during 1997–2016, Earth Syst. Sci. Data, 9(2), 697–720, doi:10.5194/essd-9-697-2017, 2017.

van Marle, M., Kloster, S., Magi, B. I., Marlon, J. R., Daniau, A.-L., Field, R. D., Arneth, A., Forrest, M., Hantson, S., Kehrwald, N. M., Knorr, W., Lasslop, G., Li, F., Mangeon, S., Yue, C., Kaiser, J. W. and van der Werf, G. R.: Historic global biomass burning emissions for CMIP6 (BB4CMIP) based on merging satellite observations with proxies and fire models (1750–2015), Geosci. Model Dev., 10(9), 3329–3357, doi:10.5194/gmd-10-3329-2017, 2017.

Vannière, B., Blarquez, O., Rius, D., Doyen, E., Brücher, T., Colombaroli, D., Connor, S., Feurdean, A., Hickler, T., Kaltenrieder, P., Lemmen, C., Leys, B., Massa, C. and Olofsson, J.: 7000-year human legacy of elevation-dependent European fire regimes, Quat. Sci. Rev., 132, 206–212, doi:10.1016/J.QUASCIREV.2015.11.012, 2016.

Wang, Z., Chappellaz, J., Park, J. Y. and Mak, J.: Large variations in Southern Hemisphere biomass burning during the last 1375   650 years, Science, 330, 1663–166, doi:10.1126/science.1197257, 2010.

Wang, Z., Chappellaz, J., Martinerie, P., Park, K., Petrenko, V. V., Witrant, E., Emmons, L. K., Blunier, T., Brenninkmeijer, C. A. M. and Mak, J.: The isotopic record of Northern Hemisphere atmospheric carbon monoxide since 1950: implications for the CO budget, Atmos. Chem. Phys., 12(10), 4365–4377, doi:10.5194/acp-12-4365-2012, 2012.

Werle, P., Mücke, R. and Slemr, F.: The Limits of Signal Averaging in Atmospheric Trace-Gas Monitoring by Tunable Diode-1380   Laser Absorption Spectroscopy (TDLAS), Appl. Phys. B-Lasers Opt., 139, 131–139, 1993.

Witrant, E., Martinerie, P., Hogan, C., Laube, J. C., Kawamura, K., Capron, E. and Montzka, S. A., E. J. Dlugokencky,D. Etheridge, T. Blunier, and W. T. Sturges: A new multi-gas constrained model of trace gas non-homogeneous transport in firn : evaluation and behaviour at eleven polar sites, Atmos. Chem. Phys., (12), 11465–11483, doi:10.5194/acp-12-11465-2012, 2012.

1385   Witrant, E. and Martinerie, P.: Input Estimation from Sparse Measurements in LPV Systems and Isotopic Ratios in Polar Firns, in 2013 IFAC Joint Conference SSSC, pp. 654–659, 5th Symposium on System Structure and Control, Grenoble, France, 2013.

Worton, D. R., Sturges, W. T., Gohar, L. K., Shine, K. P., Martinerie, P., Oram, D. E., Humphrey, S. P., Begley, P., Gunn, L., Barnola, J. M., Schwander, J. and Mulvaney, R.: Atmospheric Trends and Radiative Forcings of CF_4 and C_2F_6 Inferred from 1390   Firn Air, Environ. Sci. Technol., 41(7), 2184–2189, doi:10.1021/es061710t, 2007.

Xiao, Y., Logan, J. A., Jacob, D. J., Hudman, R. C., Yantosca, R. and Blake, D. R.: Global budget of ethane and regional constraints on U.S. sources, J. Geophys. Res., 113(D21), D21306, doi:10.1029/2007JD009415, 2008.

Yeung, L. Y., Murray, L. T., Martinerie, P., Witrant, E., Hu, H., Banerjee, A., Orsi, A. and Chappellaz, J.: Isotopic constraint on the twentieth-century increase in tropospheric ozone, Nature, 570(7760), 224–227, doi:10.1038/s41586-019-1277-1, 2019.

1395   Zheng, B., Chevallier, F., Yin, Y., Ciais, P., Fortems-Cheiney, A., Deeter, M. N., Parker, R. J., Wang, Y., Worden, H. M. and Zhao, Y.: Global atmospheric carbon monoxide budget 2000–2017 inferred from multi-species atmospheric inversions, Earth Syst. Sci. Data, 11(3), 1411–1436, doi:10.5194/essd-11-1411-2019, 2019.

Southern Hemisphere atmospheric history of carbon monoxide over the late Holocene reconstructed from multiple Antarctic ice archives

Supplementary Information

Xavier Faïn (1), David M. Etheridge (3,4), Kévin Fourteau (2), Patricia Martinerie (1), Cathy M. Trudinger (3,4), Rachael H. Rhodes (5), Nathan J. Chellman (6), Ray L. Langenfelds (2), Joseph R. McConnell (6), Mark A. J. Curran (13, 4), Edward J. Brook (7), Thomas Blunier (8), Grégory Teste (1), Roberto Grilli (1), Anthony Lemoine (1), William T. Sturges (9), Boris Vannière (10, 11), Johannes Freitag (12), Jérôme Chappellaz (1, 14).

1 Univ. Grenoble Alpes, CNRS, INRAE, IRD, Grenoble INP, IGE, 38000 Grenoble, France
2 Univ. Grenoble Alpes, Université de Toulouse, Météo-France, CNRS, CNRM, Centre d'Études de la Neige, Grenoble, France
3 CSIRO Environment, 3195, Aspendale, Victoria, Australia
4 Australian Antarctic Program Partnership, Institute for Marine and Antarctic Studies, University of Tasmania, Hobart, Tasmania
5 Department of Earth Sciences, University of Cambridge, Cambridge, CB2 3EQ, UK
6 Division of Hydrologic Sciences, Desert Research Institute, Reno, NV 89512, USA
7 College of Earth, Ocean, and Atmospheric Sciences, Oregon State University, Corvallis, OR 97331, USA
8 Physics of Ice, Climate and Earth, Niels Bohr Institute, University of Copenhagen, Copenhagen, Denmark
9 Centre for Ocean and Atmospheric Sciences, School of Environmental Sciences, University of East Anglia, Norwich, UK
10 Institute of Plant Sciences, Oeschger Centre for Climate Change Research, University of Bern, Switzerland
11 MSHE, Chrono-environnement, CNRS, Université de Franche-Comté, Besançon, France
12 Alfred Wegener Institut Helmholtz Zentrum für Polar und Meeresforschung, Bremerhaven, Germany
13 Australian Antarctic Division, Kingston, Tasmania, Australia
14 Ecole Polytechnique Fédérale de Lausanne EPFL, CH-1951, Sion, Switzerland

Correspondence to: Xavier Faïn (xavier.fain@univ-grenoble-alpes.fr)

Supprimé: 3

Supprimé: Centre for Ice and Climate

Supprimé: MSHE, CNRS, Université Bourgogne Franche-Comté, Besançon, France

Mis en forme : Anglais (Royaume-Uni)

Supprimé: Bourgogne

Summary

1. Methodology

1.1. Location of drilling and firn air sampling sites

Figure S1. Location of the different ice core drillings (DC12, Berkner Island (BKN), and TaldIce (TD)) and firn air sampling (DE08-2, DSSW19K, DSSW20K, Lock In (LI), South Pole (SP), and ABN) sites. The CSIRO stations conducting atmospheric monitoring and discussed in this study are also reported (Mawson, Casey, and South Pole).

1.2. Ice core chronologies

All gas age scales reported in this study (i.e., DC12, ABN, TD, and EDML-B40) are tied to the WDC06A-7 chronology.

Ice core	Δage (yrs)	Reference
DC12	2400	Fourteau et al., 2020
ABN	630	Servettaz et al., 2023
TaldIce	615	*This study*
EDML- B40	811	Rhodes et al., 2016

Table S1. Gas chronology for ice cores featured in this study. Δage reports the difference between gas age and ice age. All gas age scales are tied to the WDC06A-7 chronology.

55

1.3. Calibration of CO datasets

NOAA and CSIRO have maintained CO measurement programs and separate calibration scales over more than three decades. NOAA is the WMO-designated Central Calibration Laboratory for CO with their data currently reported on the WMO-X2014 scale. Long-term intercomparison
60 programs involving NOAA and CSIRO revealed large concentration-dependent differences in the 1990s (Masarie et al., 2001). Thus CSIRO elected to maintain its own calibration scale. The current version of the CSIRO scale (CSIRO2020) is closely aligned with WMO-X2014 in terms of absolute concentration but its internal consistency and long-term stability are constrained by internal CSIRO procedures and remain entirely independent of WMO-X2014 assignments.
65 Ongoing refinement of calibration scales at both laboratories has led to much improved agreement between the respective scales, with differences now within ±1 ppbv over the range of 28 - 487 ppbv (Langenfelds et al., 2023).

CO measurements (including firn and ice cores) are conducted with a SARA optical analyzer (OF-CEAS, Morville et al., 2005) at IGE. CSIRO uses gas chromatography for determination of [CO]
70 in firn air samples (Langenfelds et al., 2023). Such methodologies differ from NOAA, which applies a VURF detection (https://www.esrl.noaa.gov/gmd/ccl/co_scale.html) for CO mixing ratios. All firn air CO datasets included in this study except Berkner Island (BKN) and Lock-In (LI) datasets were analyzed at CSIRO and are reported on the CSIRO2020 scale. Ice core datasets (analyzed at IGE and DRI) and the LI firn air dataset (analyzed at IGE) are reported on the WMO-
75 X2014 scale. [CO] drifts within cylinders were quantified, either at CSIRO or at IGE. Specifically, the standard gases used for calibrating dataset at IGE were first certified at NOAA in 2012, and recertified in 2020 by the EU ICOS network (https://www.icos-cp.eu/). Very limited drifts in [CO]

were observed, ranging 0.1 - 0.2 ppbv depending on cylinders. The standard gas cylinders used
80   to calibrate the ABN ice core dataset were certified at NOAA just prior to the CFA campaign.

In this study, we combine CO data produced in different laboratories, principally CSIRO (Australia) and IGE (France). The good agreement between CSIRO2020 and WMO-X2014 (Langenfelds et al., 2023) allows for the combination of datasets reported on either scale to produce a coherent paleo-atmospheric CO history.

85   For each analytical campaign at IGE (including CFA campaigns and Lock-In firn air sample measurements), the OF-CEAS spectrometer was carefully calibrated on dry gas by direct injection of a synthetic standard gas (Scott Marin, artificial gas mixtures). Finally, during each analytical campaign (CFA and firn air measurements), routine measurements of a gas standard verified that no drift was occurring, and that the calibration of the OF-CEAS analyser was remaining stable.

90

1.4. Internal precision of CO CFA analyses

Allan-Werle variance tests (Allan, 1966, Werle et al., 1993) applied to calibration loop dataset (deionized degassed water mixed with a single standard gas) in order to evaluate Internal precision and stability of gas-CFA measurements are reported on Fig. S2. Internal precision,
95   defined as twice the Allan-Werle deviation at chosen integration time, was 0.7 and 1.0 ppbv for the IGE (i.e., DC12 and TD) and DRI (i.e., ABN) analytical campaigns (Table S2).
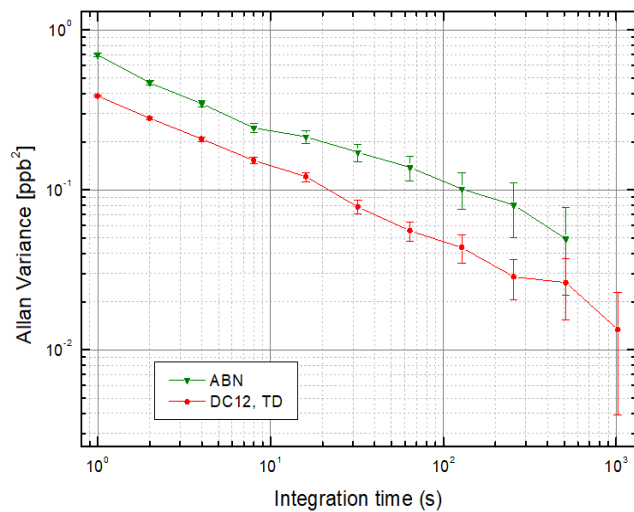
Figure S2. Allan-Werle variance results for calibration loop dataset (DI degassed water mixed with a single standard gas) collected for the different CFA setups: DRI (ABN core) and IGE (DC12 and TD cores).

Ice core	Laboratory of analysis	Analysis date	Mean gas sample flow (sccm min^{-1})	Optimal Integration Time (s)	Integration Time applied (s)	Internal precision at IT (ppbv) (2σ)	External precision (ppbv) (2σ)	System response time (min)	CO blank (ppbv)	CO solubility losses (%)
EDML-B40	DRI	10-14/10/2013	1.50	n.d.	10	n.d.	n.d.	14.2	n.d.	6.0%
DC12	IGE	6-24/06/2014	1.35	>1000	10	0.7	2.8	1.6	4.1	7.4%
TD	IGE	17-21/10/2014	1.45	>1000	10	0.7	2.8	1.6	4.1	7.4%
ABN	DRI	5-14/10/2015	1.62	>500	10	1.0	8.8	9.3	7.4	6.0%
Solarice	IGE	15/01/2019	1.30	>1000	10	0.7	8.8	1.6	4.1	7.4%

Table S2. CFA setup specifications and performances of the different analytical campaigns.

1.5. External precision of CO CFA analyses

External precision of the continuous CO measurements (i.e., including all sources of errors or bias) can be investigated by melting replicate ice sticks on different days on a gas-CFA setup. Such an approach has been applied before to CFA gas setups (Faïn et al., 2022). Specifically, we define the external precision as the pooled standard deviations calculated on the differences of CO concentrations from main and replicate analysed ice sticks, averaging continuous CO data over few cm long intervals.

No long sections (i.e., > 1 meters) of replicate ice sticks were available or analysed in the frame of this study to evaluate external precision directly on Antarctica ice samples. External precision for the IGE and DRI continuous CO measurements are thus extracted from the comparison of main and replicate analyses conducted on the PLACE core, although this archive exhibits higher [CO] compared to Antarctic ice. The PLACE core was drilled in 2015 nearby Summit Station, Central Greenland, and analysed in 2015 and 2017 at DRI and IGE, respectively (Faïn et al., 2022).

[CO] patterns extracted from the PLACE core exhibit high frequency variability, with high amplitude spike (i.e., amplitude larger than 100 ppbv is observed, Faïn et al., 2022). Such patterns are different from continuous [CO] extracted from Antarctica ice, which reveals no in-situ production and no high-frequency, non-atmospheric, features (Fig. 2). Specifically, the difference between the maxima and minima of [CO] observed in our Antarctic high resolution CFA records is ~15 ppbv (Fig. 2). Therefore, only sections of the PLACE record exhibiting minimum [CO] but within a range of 15 ppbv were considered for the evaluation of external precisions for Antarctica samples.

In practice, 14.2 m (resp., 1.9 m) of replicate PLACE sticks analysed at DRI in 2015 (resp., at IGE in 2017) were first considered. CO concentrations measured on both main and replicate ice sticks were averaged by binning over 142 10-cm long (resp., over 190 1-cm long) intervals at DRI (resp., at IGE). Second, 33 (resp., 33) intervals were selected at DRI (resp., IGE) for exhibiting minimum [CO] of the Greenland records, and within a range of 15 ppbv. Figure S3 reports significant correlations between averaged [CO] from main cuts versus averaged [CO] from replicate cuts for

135 both CFA setups. Finally, 2σ external precision of 4.0 ppbv (resp. 8.8 ppbv) was calculated for the IGE CFA setup (resp., the DRI CFA setup).
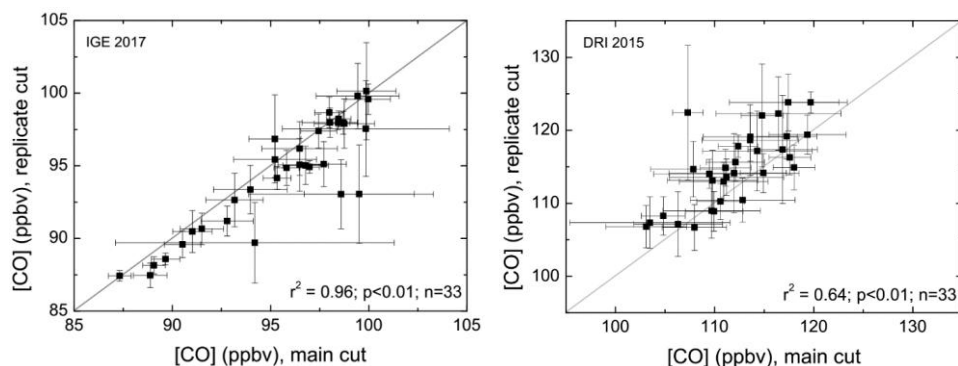
Figure S3. CO mixing ratios measured on both main and replicate PLACE ice sticks at IGE (left panel) and DRI (right panel), after averaging data over 1-cm long (resp., over 10-cm long) intervals at IGE (resp., at DRI). The 1:1 line is shown in grey.

140

1.6. Absolute calibration of continuous CO datasets: accuracy

A fraction, or all, of gases dissolved in the water CFA sample flow are not recovered by the Idex degassers used in this study. CO solubility is higher than N_2 or O_2 solubility. This preferential dissolution of CO in comparison to N_2 and O_2 results in underestimated CO mixing ratios when
145 detected at the gas outlet of the degasser. This underestimation of CO mixing ratios need to be accurately quantified so as to provide an absolute calibration of CO continuous dataset.

In this study, we follow the rationale reported by Faïn et al. (2022) and use the calibration loop (CL) to calibrate internally (i.e., with CFA data) continuous CO datasets. We hypothesise that CO and methane dissolution follow the same physical laws: consequently, if a calibration loop is able
150 to reproduce methane preferential dissolution, it should also reproduce CO losses related to dissolution. Estimates of methane losses related to dissolution, independent of the calibration loop, from each ice core analyzed, was thus required. For the ice core DC12, preferential methane dissolution was already known (Fourteau et al., 2020). For the ABN and TD archives, it was evaluated by direct comparison of CFA dataset with WAIS-Divide discrete record (Mitchell et al.,
155 2013). Finally, we observed an underestimation of methane mixing ratios of 11.1%, 9.5%, and 11.1% when measuring the DC12, ABN, and TD cores, respectively.

Each continuous CO dataset, after initial calibration of the OF-CEAS analyser (Sect. 1.2), was calibrated according to the following: $[CO]_{COR} = ([CO]_{SAMPLE} - CO_{BLANK}) / SC$

With SC the Solubility Correction evaluated with CL experiment, and CO_{BLANK}, the CO blank of the CFA setup.

SC was extracted from multi-standards (with [CO] ranging 30-100 ppbv) CL experiments. We operated the CL with different artificial gas cylinders of known CO and CH_4 mixing ratios. Liquid and gas flows injected through the CL were chosen to reproduce ice air content value. Gas flow was later adjusted if required so as the calibration loop reproduces nicely the expected methane preferential dissolution. At IGE, we were also able to add to the CL experiment an injection of CO-depleted air (so called "Air Zero" later), produced by flushing room air on PtO trap heated at 200°C. After and/or before each calibration loop experiment, gas from all cylinders and Air Zero were analysed directly with the OF-CEAS analyser. The CL data were not calibrated onto the WMO-X2014 scale, but instead directly compared to these direct measurements from cylinders or Air Zero. The same calibration was applied to both datasets collected with the IGE setup, i.e. DC12 and TD (Fig. S4). Indeed (i) similar CH_4 preferential dissolutions were observed during the DC12 and TD analyses, and (ii) configuration of IGE CFA setup remains identical for the DC12 and TD analytical campaigns. Similarly, the calibration applied to the ABN dataset is identical to the one previously used by Faïn et al., (2022) to calibrate the PLACE dataset. The ABN core was analysed immediately after the PLACE core, with no changes within the CFA setup, and similar CH_4 preferential dissolution was observed during the PLACE and ABN analyses. The CO blanks of the IGE and DRI setups have been reported previously (Faïn et al., 2022) and are reported in Table S2, along with SC.
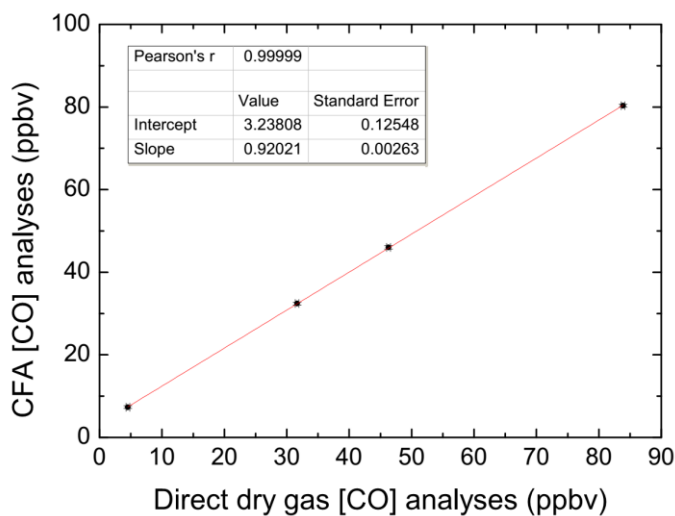
180 **Figure S4.** Multi-standard Calibration Loop experiment conducted on the IGE CFA setup: CO preferential dissolution representative of the DC12 and TD melting conditions. The intercept indicates the CO blank level during the experiment, and is in agreement with the CO system blank established previously for the IGE CFA setup (i.e., 4.1±1.2 ppbv, Table S2; Faïn et al., 2022).

185 **2. Supporting Data**

2.1. CSIRO atmospheric [CO] monitoring in Antarctica

CSIRO has measured CO in flask samples of background air from a range of SH sites since the 1980s. Antarctic sites with long CO records include Mawson (MAA, since 1984), South Pole (SPO, since 1991) and Casey (CYA, since 1996). Samples were pressurized in CSIRO's 0.5L or
190 5.0L glass flasks using customised pump units equipped with either chemical (anhydrous magnesium perchlorate) or cryogenic drying (Francey et al., 2003; Langenfelds et al., 2023). The MAA dataset is used as the primary link to firn/ice data in this study due to its longer duration and MAA's coastal Antarctic location being similar to that of Law Dome.

Gas chromatographic (GC) measurements since 1991 were made using a Trace Analytical
195 Reduction Gas Analyser (RGA). These records are supported by extensive measurements of a large suite of calibration standards, including ten CO-in-synthetic-air standards in the range of

approximately 23 - 200 ppbv that were prepared by Scott Marrin, USA in 1992 and which retain about 1/3 of their original contents. Random uncertainties applying to these flask sample CO data are generally within ±1 ppbv. Systematic uncertainties relevant to comparison with firn/ice data are dominated by two components:

(i) Correction for flask storage effects. Measured CO in CSIRO's 0.5L glass flasks with PFA o-rings is corrected by -0.0058 ppbv/day of storage (equivalent to -2.1 ppbv yr^{-1}), as derived from multiple, mainly laboratory-based storage tests. However, drift rates can vary depending on flask history, condition and CO content of the atmosphere in which the flasks are stored. Because MAA samples are returned to CSIRO in annual batches, mean corrections are approximately -1.4 ppbv with an estimated uncertainty of ±1 ppbv in MAA annual means.

(ii) Long-term calibration drift. Uncertainty in stability of the CSIRO2020 scale over three decades is estimated at ±0.1 ppbv yr^{-1}, based on the measured relative stability of a large number of air samples/standards stored in a range of different cylinder types, and supporting results from other experimental tests of instrument and air standard stability (Masarie et al., 2001).

GC measurements of earlier MAA samples (1984 - 1990) were made with one of two Carle instruments where CO was catalytically converted to CH_4 for flame ionisation detection (FID). Data from this period are not supported by similar levels of calibration and other diagnostic data as applied to the RGA data (Langenfelds et al., 2023). These early data are noisier and carry larger uncertainty in scale stability of ±0.57% yr^{-1} (equivalent to approx. ±0.24 ppbv yr^{-1} in CO mole fraction observed at that time; Langenfelds et al., 2023). Consequently, they are not used in this study.
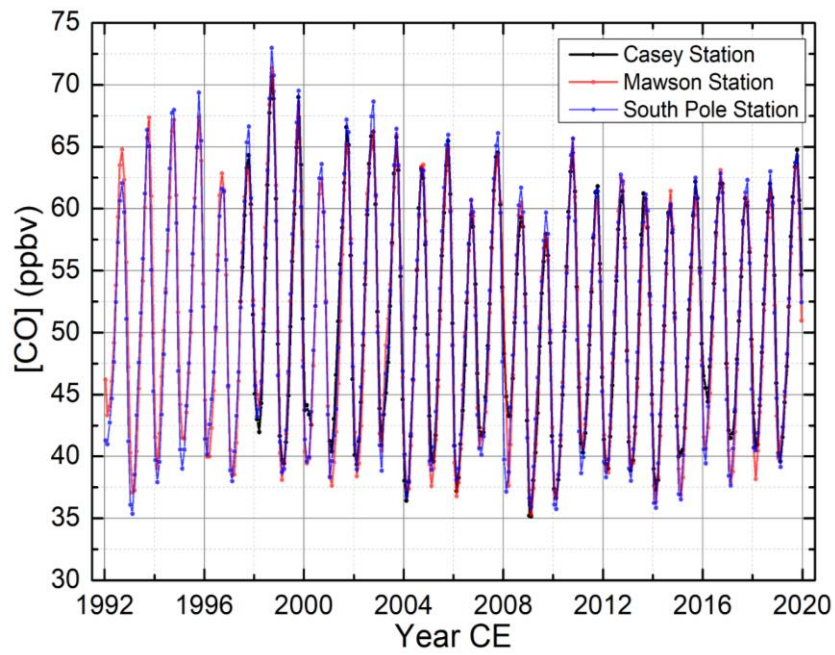
Figure S5. Monthly mean records from flask measurements of [CO] by CSIRO at Casey (Loh et al., 2021a),
South Pole (Loh et al., 2021b), and Mawson (Loh et al., 2021c) stations (Antarctica), for the time period
spanning 1992-2020 CE. Data are reported on the CSIRO2020 CO scale.
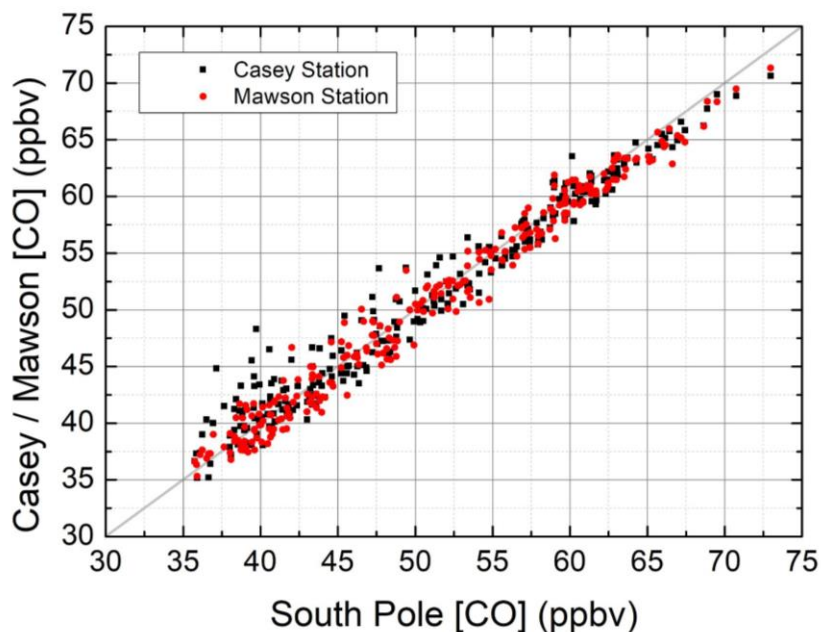
Figure S6. Correlation (r^2 = 0.96) of the CSIRO monthly mean records from flask measurements of [CO] from Casey (Loh et al., 2021a), South Pole (Loh et al., 2021b), and Mawson (Loh et al., 2021c) stations, for the period spanning 1997-2020 CE. Data are reported on the CSIRO2020 CO scale. The grey line indicates the 1:1 line.

2.2 Firn air measurement uncertainty

The precision of the firn air [CO] measurements can be estimated from replicate measurements of samples collected at the same level for each site. The 2-sigma precision is about 1 ppbv for all sites, except for DE08-2 where it is about 2 ppbv. The accuracy, including possible effects of the firn air sampling device (FASD) tubing, bladder and pumps, sample storage in the flask and subsequent measurement, is more difficult to estimate. Comparisons of "surface" firn air [CO], where the FASD inlet is at the snow surface, with "reference" atmospheric [CO] concentrations from air sampled into flasks directly at the site, or with the CO measurements at the coastal stations, mainly Mawson (both firn measurements and station measurements being on the same scale) may reveal sampling artifacts. This assumes that the "reference" measurements are accurate and are representative of the air being sampled at the firn air sampling location and time by the FASD. The comparison is also limited by the sample size- typically only a few surface firn

air sample measurements are made. Also, the deepest levels, where the firn air sample flow can be very low and pumped at well below ambient pressures, can be challenging to sample reliably, and may not be closely simulated by the FASD at the surface (sampling at ABN simulated sub ambient pressure in the inlet line by placing a restriction on the FASD inlet, with no detectable systematic effect on [CO]). The comparison of surface firn [CO] with reference atmospheric [CO] gives differences of about +/- 1 ppbv.

2.3. IGE-GIPSA firn inversion

2.3.1. Depth-concentration firn [CO] profiles

As mentioned in the caption of Fig. 1 in the main manuscript, comparing the [CO] firn data plotted as a function of mean age with the modeled atmospheric trend is not entirely rigorous due to the distributed gas ages resulting from diffusive mixing in the firn. Here we more appropriately compare the [CO] observed and modelled in the firn air. To model [CO] we used the atmospheric trend obtained by inverse firn modeling as input to the forward firn model. The best guess results and uncertainty envelopes illustrate the ability of the model to simultaneously represent the five datasets (Fig. S7).
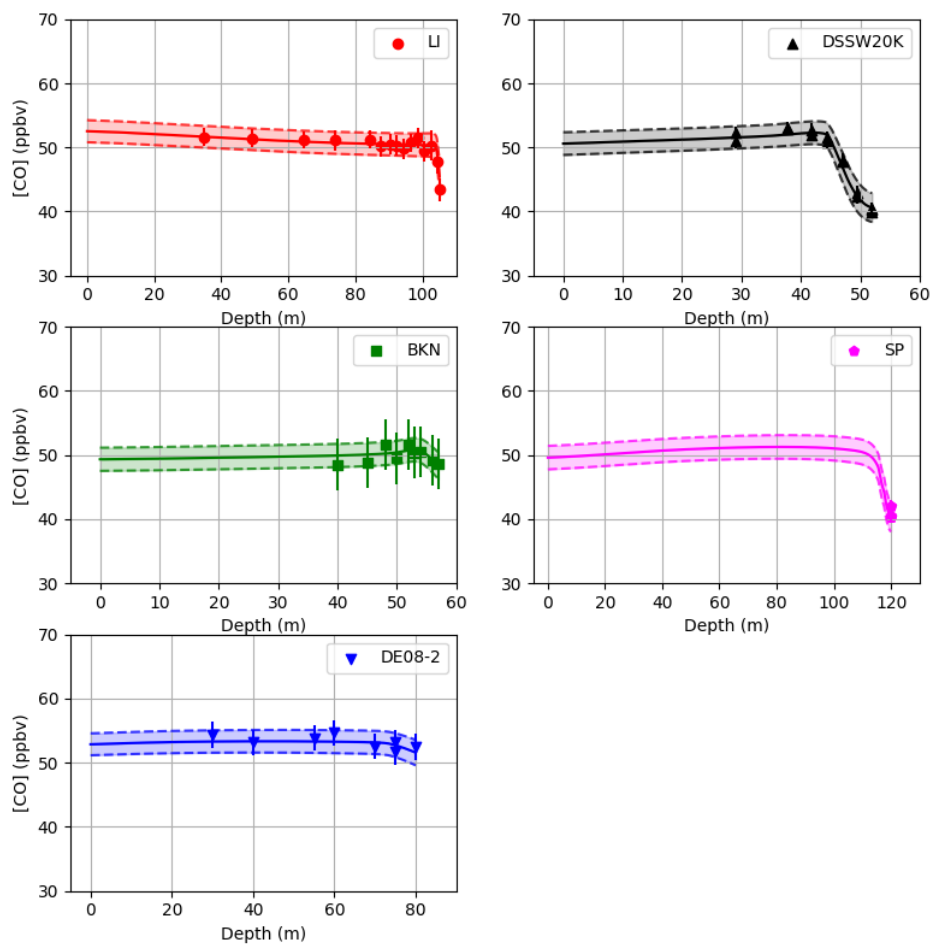
Figure S7. Concentration-depth profiles in the firn air at the five sites investigated with the IGE-GIPSA model. The measurements are reported with symbols with error bars indicating 2σ uncertainties (when available). The solid lines are best fits of the firn IGE-GIPSA model, with envelopes indicating the 2σ uncertainties.

2.3.2. Constraints from ice core dataset

As introduced in Sect. 2.4 of the main manuscript, simulations were performed with the IGE-GIPSA model with and without constraints from ice core data in addition to firn air data. The two

tests are compared in Fig. S8. The multi-site record based on a spline-fit to the ice core data presented in Section 3.3.2 is used to build five synthetic data points in BKN ice at 70, 71, 72, 73 and 74 meters depth. BKN is used as a substitute for the ABN site, which has almost the same accumulation rate. The Green's function approach was used to calculate mean gas ages at the

270   selected depth levels in BKN ice, then CO mixing ratios at the same gas-age in the multi-site spline-fit, ranging between 1862 and 1889 CE, were used to build the five synthetic data points shown on the lower left side of Fig. S8. The time trend scenarios obtained with (in black) and without (in grey) constraints in ice remain within the uncertainty envelopes of one another on their common time frame. Using the ice constraint allows us to reconstruct a trend that goes further

275   back in time.
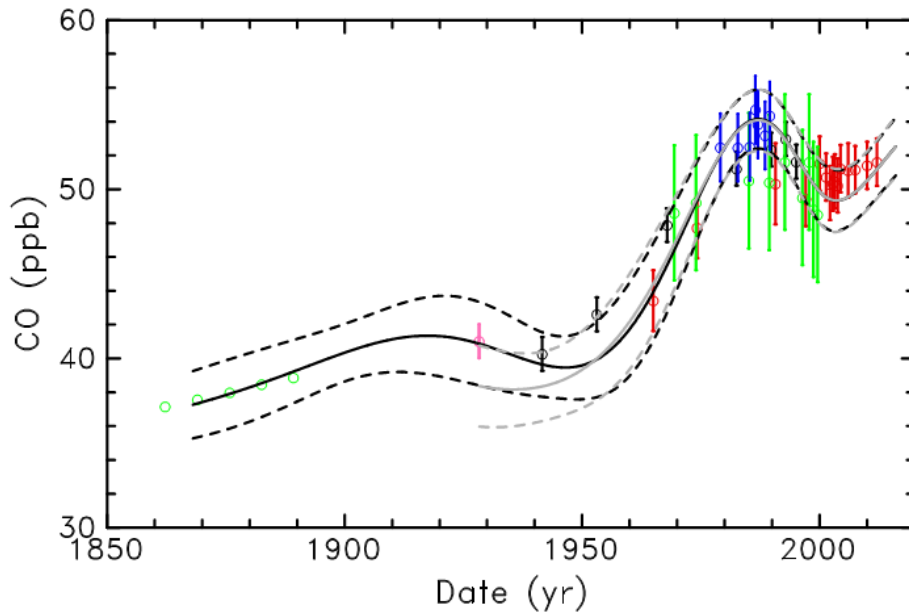
Figure S8. Modelled time trends of CO mixing ratios (continuous lines) with uncertainty envelopes (2σ, dashed lines) obtained with (in black) and without (in grey) synthetic ice core constraint. Synthetic ice core data are shown as green open circles on the left side of the plot (before 1900 CE) whereas firn air data are
280   shown as open circles with uncertainties plotted as vertical bars, LI in red, DSSW20K in black, BKN in green, SP in pink, and DE08-2 in blue. We should note that firn air data plotted versus mean age are not strictly comparable to the modelled time trends which are determined using the age distributions for the

samples from the firn model. This effect is most important near maxima or minima of the trend that are smoothed in the data.

285

2.4. CSIRO firn inversion

The results from the CSIRO inverse model described in the main paper are obtained by using the CO ice reconstruction up to 1897 and the Mawson atmospheric record from 1993, and inferring the atmospheric history between 1898 and 1992 from the firn measurements. Here we give more
290   details about that calculation, and show results from alternative calculations that do not use the ice reconstruction or the Mawson record. The CSIRO inverse model is implemented in IDL (Exelis Visual Information Solutions, Boulder, Colorado) using the constrained_min routine. Non-negativity constraints such as those used by Trudinger et al. (2016) for PFCs are not useful in our inversion for CO because the mole fraction is far from zero and can decrease in time. A simple
295   prior estimate of the CO atmospheric history is used as a starting point for the inversion, but is not included in the cost function. The results were found not to be sensitive to the prior estimate (after 1898, see next paragraph).

We include the ice reconstruction (black line in Fig. 3) in the inversion by setting the prior estimate to match the ice reconstruction up to 1897 and not allowing the inversion to update these values.
300   The Green's functions for the deep firn that extend before 1898 are therefore convolved with a history that is part ice reconstruction and part firn reconstruction. We include the Mawson atmospheric history by using the firn model to calculate the influence at the measurement depths of the Mawson record interpolated to daily resolution from mid-1992 and mean seasonality before 1992, then subtracting this from the firn measurements prior to the inversion. We include the
305   Mawson record in this way because the Mawson record needs to be modelled at about daily resolution to give accurate variation of CO with depth in the upper firn, and the Green's functions (saved at annual resolution) could not do this. Figure S9 shows the contribution of the different parts of the atmospheric history (i.e., up to 1897, between 1898 and 1992 and after 1993) to the modelled firn depth profiles.

310
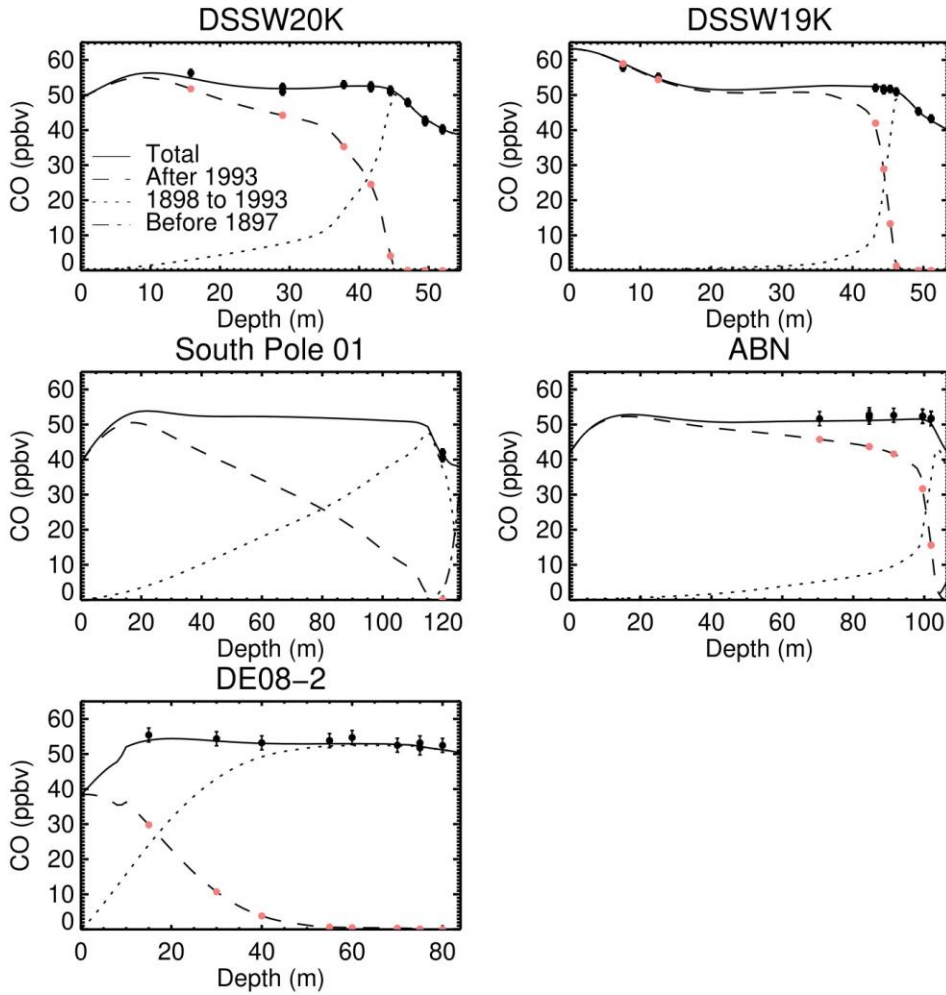
Figure S9. Modelled depth profiles of [CO] inversions from the CSIRO firn model at five sites (DSSW20K, DSSW19K, South Pole 01 (SP), ABN and DE08-2) showing the contribution of the atmospheric history up to 1897 (from the ice reconstruction), between 1898 and 1992 (inferred from the firn measurements) and after 1993 (from the Mawson atmospheric record). The black symbols show the actual firn measurements, and the pink symbols show the modelled influence of the Mawson record at the measurements depths.

The CSIRO inverse model uses bootstrapping to estimate uncertainties in the atmospheric CO reconstruction due to uncertainties in the firn measurements, the firn model, the ice reconstruction and the Mawson record. That is, we repeat the inversion more than 1000 times with the firn observations perturbed according to their uncertainty, using different firn model Green's functions from an ensemble generated during firn model calibration (Trudinger et al., 2013), and ice reconstruction and Mawson record realisations that have been perturbed according to their respective uncertainties. The ice reconstruction is taken to have random uncertainties of 3.7 ppbv before 1880 and 8.8 ppbv after 1880 (see Sections 2.6.2 and S1.5, these are 2σ estimates of external precision from replicate ice sticks, modelled in the CSIRO inversion as random perturbations to annual values of the ice reconstruction) and systematic uncertainties due to the blank (2.8 ppbv) and solubility (0.4 ppbv), both 2σ, each modelled as a separate perturbation that is constant for each realisation of the ice reconstruction in the inversion). In general, realisations of the ice reconstruction that are higher (on average) lead to firn reconstruction solutions that are lower, and vice versa, so that the convolution with the Green's function provides a similar match to the firn observations. The Mawson record uncertainties are dominated by systematic uncertainty due to the correction for flask storage effects (the same uncertainty for all years) and long-term calibration drift (higher uncertainty in early years, decreasing linearly with time) - see Sect. 2.1 and Langenfelds et al., (2023). These uncertainties are modelled in the CSIRO inversion by including random perturbations in the influence of the Mawson records at the firn measurement depths that are subtracted from the firn measurements before the inverse calculation. The maximum size of the perturbations has been determined with the firn model based on worst-case scenarios (specified at daily resolution) for errors in the Mawson record; the flask storage effect varies seasonally but averages about 1.4 ppbv over a year, and the calibration drift is 3 ppbv in 1992 decreasing linearly to zero now (these are taken to be 3σ).

We also consider a case without the ice reconstruction. In this case, the inversion infers the CO history back to 1900 and assumes constant CO levels up to 1900. No information about the ice reconstruction is used in this case. The inferred history differs by up to about 1 ppbv from the case that uses the ice reconstruction, well within the uncertainty range. In addition, we consider a case without the Mawson record, and instead infer the atmospheric history up to 2004 from firn measurements below 25m (to avoid the influence of the seasonal cycle). These results are shown in Fig. S10, with all solutions showing good consistency.
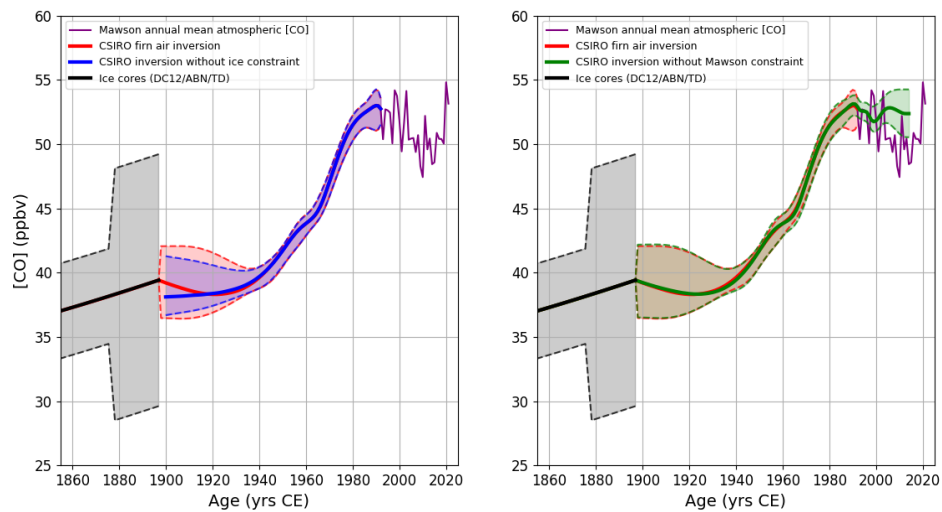
Figure S10. [CO] atmospheric reconstruction from the CSIRO inverse model with ice constraint (red line), and without ice constraint (blue line). The difference between the two inversions in 1897 CE is 1 ppbv. The grey envelope shows the ice core record.

350

355

360

### 2.4.1. Depth-concentration firn [CO] profiles

Figure S11 shows modelled concentration-depth profiles of CO in firn air from the CSIRO model. The solid lines correspond to the best fit cases in Fig 1f. The 2-sigma uncertainty band is generated by calculating firn depth profiles from the multiple atmospheric histories that result from the bootstrap method, thus corresponding to the uncertainty range in Fig 1f.
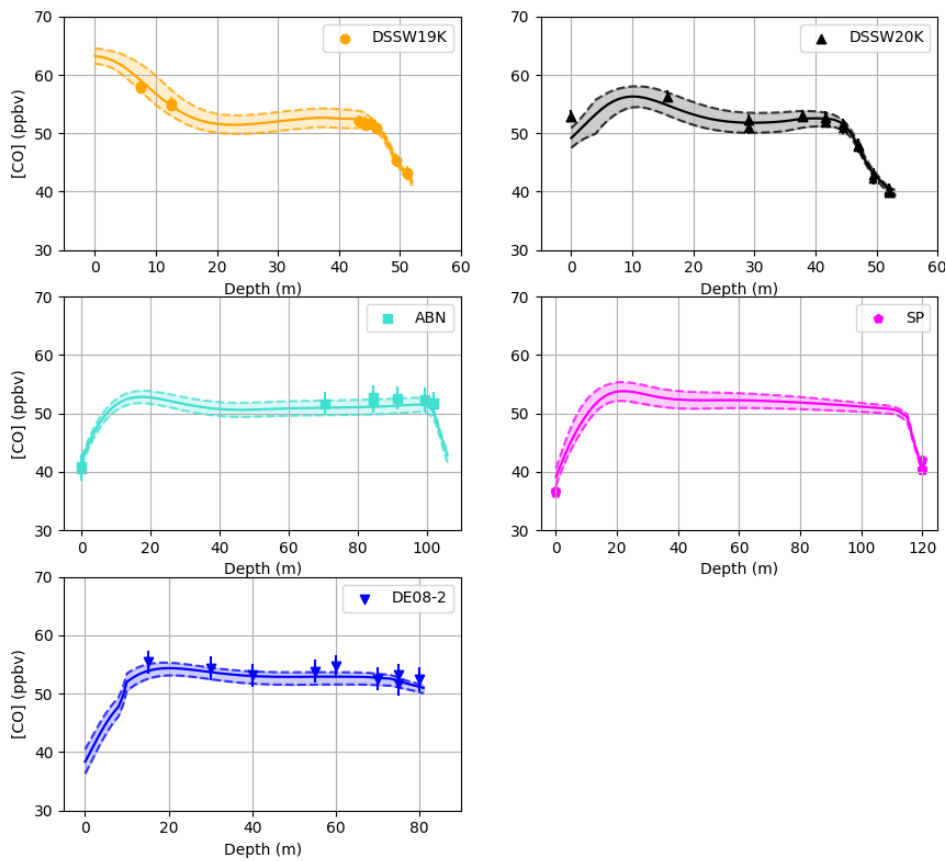
Figure S11. Concentration-depth profiles in the firn air at the five sites investigated with the CSIRO model. The measurements are reported with symbols with error bars indicating 2σ uncertainties. The solid lines are best fits of the firn CSIRO model, with envelopes indicating the 2σ uncertainties.

2.5. Combining IGE-GIPSA and CSIRO firn reconstructions

In this study, we use two independent models as a way to incorporate firn model uncertainty. Over the period spanning 1905 to 1992, we average the IGE-GIPSA and CSIRO records' annual values to produce a multimodel firn air CO reconstruction. For the 1897-1904 CE period, a third order polynomial weight was introduced in the annual averaging of the two firn records. Such approach (Fig. S12) allowed (i) to weight the multimodel record toward the CSIRO reconstruction in 1897 CE (because it is continuous with the ice reconstruction), and (ii) to match the [CO] growth rates (ie. in ppbv/yr) of the firn and ice core reconstructions in 1897 and 1905 CE. The multimodel firn air reconstruction is reported in Fig. S12, along with IGE-GIPSA and CSIRO reconstructions. The envelopes represent 2σ uncertainty intervals.
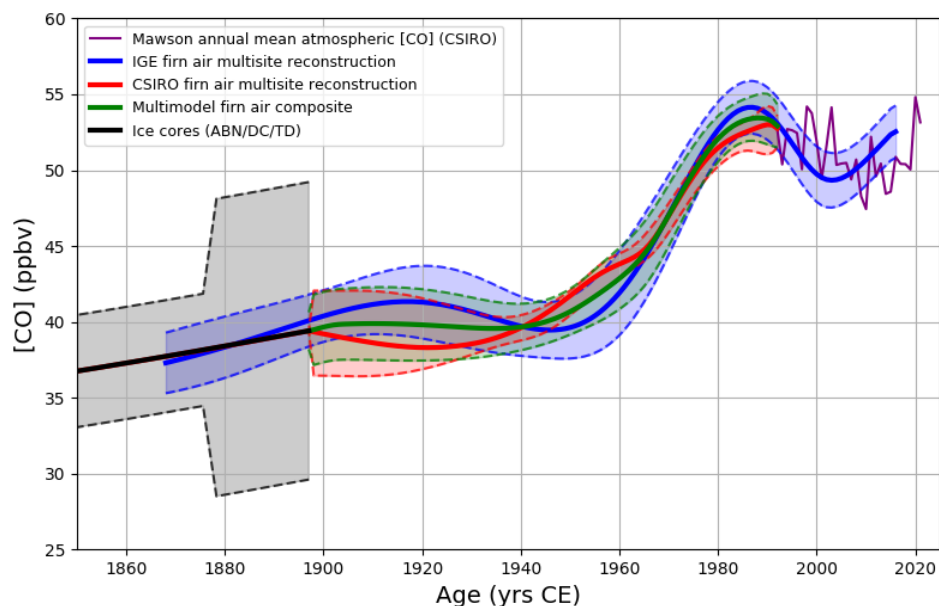
Figure S12. Optimal atmospheric [CO] history obtained with IGE-GIPSA (blue line) and CSIRO (red line) models. The green line shows the multimodel record obtained by averaging the IGE-GIPSA and CSIRO records.

2.6. The EDML-B40 continuous CO dataset

The EDML-B40 (later referenced as B40 in this section) ice core was drilled close to Kohnen Station, Dronning Maud Land, East Antarctica, by the Alfred Wegener Institute (drilling site : 75.001∘ S, 0.068∘ E, 2911 m elevation, Fig. S1 and Table S3). This core was analyzed on the DRI

CFA setup in September 2013 with a focus on methane mixing ratio (Rhodes et al., 2016). However, we were able to simultaneously measure CO concentrations, making the B40 core the first Antarctic ice archive measured for CO by CFA. As a first attempt to analyze continuously low-levels [CO] preserved in Antarctica ice, the B40 dataset is affected by memory effects and unexplained contaminations when initializing melting. Consequently, these data are not robust, and could not be calibrated and reported as absolute values. The configuration of the B40 analyses is reported in Table S2.

Ice core & location (Fig. S1)	Depth intervals (m)	Gas age interval (yrs CE)	Accum. Rate (cm weq yr^{-1})	Mean annual Temp. (°C)
EDML - B40	97.0 - 99.0	1849 ;1878	6.3 [a]	-46 [a]
Dronning Maud Land	100.3 - 103.9	1781 ; 1833		
75°S, 0° E	107.2 - 109.9	1698 ; 1736		
2911 m elevation	115.2 - 116.3	1606 ;1623		
	117.6 - 119.7	1560 ; 1590		
Solar-Ice	150.0 - 158.7	-71 ; 27	2.5 [b]	-53 [c]
Dôme Concordia				
75°0.6' S, 133°2' E				
3233 m elevation				

Table S3. Locations, site characteristics and other relevant information for the EDML-B40 and Solar-Ice ice cores. [a]Klein et al. (2014), [b]Gautier et al. (2016), [c]Fabre et al. (2000).

Figure S13 reports raw CO data from the B40 core, and highlights in red decreasing CO trends systematically observed when initializing melting.
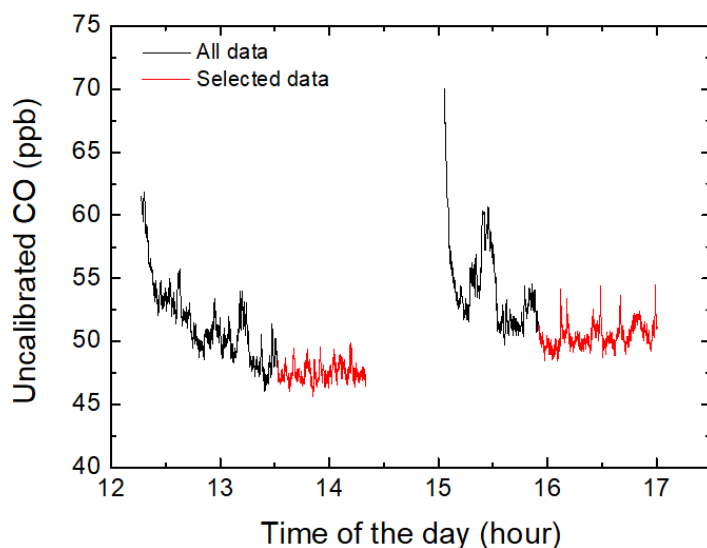
Figure S13. Typical EDML-B40 raw continuous CO data collected at DRI in September, 2013. Each analytical run lasts ~2 hours, and no sample is melted between runs. Decreasing trends in CO mixing ratio were observed at the beginning of each run, lasting for about half of the run.

410

In this Supplement, we extract the fraction of the B40 that we consider not affected by these contamination, i.e., for each melting run lasting about 2 hours, we kept the last hour of measurement (reported in red on Fig. S13). This is a conservative approach, but we preferred not applying CFA calibration to these data as the contamination processes were unexplained.

415   Finally, the selected, uncalibrated, B40 CO data are compared with other continuous Antarctica [CO] reconstruction (Fig. S14). To ease this comparison, we further apply an arbitrary offset of -19 ppbv to the B40 data. B40 data shows a trend similar to the DC12, ABN, and TD records. Specifically, the adjusted B40 data reproduces the minimum in [CO] observed at the beginning of the XVIII century, and the 10 ppbv increases during the period extending to the onset of the
420   Industrial Era. Although not accurate, the B40 data strengthen the pattern extracted from the calibrated record of the DC12, ABN and TD ice cores.
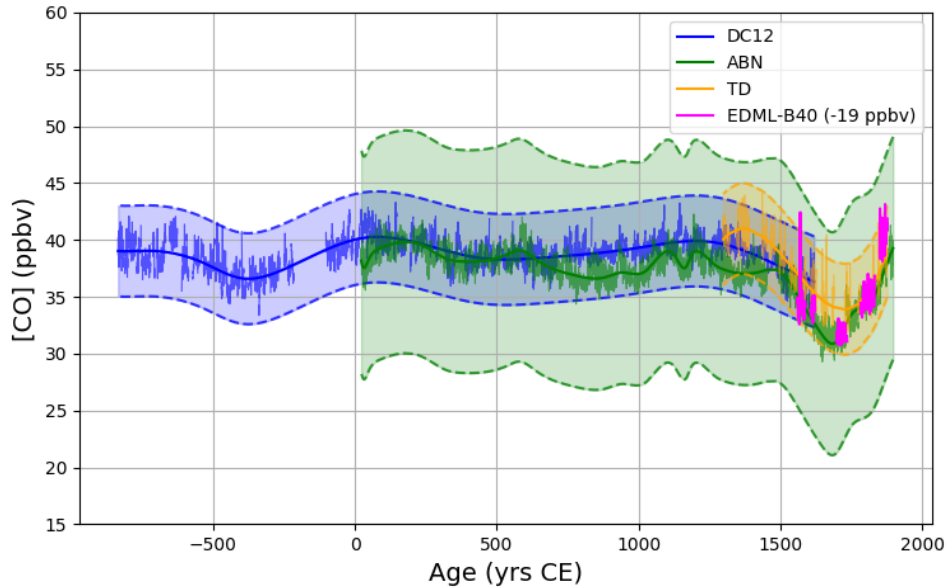
Figure S14. A selection of EDML-B40 [CO] data compared to continuous CO records of DC12, ABN and TD. The EDML-B40 data could not be CFA-calibrated, and were adjusted with an arbitrary offset of -19 ppbv for the purpose of this comparison.

2.7. Filling a gap in the DC12 dataset with the Solarice archive

The DC12 ice core was of extremely good quality, with very few breaks. However, a single section, spanning [154-158] m depth, was damaged during transportation and could not be analysed. To fill up this gap, we took advantage of the Solarice core, drilled in 2016 at Concordia Station (75°0.6' S, 123°2' E) closely from the DC12 drilling site

A Solarice core section spanning [151.0 – 158.8] m depth was analysed in January 2019 with the IGE CFA setup. Fig. S15 reports DC12 and Solarice dataset, with both cores calibrated with the same SC and Blank value (Table S2). The IGE CFA setup indeed remains unchanged between the two analytical campaigns, and the two ice cores originate from the same location.
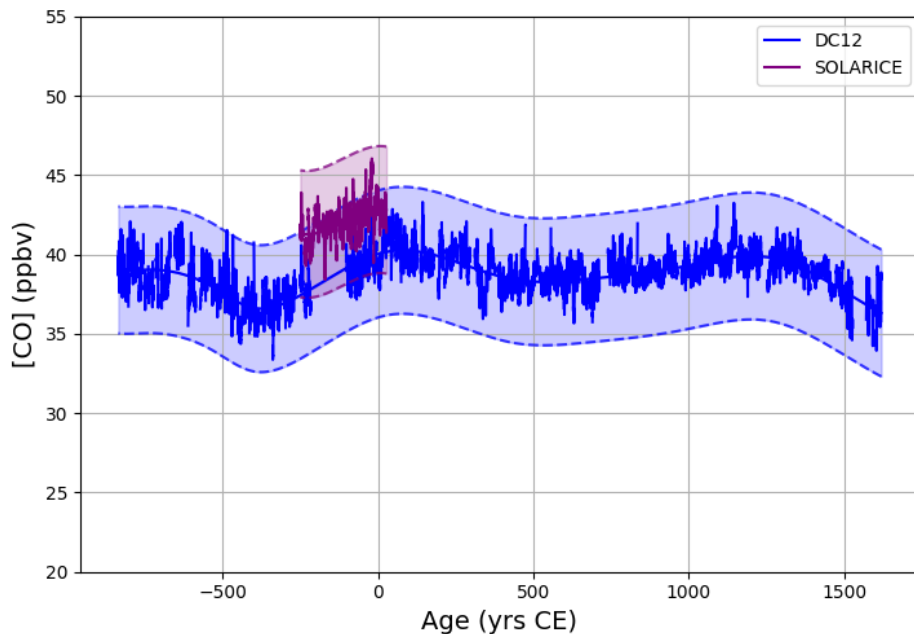
Figure S15. Solarice [CO] measurements conducted on the 150-158 m depth interval, overlapping with the gap in the DC12 record. Both Solarice and DC12 cores were drilled at Concordia Station (in 2016 and 2012, resp.), with boreholes located 2 km apart.

440

Although we observed slightly higher CO mixing ratios for Solarice compared to DC12, both records agree within their uncertainty envelope (2σ). The Solarice dataset reveals that [CO] remains very stable over the [151.0 – 158.8] depth range for ice drilled at the Dome Concordia, Antarctica. Consequently, we used a continuous spline to extract an average CO history from the
445   high resolution DC12 signals.

### 2.8. Evaluation of the smoothing effect of firn on ice core data

Using a similar approach as in Sect. 2.4 of the main article for firn data, this paragraph aims at showing that the smoothing effect from gas transport in firn and from progressive trapping in ice
450   on the CO records in ice is insignificant. The magnitude of the smoothing is primarily dependent on the relative time scales of atmospheric variations and physical processes in firn. For instance,

CO atmospheric seasonal variations are fast compared to gas transport in firn and entirely smoothed in the upper 30-40m. On the other hand, the CO trend variations recorded in the ice for the -835 to 1897 CE period are much slower.

455   Gas trapping in ice bubbles is the slowest firn process: it operates at the decadal to multi-century time scales depending in first instance on the snow accumulation rate at the study site, which controls the sinking speed of firn layers. Among our ice core study sites, the strongest smoothing effect is thus expected at Dome C. Two approaches are used to evaluate the smoothing of the CO signal: (1) A forward model approach comparing the results obtained at our three sites when
460   using the ice core signal + firn based reconstruction as the atmospheric input trend and (2) an inverse model approach constrained with the ice core data in order to reconstruct an atmospheric signal. Although more relevant, the inverse model approach has a major limit: it is a multiple solutions mathematical problem (Rommelaere et al., 1997, Witrant and Martinerie, 2013). The result is strongly dependent on the ability of the model to discriminate between signal and noise
465   in the data, as very well illustrated by Fig. 11 in Rommelaere et al. (1997).

As expected, the forward model approach (Fig. S16) produces a slightly smoother signal at Dome C than other sites. The IGE-GIPSA model has not been directly tuned to ABN and TD, thus drill sites with similar accumulation rates were used: South Pole (7.4 cm weq. yr^{-1}) instead of TD (8.6 cm weq. yr^{-1}) and BKN (13.0 cm weq. yr^{-1}) instead of ABN (11.9 cm weq. yr^{-1}). The model results
470   for South Pole and Berkner remain very close to the input spline signal whereas Dome C signal suggest that some smoothing is occurring. The smoothing is most pronounced around the 1700 CO minimum, which is not part of the Dome C ice core record as it is too close to the bubble closure zone. All results remain well within the uncertainty envelope of the spline fit to the ice core data.
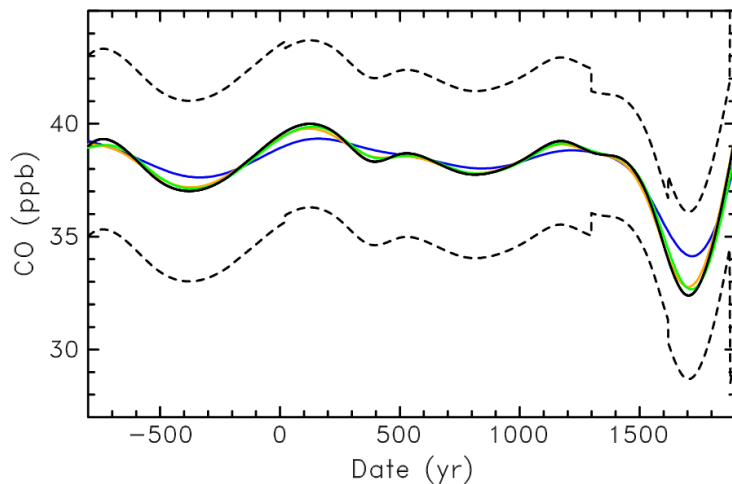
Figure S16. Forward firn model results in ice using the spline fit to ice core data (in black) as atmospheric input. In order to run the model until present day, the spline was combined with the atmospheric scenario reconstructed from firn air data for recent decades. Modelled mixing ratios in the ice are plotted versus gas age in blue for Dome C, orange for South Pole (representative of TD) and green for BKN (representative of ABN).

Two ways of forcing the inverse model, in Dome C configuration, were used (Fig. S17). First the model was directly constrained by the DC12 CO dataset binned at a 4 cm resolution. The reconstructed atmospheric trend (dark blue) is slightly smoother than the spline fit to the overall fit to the 3 sites dataset (in black) also based on higher accumulation sites. The model was further constrained with the spline fit, but its ability to properly discriminate signal and noise is more uncertain in this case. This leads to the slightly less smooth light blue trend on Fig. S17 which also remains within the uncertainty envelope of the data. Consistently with the forward model approach, the largest difference is observed near the CO minimum at ~1700 CE. However, the spline fit of the data is not constrained by Dome C data in that time period and Figure S16 suggests very limited smoothing at the other sites.
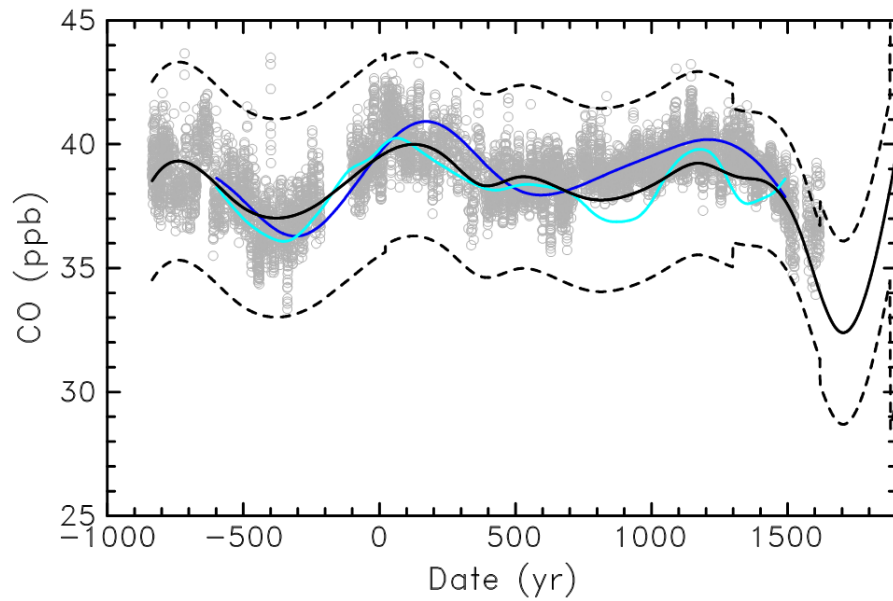
Figure S17. Inverse model reconstructions of atmospheric CO trend using Dome C firn physics conditions constrained with (i) the Dome C dataset binned at 4 cm resolution (grey circles) which leads to the smooth dark blue trend, or (ii) with the spline fit to the multi-site CO dataset (black line) leading to the light blue trend.
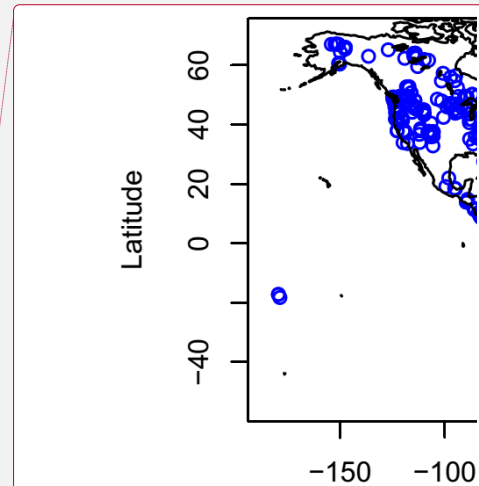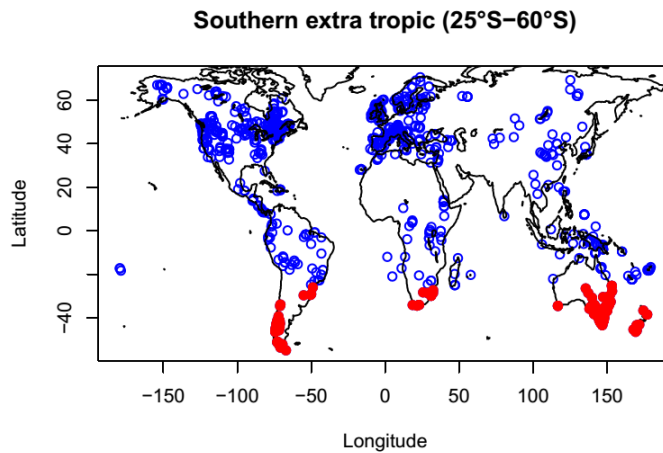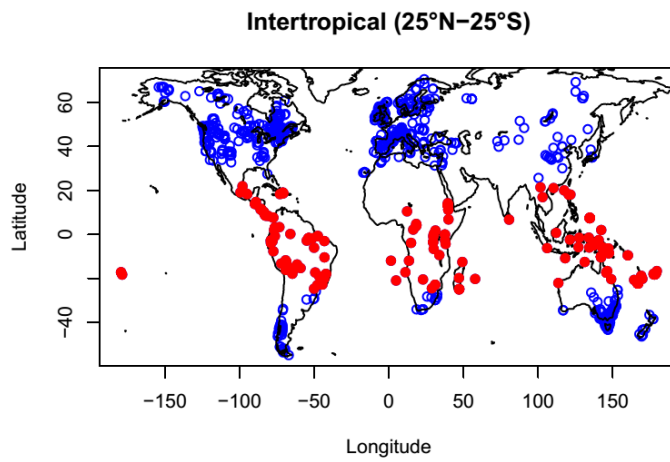
~~Overall, we conclude that no significant smoothing by firn related processes affects our spline fit to the ice core signals.~~

2.9. Localisation of charcoal records

Intertropical (25°N−25°S)

Southern extra tropic (25°S−60°S)

510 **Figure S18.** Localisation of charcoal records included in the composites discussed in this study (Fig. 5). Extracted from the Global Paleofire Database (https://database.paleofire.org).

515

Supprimé:

Supprimé: included

Supprimé: in the 30-60°S Oceania, and America composites

3. References

520

Allan, D. W.: Statistics of atomic frequency standards, Proc. IEEE, 54(2), 221–230, doi:10.1109/PROC.1966.4634, 1966.

Fabre, A., Barnola, J. M., Arnaud, L. and Chappellaz, J.: Determination of gas diffusivity in polar firn: comparison between experimental measurements and inverse modeling, Geophys. Res.
525 Lett., 27(4), 557–560, 2000.

Faïn, X., Rhodes, R. H., Place, P., Petrenko, V. V., Fourteau, K., Chellman, N., Crosier, E., McConnell, J. R., Brook, E. J., Blunier, T., Legrand, M. and Chappellaz, J.: Northern Hemisphere atmospheric history of carbon monoxide since preindustrial times reconstructed from multiple Greenland ice cores, Clim. Past, 18(3), 631–647, doi:10.5194/cp-18-631-2022, 2022.

530 Fourteau, K., Martinerie, P., Faïn, X., Ekaykin, A. A., Chappellaz, J. and Lipenkov, V.: Estimation of gas record alteration in very low-accumulation ice cores, Clim. Past, 16(2), 503–522, doi:10.5194/cp-16-503-2020, 2020.

Francey, R. J., L. P. Steele, D. A. Spencer, R. L. Langenfelds, R. M. Law, P. B. Krummel, P. J. Fraser, D. M. Etheridge, N. Derek, S. A. Coram, L. N. Cooper, C. E. Allison, L. Porter and S. Baly,
535 The CSIRO (Australia) measurement of greenhouse gases in the global atmosphere, *Baseline Atmospheric Program (Australia) 1999-2000,* N. W. Tindale, N. Derek and P. J. Fraser (eds.), Bureau of Meteorology and CSIRO Atmospheric Research, Melbourne, Australia, 42-53, 2003.

Fraser, P., S. Coram and N. Derek (1994), Atmospheric methane, carbon monoxide and carbon dioxide by gas chromatography, Baseline Atmospheric Program (Australia) 1991, A. L. Dick and
540 J. L. Gras (eds.), Bureau of Meteorology and CSIRO Division of Atmospheric Research, Melbourne, Australia, 60-64

Gautier, E., Savarino, J., Erbland, J., Lanciki, A. and Possenti, P.: Variability of sulfate signal in ice core records based on five replicate cores, Clim. Past, 12(1), 103–113, doi:10.5194/cp-12-103-2016, 2016.

545 Klein, K.: Variability in dry Antarctic firn – Investigations on spatially distributed snow and firn samples from Dronning Maud Land, Antarctica, PhD thesis, University of Bremen, Bremen, Germany, 2014.

Langenfelds, R. L., Guerette E-A., Steele L. P., Krummel P. B., Spencer D. A., Loh Z. M., Gregory R. L., Thornton D. P., Howden R. T. and Fraser P. J.: Atmospheric methane, carbon dioxide,

550   carbon monoxide, hydrogen and nitrous oxide from Cape Grim flask samples analysed by gas chromatography, in Baseline Atmospheric Program (Australia), 2014-16, R. Langenfelds, N. Derek and S. L. Cleland (eds.), Bureau of Meteorology and CSIRO Environment, Melbourne, Australia, 2023.

Loh, Z., Langenfelds, R., Krummel, P.: Atmospheric CO at Casey by Commonwealth Scientific

555   and   Industrial   Research   Organisation,   dataset   published   as   CO_CYA_surface-flask_CSIRO_data1 at WDCGG, ver.2021-04-08-1004, https://doi.org/10.50849/WDCGG_0016-7004-3001-01-02-9999, 2021a.

Loh, Z., Langenfelds, R., Krummel, P.: Atmospheric CO at South Pole by Commonwealth Scientific and Industrial Research Organisation, dataset published as CO_SPO_surface-

560   flask_CSIRO_data1 at WDCGG, ver.2021-04-08-1004, https://doi.org/10.50849/WDCGG_0016-7011-3001-01-02-9999, 2021b.

Loh, Z., Langenfelds, R., Krummel, P.: Atmospheric CO at Mawson by Commonwealth Scientific and   Industrial   Research   Organisation,   dataset   published   as   CO_MAA_surface-flask_CSIRO_data1 at WDCGG, ver.2021-04-08-1004, https://doi.org/10.50849/WDCGG_0016-

565   7005-3001-01-02-9999, 2021c.

Masarie, K. A., R. L. Langenfelds, C. E. Allison, T. J. Conway, E. J. Dlugokencky, R. J. Francey, P. C. Novelli, L. P. Steele, P. P. Tans, B. Vaughn and J. W. C. White, NOAA/CSIRO Flask Air Intercomparison Experiment: A strategy for directly assessing consistency among atmospheric measurements made by independent laboratories, J. Geophys. Res., 106, 20445-20464, 2001.

570   Mitchell, L. E., Brook, E. J., Lee, J. E., Buizert, C. and Sowers, T.: Constraints on the late holocene anthropogenic contribution to the atmospheric methane budget, Science, 342(6161), 964–6, doi:10.1126/science.1238920, 2013.

Morville, J., Kassi, S., Chenevier, M. and Romanini, D.: Fast, low-noise, mode-by-mode, cavity-

575   enhanced absorption spectroscopy by diode-laser self-locking, Appl. Phys. B-Lasers Opt., 80(8), 8 1027–1038, doi:10.1007/s00340-005-1828-z, 2005.

Rhodes, R. H., Faïn, X., Brook, E. J., McConnell, J. R., Maselli, O. J., Sigl, M., Edwards, J. S., Buizert, C., Blunier, T., Chappellaz, J. and Freitag, J.: Local artifacts in ice core methane records

caused by layered bubble trapping and in situ production: a multi-site investigation, Clim. Past, 12(4), 1061–1077, doi:10.5194/cp-12-1061-2016, 2016.

580 Rommelaere, V., Arnaud, L. and Barnola, J. M.: Reconstructing recent atmospheric trace gas concentrations from polar firn and bubbly ice data by inverse methods, J. Geophys. Res., 102, 30 069-30 083, 1997.

Servettaz, A. P. M., Orsi, A. J., Curran, M. A. J., Moy, A. D., Landais, A., McConnell, J. R., Popp, T. J., Le Meur, E., Faïn, X. and Chappellaz, J.: A 2000-year temperature reconstruction on the 585 East Antarctic plateau from argon–nitrogen and water stable isotopes in the Aurora Basin North ice core, Clim. Past, 19(6), 1125–1152, doi:10.5194/cp-19-1125-2023, 2023.

Trudinger, C. M., Enting, I. G., Rayner, P. J., Etheridge, D. M., Buizert, C., Rubino, M., Krummel, P. B. and Blunier, T.: How well do different tracers constrain the firn diffusivity profile?, Atmos. Chem. Phys., 13(3), 1485–1510, doi:10.5194/acp-13-1485-2013, 2013.

590 Trudinger, C. M., Fraser, P. J., Etheridge, D. M., Sturges, W. T., Vollmer, M. K., Rigby, M., Martinerie, P., Mühle, J., Worton, D. R., Krummel, P. B., Steele, L. P., Miller, B. R., Laube, J., Mani, F. S., Rayner, P. J., Harth, C. M., Witrant, E., Blunier, T., Schwander, J., O'Doherty, S. and Battle, M.: Atmospheric abundance and global emissions of perfluorocarbons CF4, C2F6 and C3F8 since 1800 inferred from ice core, firn, air archive and in situ measurements, Atmos. Chem. 595 Phys., 16(18), 11733–11754, doi:10.5194/acp-16-11733-2016, 2016.

Werle, P., Mücke, R. and Slemr, F.: The Limits of Signal Averaging in Atmospheric Trace-Gas Monitoring by Tunable Diode-Laser Absorption Spectroscopy (TDLAS), Appl. Phys. B-Lasers Opt., 139, 131–139, 1993.

Witrant, E., Martinerie, P., Hogan, C., Laube, J. C., Kawamura, K., Capron, E. and Montzka, S. 600 A., E. J. Dlugokencky,D. Etheridge, T. Blunier, and W. T. Sturges: A new multi-gas constrained model of trace gas non-homogeneous transport in firn : evaluation and behaviour at eleven polar sites, Atmos. Chem. Phys., (12), 11465–11483, doi:10.5194/acp-12-11465-2012, 2012.

Witrant, E. and Martinerie, P.: Input Estimation from Sparse Measurements in LPV Systems and Isotopic Ratios in Polar Firns, in 2013 IFAC Joint Conference SSSC, pp. 654–659, 5th 605 Symposium on System Structure and Control, Grenoble, France, https://www.gipsa-lab.grenoble-inp.fr/~emmanuel.witrant/papers/13_ifac_firn.pdf, 2013.

Supprimé: Rommelaere, V., Arnaud, L., and Barnola, J.-M. (1997), Reconstructing recent atmospheric trace gas concentrations from polar firn and bubbly ice data by inverse methods, J. Geophys. Res., 102(D25), 30069– 30083, doi:10.1029/97JD02653.¶

Supprimé: Servettaz, A. P. M., Orsi, A. J., Curran, M. A. J., Moy, A. D., Landais, A., McConnell, J. R., Popp, T. J., Le Meur, E., Faïn, X. and Chappelaz, J.: A 2000-year temperature reconstruction on the East Antarctic plateau, from argon-nitrogen and water stable isotopes in the Aurora Basin North ice core, Clim. Past Discuss., 2022, 1–58, doi:10.5194/cp-2022-91, 2022. ¶